Texas A&M University

Department of

OCEANOGRAPHY

MICROWAVE RADIOMETRY AND ITS APPLICATION TO MARINE METEOROLOGY AND OCEANOGRAPHY

by
Jack F. Paris

January 1969

Office of Naval Research
Contract Nonr 2119(04)

Project NR 083-036
A&M Project 286-13
Ref. No. 69-1T

Funded by
National Aeronautics and Space Administration
through the
Office of Naval Research

Research Conducted through the
Texas A & M Research Foundation
COLLEGE STATION, TEXAS

ERRATA SHEET

for

MICROWAVE RADIOMETRY AND ITS APPLICATION
TO MARINE METEOROLOGY AND OCEANOGRAPHY

by

Jack F. Paris
January, 1969

1. Page 14 - Line 12 - (henrys per meter) . . .
2. Page 19 - Line 22 - since (30) is to be used . . .
3. Page 34 - Line 3 - . . . farads per meter.
4. Page 34 - Line 7 - detect ice-ocean boundaries . . .
5. Page 61 - Line 17 - Equation (99) - . . . (db/km), (99)
6. Page 84 - Line 9 - Equation (128) - = $4.093\ C_1 M\nu/c\rho_L$
7. Page 85 - Line 8 - δ^7 or higher, . . .

Attention:

In order to keep our distribution list up to date, please check your address at the back of this report. If it is incorrect, please correct it on the form below, and return it to:

Mrs. June Hagler
Spacecraft Oceanography Project
Department of Oceanography
Room 325, Teague Research Center
Texas A & M University
College Station, Texas 77843

Corrected Address: _____

_____

_____

_____

_____

_____

April/69

Texas A&M University
Department of Oceanography
College Station, Texas 77843

Research conducted through the
Texas A&M Research Foundation
A&M Project 286-13

MICROWAVE RADIOMETRY AND ITS APPLICATIONS TO MARINE METEOROLOGY AND OCEANOGRAPHY

by

Jack F. Paris
January 1969

PREFACE

Project 286 is sponsored by the Office of Naval Research [Project NR 083-036, Contract Nonr 2119(04)]. The Project 286-13 portion is operated through funding provided by the Spacecraft Oceanography Project of the Naval Oceanographic Office and is part of the National Aeronautics and Space Administration's Earth Resources Survey Program.

Dr. Luis R.A. Capurro
Project Supervisor

ABSTRACT

MICROWAVE RADIOMETRY AND ITS

APPLICATIONS TO MARINE

METEOROLOGY AND OCEANOGRAPHY

January 1969

Jack Frederick Paris

B.S., Texas A&M University

B.S., University of Washington

Directed by Dr. George L. Huebner, Jr.

Past developments in microwave radiometry, a discipline of remote sensing, are reviewed comprehensively to establish a continuity between microwave physics, microwave engineering, and applications to marine meteorology and oceanography. Molecular oxygen, water vapor, and liquid water absorb, emit, and scatter microwave radiation. The ocean reflects or scatters a majority of the microwave radiation incident upon its surface and emits microwave energy. The functional relationships between these interactions and the physical state of the atmosphere and hydrosphere are described in detail.

The emission of sea water is almost constant with temperature and salinity for frequencies of 8 GHz to 30 GHz, is linearly proportional to temperature for frequencies near 5.4 GHz, and is strongly dependent upon salinity for frequencies near 1 GHz. Sea foam causes the microwave emission of the sea to increase

greatly for all microwave frequencies and angles of viewing.

The natural variability of water vapor in the atmosphere affects the absolute value of upwelling microwave radiation greatly for frequencies near 22.235 GHz. The attenuation and emission of the atmosphere are predictable for frequencies less than 8 GHz.

Microwave measurements near 5.4 GHz and 1 GHz may be used to survey, remotely, the temperature and salinity of coastal water. Microwave measurements near 22.235 GHz may be used to measure the precipitable water in the atmosphere.

It is recommended that (1) electric properties of sea water be measured precisely, (2) controlled environmental tests of current microwave theory be conducted, (3) the problem of the microwave emission and extinction of raining clouds over water be studied in great detail using realistic models of clouds and using the Mie theory, and (4) the emissive properties of sea foam, bubbles, and rough sea surfaces be determined through empiricism.

ACKNOWLEDGMENTS

The author wishes to express his appreciation to Dr. George L. Huebner, Dr. Guy A. Franceschini, and Dr. H. A. Luther. The author expresses his appreciation to Mrs. Rosemary Boykin, Mr. Hector Cornelio, and Mrs. Melanie Fuller who assisted in the preparation of this report and the reduction of the data used in it.

Dr. William Nordberg and Dr. Jack Conaway of the Goddard Space Flight Center, Greenbelt, Maryland, furnished the author with timely microwave data obtained over the Gulf of Mexico. Mr. Sid Whitley of the Manned Spacecraft Center and Mr. John Blinn of Jet Propulsion Laboratories furnished the author with microwave data taken over the Mississippi Delta.

The research was conducted under the sponsorship of the U. S. Naval Oceanographic Office under the Office of Naval Research, Contract Nonr 2119(04). Dr. Luis R. A. Capurro is the principal investigator for this research.

The author is grateful for the two years of support given under the National Defense Education Act Title IV Fellowship.

Appreciation is given to my wife, Mary, and our children for their support and love throughout this period of research.

The author appreciates the many helpful suggestions and editing by Dr. Vance Moyer.

TABLE OF CONTENTS

		Page
ABSTRACT		iii
ACKNOWLEDGMENTS		v
LIST OF TABLES		x
LIST OF FIGURES		xiii
LIST OF SYMBOLS AND ABBREVIATIONS		xvii
Chapter		
I.	INTRODUCTION	1
	Nature of Problem	1
	Past Studies	6
	Objective and Scope	11
II.	ELECTRIC AND MAGNETIC PROPERTIES OF MATTER	14
	Maxwell's Equations	14
	Complex Dielectric Constant	15
	Theory	15
	Practical treatment	23
	Electric and magnetic properties of water	26
	Electric and magnetic properties of ice	33
III.	RADIATIVE TRANSFER	35
	Elementary Radiation	35
	Intensity	35
	Poynting's theorem	37
	Polarization	39
	Blackbody radiation	40
	Brightness Temperature	43
	Cosmic temperature	44
	Sky temperature	44
	Emissive temperature of the surface	45
	Reflective temperature	45

Equations of Transfer 45
Extinction and emission 46
General equation of transfer 47
Transfer equation in a non-scattering medium under local thermodynamic equilibrium in terms of brightness temperature 49
Extinction and emission at the air-sea interface 51
Upwelling microwave radiation 56

IV. EXTINCTION AND EMISSION IN THE ATMOSPHERE..... 58

General 58
Atmospheric Gases 60
Molecular oxygen 60
Water vapor 64
Total gaseous absorption 65
Total atmospheric attenuation for a clear atmosphere 69
Sky temperature 72
Hydrometeors 80
General 80
Mie theory 81
Approximations to the Mie theory 83
Emission of clouds and rain 88
Summary 95

V. EXTINCTION AND EMISSION IN THE HYDROSPHERE.... 98

General 98
Flat Sea Surface 100
Fresnel's Laws of Reflection 100
Reflective temperature of a flat sea surface 101
Emissive temperature of a flat sea surface 102
Brightness temperature of a flat sea surface 102
Smooth Irregular Sea Surface 109
Rough Sea Surface 112
General 112
Kirchhoff approximation 113

Foam, Bubbles, and Ice 114
General 114
Foam and bubbles 115
Ice 117

VI. INTENSITY OF UPWELLING MICROWAVE RADIATION..... 120

General 120
Salinity Effect 122
Effect of Water Vapor 128
Effect of Roughness 130
Effect of Liquid Water 135

VII. MICROWAVE RADIOMETRY..... 139

General 139
Microwave Receivers 140
Antenna Effects 145

VIII. RESULTS OF MICROWAVE MEASUREMENTS..... 153

General 153
Microwave Radiometers in the NASA 926 155
System description 155
Mission 41 161
Mission 50 166
Mission 66 166
Implications for future missions 176
Microwave Radiometers in the Convair 990 180
Systems description 180
Roughness 181
Precipitable water 184
Liquid water 184

IX. CONCLUSIONS AND RECOMMENDATIONS 190

Conclusions 190
Dielectric properties of water 190
Radiative transfer 191
Thermodynamic equilibrium 192
Water vapor and molecular oxygen 192
Hydrometers 193
Air-sea interface 194
Sea temperature 194
Salinity 195
Foam, bubbles, ice, and land 195
Microwave radiometry 196
Applications 196

Recommendations 196

BIBLIOGRAPHY..... 199

VITA..... 211

LIST OF TABLES

Table		Page
I.	Atmospheric windows in the electromagnetic spectrum.....	4
II.	Microwave bands reserved for radio astronomy (after Smith-Rose, 1964).....	11
III.	Principal ionic constituents of sea water (34.4 o/oo salinity) (after McLellan, 1965).....	22
IV.	Specific gravity of solution of sodium chloride and water as a function of temperature and salinity at one atmosphere of pressure.....	24
V.	Static relative permittivity (ε_s), relaxation time (τ, seconds), and ionic conductivity (σ_i, mhos per meter) of a solution of sodium chloride and water for specific values of temperature (T, °C) and salinity (S, o/oo) (after Saxton and Lane, 1952)...	25
VI.	Calculated values of ε' and ε'' for selected values of temperature (T, °C), salinity (S, o/oo), and frequency (ν, GHz).....	28
VII.	Dielectric constant of ice (after Gunn and East, 1954).....	33
VIII.	Theoretical values of the absorption coefficient of molecular oxygen (α_{ox}, db/km) at a pressure of 1013.25 mb and a temperature of 293.0° K (after Van Vleck, 1951).....	62
IX.	Theoretical values of the absorption coefficient of water vapor (α_w, db/km) per unit of water-vapor density (ρ_w, g/m^3) at a pressure of 1013.25 mb and a temperature of 293° K (after Van Vleck, 1951)....	67
X.	Total absorption coefficient for molecular oxygen and and water vapor (α_g, db/km) for a pressure of 1013.25 mb, for a temperature of 293° K and for water vapor densities of 3, 7.5 and 17 g/m^3.....	68

XI. Zenith attenuation ($L_g(z)$, db) in a 1960 ARDC model atmosphere with a density of water vapor of 9.35 exp (-5z) grams per cubic meter versus altitude (z, km) (after Stogryn, 1967)..... 71

XII. Summary of calculated and observed values of total zenith attenuation (L_g, db)..... 73

XIII. Summary of calculated and observed values of polarized sky temperature (T_p^{sky}, °K)..... 78

XIV. The attenuation coefficient of non-raining clouds and fog (α_c, db/km) per unit concentration of liquid water (M, g/m^3) for temperatures of 0° C and for 20° C and for frequencies of 3, 6, 10, 15 and 30 GHz (after Ryde, 1946)..... 84

XV. Absorption coefficient of non-raining clouds and fog (α_c, db/km) per unit concentration of liquid water (M, g/m^3) for a temperature of 18° C (after Goldstein, 1951)..... 87

XVI. Correction factor, $F_1(T)$ (dimensionless), for α_c in Table XV (after Goldstein, 1952)..... 88

XVII. Extinction coefficient for raindrops (e_R, db/km) for various precipitation rates (R, mm/hr) for a temperature of 18° C (after Goldstein, 1951)..... 89

XVIII. List of cases considered by Kreiss (1968)..... 91

XIX. Some values of polarized sky temperature (T_p^{sky}, °K), under various meteorological conditions (from Kreiss, 1968)..... 93

XX. Average values of measured vertically-polarized sky temperatures (T_v^{sky}, °K) at Columbus, Ohio, for frequencies of 23 GHz and 35 GHz taken in the summers of 1964 and 1965 (after Cummings and Hull, 1966).... 94

XXI. Values of vertically polarized sky temperature (T_v^{sky}, °K) by Weger (1960) for various meteorological conditions..... 95

XXII. Measured values of polarized zenith sky temperature by Wulfsberg (1964) for various meteorological conditions..... 96

XXIII. Reflectivity, emissivity, emissive temperature, reflective temperature, and brightness temperature of a flat sea surface for various frequencies, temperatures, and salinities and for an incidence angle of 0° 104

XXIV. Results of ground measurements of the emission of the sky, smooth water, bubbles, and foam by Williams (1968) 116

XXV. List of special cases considered in Chapter VI 123

XXVI. Assumed atmospheric parameters and derived quantities used in calculating values of brightness temperature given in Figure 10 127

XXVII. Difference between the horizontally polarized brightness temperature of sea water at an incidence angle of 0° (T_h (0°)) and that of sea water at an incidence angle of 45° (T_p (45°)) for a frequency of 19.4 GHz versus the speed of the wind at 41 ft. above sea level (w, m/sec) for a fully developed sea 134

XXVIII. Significant parameters of the MR-62 and MR-64 microwave radiometers on board the NASA 926 (after Blinn, 1967a) 157

XXIX. Flight parameters and radiometric parameters for Mission 41 162

XXX. Mean values of brightness temperatures for Mission 41 164

LIST OF FIGURES

Figure	Caption	Page
1.	The electromagnetic spectrum.....	3
2.	Real part of the complex dielectric constant of pure, fresh and sea water versus frequency for 0° C and 20° C.....	31
3.	Imaginary part of the complex dielectric constant of pure, fresh and sea water versus frequency for a water temperature of 0° C and 20° C.....	32
4.	Geometry of intensity.....	36
5.	Geometry of radiative transfer in a horizontally uniform, plane, parallel atmosphere.....	50
6.	Geometry of surface scattering.....	54
7.	The absorption coefficient of molecular oxygen and water vapor at sea level versus frequency for a temperature of 293° K and for water-vapor densities of 0, 3, 7.5, and 17 grams per cubic meter.....	66
8.	The polarized emissive temperature of a flat sea surface versus the thermometric temperature of the sea surface for frequencies of 1, 5.4, 9.2, 15.8, 19.35, 22.235, and 34 GHz and for various salinities.....	108
9.	The change in polarized emissive temperature of a flat sea surface due to a change in water temperature from 273° K to 300° K versus frequency (after Marandino, 1967).....	110
10.	The polarized brightness temperature of sea water versus salinity for a water temperature of 283° K, for an incidence angle of 0°, for frequencies of 1, 5.4, 9.2, 15.8, 19.35, 22.235, and 34 GHz, and for an altitude of 1 km.....	125

11. The polarized brightness temperature of sea water versus salinity for a water temperature of 303° K, for an incidence angle of 0°, for frequencies of 1, 5.4, 9.2, 15.8, 19.35, 22.235, and 34 GHz, and for an altitude of 1 km..... 128

12. The polarized brightness temperature of sea water versus precipitable water in the atmosphere for frequencies of 19.35 GHz and 22.235 GHz, for an incidence angle of 0°, and for an altitude in excess of 20 km..... 131

13. The polarized brightness temperatures of sea water versus incidence angle for horizontal and vertical polarization, for fully developed sea driven by surface winds of 0, 4, and 14 m/sec, for an altitude of 1 km, and for a frequency of 19.4 GHz (after Stogryn, 1967)..... 133

14. The polarized brightness temperature of sea water versus the concentration of liquid water in intervening clouds for a frequency of 19.35 GHz and for an incidence angle of 0°..... 136

15. The polarized brightness temperature of sea water versus the product of the thickness of intervening clouds and their concentration of liquid water for a frequency of 19.35 GHz and for an incidence angle of 0°..... 137

16. Block diagram of a typical microwave radiometer.. 141

17. Geometry of antenna parameters..... 145

18. Antennas of the MR-62 and MR-64 microwave radiometers..... 156

19. Location of remote sensors in the NASA 926..... 158

20. Basic flight lines flown over Mississippi Delta over past two years..... 160

21. Flight lines flown over Mississippi Delta during Mission 50 and during Flight 13..... 167

22. Cruise track of R/V ALAMINOS during Cruise 68-A-1..... 169

23. Analysis of surface temperature for 68-A-1, February 1968..... 170

24. Analysis of surface salinity for 68-A-1, February 1968..... 171

25. The distribution of temperature and salinity along Line 1 from analyses in Figures 23 and 24 .. 172

26. Estimated brightness temperatures measured over Line 1 of Mission 66 at altitudes of 3048 meters (squares) and 458 meters (circles) and corresponding theoretical values of brightness temperatures (solid lines) versus distance from South Pass for frequencies of 9.2 GHz and 15.8 GHz..... 174

27. Estimated brightness temperatures measured over Line 1 of Mission 66 at altitudes of 3048 meters (squares) and 458 meters (circles & triangles) and corresponding theoretical values of brightness temperatures (solid lines) versus distance from South Pass for frequencies of 22.234 GHz and 34 GHz..... 175

28. Theoretical polarized brightness temperatures versus distance from South Pass for the distribution of temperature and salinity given in Figure 24, for frequencies of 5.4 GHz and 1.0 GHz and for an incidence angle of 0°..... 177

29. Analysis of surface temperature for 67-A-7 based on readings of the infrared radiometer on the R/V ALAMINOS..... 178

30. Analysis of surface salinity for 67-A-7, August 1967..... 179

31. The average value of the horizontally polarized brightness temperature (circles and dashed line) measured during Flight 12 from 18:13:00Z to 18:13:30Z versus incidence angle and corresponding theoretical values (solid lines) from Stogryn (1967) for a frequency of 19.35 GHz..... 183

32. Measured values of the horizontally polarized brightness temperature from 17:24 Z to 17:25 Z during Flight 12 versus time for an incidence angle of 0° and for a frequency of 19.35 GHz as the aircraft flew from land to water..... 185

33. The estimated horizontally polarized brightness temperature from 13:53:00 Z to 13:54:30 Z during Flight 13 versus time for an incidence angle of 0° and for a frequency of 19.35 GHz as the aircraft flew over raining clouds at sea..... 187

34. The distribtion of the concentration of liquid water in the clouds under the aircraft as derived from the measurements given in Figure 33..... 188

LIST OF SYMBOLS AND ABBREVIATIONS

SYMBOLS

a	radius of a water droplet
$\vec{a}$	unit vector denoting direction of travel of a pencil of radiation
$\vec{a}_s$	unit vector denoting direction of scattered radiation
$\vec{a}_z$	unit vector denoting the vertical direction
$\vec{a}_\Omega$	unit vector denoting direction when integrating over the solid angle, Ω
a_m	maximum radius of a cloud of water droplets
a_n	complex scattering-amplitude-coefficient of a homogenous dielectric sphere
a_o	absorptivity of a natural body
b_n	complex scattering-amplitude-coefficient of a homogenous dielectric sphere
c	speed of propagation of an electromagnetic wave in a vacuum
d	distance from South Pass, Mississippi Delta
e	extinction coefficient of a medium
e_R	volume extinction coefficient of raindrops
g_x	root-mean-squared wave slope of the sea surface along the direction perpendicular to the direction of the surface wind
g_y	root-mean-squared wave slopes of the sea surface along the direction of the surface wind
h	Planck's constant, approximately $6.62? \times 10^{-34}$ joule-seconds
h_o	altitude of observation
k	Boltzman's constant, approximately 1.38×10^{-23} joules per degree Kelvin

ℓ	thickness of a layer of ice overlying ice
m	complex index of refraction of a medium
n	real part of the complex index of refraction
p	atmospheric pressure
p	symbol denoting either vertical or horizontal polarization; p = v or h (subscript)
r_h	horizontally polarized reflectivity of a flat sea surface
r_p^i	polarized reflectivity of ice
r_v	vertically polarized reflectivity of a flat sea surface
s	volume scattering-coefficient of a medium
t	time
t_i	integration time of a microwave radiometer
u	dummy variable
v	speed of propagation of an electromagnetic wave through a medium
w	wind speed
z	altitude
A	area
$\bar{A}$	area vector
A_e	effective area of an antenna
B_p	polarized intensity of radiation emitted by a blackbody
B	intensity of radiation emitted from a blackbody
C_1	constant of proportionality in Equation (128)
C_2	term defined by Equation (130)
C_3	term defined by Equation (131)
C_4	term defined by Equation (132)

D	distance from scatterer
E	radiant energy
$\vec{E}$	electric field vector
$\vec{E}_o$	initial value of the electric field vector
$\vec{E}_M$	maximum value of the instantaneous electric field vector
$\vec{H}$	magnetic field vector
$\vec{H}_o$	initial value of the magnetic field vector
$\vec{H}_M$	maximum value of the instantaneous magnetic field vector
I	specific intensity of radiation
I_h	horizontally polarized intensity of radiation
I_p	polarized intensity of radiation
I_p^c	polarized intensity of radiation coming from cosmic sources
I_p^e	polarized intensity of radiation emitted by a natural body
I_p^r	polarized intensity of radiation reflected from a natural body
I_p^{sky}	polarized intensity of radiation incident upon the surface of Earth and originating from the atmosphere
I_v	vertically polarized intensity of radiation
J_p	polarized source function
L_g	total zenith attenuation
L_R	transmissivity of an aircraft radome
M	concentration of liquid water
N	concentration of a solution in terms of normal units
P	position
$\vec{P}$	Poynting's vector
$\overline{P}$	average power radiated by an antenna per unit solid angle

P_a	power intercepted by a receiving antenna
P_A	rate of extinction of energy due to absorption by a medium
P_i	power supplied to the input terminals of a microwave receiver by its antenna system, or power supplied to the terminals of a radiating antenna
P_J	Johnson noise
P_s	rate of extinction of energy due to scattering in a medium
P_t	power transmitted to an antenna
Q_A	effective absorption cross section of a medium
Q_B	backscattering cross section of a medium
Q_S	effective scattering cross section of a medium
Q_T	total extinction cross section of a medium
R	precipitation rate
S	salinity of a solution or of sea water
T	temperature of a medium
$\overline{T}$	mean temperature of an intervening layer of atmosphere
T_G	temperature of the surface layer of atmosphere
T_m	effective radiating temperature of a natural body
T_R	temperature of an aircraft radome
T_{sea}	temperature of the active sea surface
W_i	power density of electromagnetic radiation present at some distance from a radiating microwave antenna
V	volume
Z	Greenwich Meridian Time
Z_l	impedence of air, 377 ohms
Z_i	impedence of ice

Z_L effective impedence of ice overlying water

Z_W impedence of sea water

α attenuation factor, real part of the complex propagation factor, or absorption coefficient of a medium

$\bar{\alpha}$ mean volume absorption coefficient of a layer of intervening atmosphere

α_c volume absorption coefficient of a non-raining cloud

α_d volume absorption coefficient of a cloud of water droplets

α_o integrated absorption coefficient of a natural body

α_{ox} volume absorption coefficient of molecular oxygen

α_w volume absorption coefficient of water vapor

β phase factor or imaginary part of the complex propagation factor

β_h horizontally polarized albedo of the sea surface

β_v vertically polarized albedo of the sea surface

γ_{12} the bistatic cross-section per unit area which gives the percentage of incident radiation of polarization 2 scattered as radiation of polarization 1.

δ ratio of the circumference of a spherical water droplet to the wavelength of the microwave radiation under consideration

ε' real relative permittivity of a medium

ε'' imaginary relative permittivity of a medium, imaginary part of the complex dielectric constant of a medium, or relative loss factor

ε_1 dielectric constant of medium 1

ε_2 complex dielectric constant of medium 2

ε_i complex dielectric constant of ice

ε_o permittivity of a vacuum, approximately $10^{-9}/36\pi$ farads per meter

ε_s	static relative permittivity of sea water
ε'_w	real part of the complex dielectric constant of sea water
ε_∞	relative permittivity of sea water at high frequencies assumed to be equal to 4.9
η_a	antenna efficiency factor
θ	direction angle relative to an antenna axis (see Figure 17)
θ'	angle between a given direction and the axis of an antenna
κ	index of absorption or imaginary part of the complex index of refraction of a medium
λ	wavelength of electromagnetic wave
λ_i	wavelength of electromagnetic radiation of ice
μ_o	permeability of a vacuum, 4×10^{-7} henrys per meter
ν	electromagnetic frequency
ξ_p	polarized emissivity of a natural body
π	ratio of the circumference of a plane circle to its diameter approximately 3.14159
ρ_h	horizontally polarized reflection coefficients for the electric field
ρ_v	vertical polarized reflection coefficients for the electric field
ρ_w	density of water vapor
σ	conductivity
σ_i	ionic conductivity of sea water
τ	relaxation time of sea water
τ_o	transmissivity of a natural body
ϕ	direction angle relative to an antenna axis (see Figure 17)
ψ	incidence angle, angle of observation or zenith angle

ω angular frequency of an electromagnetic wave

Γ_{12} coefficient of scattering which gives the percentage of radiation of polarization 2 scattered as radiation of polarization 1.

Θ beamwidth of an antenna in the θ-plane

Θ_M beamwidth of the main lobe of an antenna in the θ-plane

Λ optical path length

Λ_m optical path length or optical thickness of the atmosphere in the vertical

Φ beamwidth of an antenna in the ϕ-plane.

Φ_M beamwidth of the main lobe of an antenna in the ϕ-plane

T_a antenna temperature of a microwave radiometer, the temperature of a matched resister that produces a power equal to that intercepted by the antenna system of a microwave radiometer

T_i power measured by a microwave radiometer in terms of the equivalent temperature of a matched resistar; input temperature

T_N internal noise temperature of a microwave radiometer

T_p polarized brightness temperature of a natural body; used to relate an intensity of radiation to the emission of a blackbody at the same temperature

$\overline{T}_p$ mean value of the polarized brightness temperature of the sea

T_p^{air} polarized brightness temperature of radiation originating in the layer of air between an observer and the surface of Earth

T_p^c polarized brightness temperature of radiation coming from cosmic sources

T_p^e polarized brightness temperature of radiation emitted by a natural body

T_p^r polarized brightness temperature of the radiation reflected from a natural body

T_p^{sky}	polarized brightness temperature of radiation incident upon the surface of Earth and originating from the atmosphere
χ	slab thickness
Ω	solid angle
Ω_B	equivalent solid angle of the back lobes of an antenna
Ω_M	equivalent solid angle of the main lobe of an antenna
Ω_S	effective solid angle of the side lobes of an antenna

Compound Symbols

$D(\theta,\phi)$	directive gain pattern of an antenna
$G(\theta,\phi)$	gain pattern of an antenna
H-O-H	water vapor
NF	noise figure of a microwave radiometer
OH	hydroxyl molecule
$P(\theta,\phi)$	distribution of power radiated by an antenna
$\Delta\nu$	bandpass of a microwave radiometer
$\Delta\nu/c$	line-breadth constant for gaseous absorption
$\Delta\nu_d/c$	line-breadth constant for Doppler broadening
$\overline{\Delta T_i}$	root-mean-square deviation of the measured apparent input temperature
ΔT_p^e	change in the polarized emissive temperature of a flat sea surface due to a change in surface temperature from 273° K to 300° K
$\Delta\nu_z/c$	line-breadth constant for Zeeman splitting

ABBREVIATIONS

amps	ampheres
cm	centimeter
cos	cosine
°C	degrees Celsius
CO^2	carbon dioxide
db	decibel
.	grams
GHz	unit of electromagnetic frequency, 10^9 cycles per second
H_2O	water vapor
Hz	Hertz, one cycle per second
Im	operator which indicates that only the imaginary part of a complex quantity is taken
km	kilometer, 10^3 meters
°K	degrees Kelvin, unit of absolute temperature
KHz	unit of electromagnetic frequency, 10^3 cycles per second
m	(units) meter
mb	millibar
mm	millimeter
MHz	unit of electromagnetic frequency, 10^6 cycles per second
MR-62	dual-frequency microwave radiometer built by Jet Propulsion Laboratory
MR-64	dual-frequency microwave radiometer built by Jet Propulsion Laboratory
NASA	National Aeronautics and Space Administration

o/oo	unit of salinity or chlorinity, parts per thousand, grams of solute per kilogram of solution
O_2	molecular oxygen
O_3	ozone
R_e	operator which indicates that only the real part of a complex quantity is taken
sec	second
sin	sine
∇	del operator
∇A	gradient of $\vec{A}$
$\nabla^2 A$	Lapecian of $\vec{A}$
$\nabla \cdot \vec{A}$	divergence of $\vec{A}$
$\nabla \times \vec{A}$	curl of $\vec{A}$
$\lvert\vec{A}\rvert$	magnitude of $\vec{A}$
exp(A)	exponential, e^A
∞	infinity

CHAPTER I

INTRODUCTION

Nature of the Problem

Meteorological and oceanographic studies are based upon observations of the environment. Although much progress has been made during this century in the art and science of environmental observations, much of the hydrosphere and atmosphere goes unsurveyed or is inadequately surveyed. An artificial satellite in Earth orbit is a platform from which observations of phenomena on Earth can be made with unprecedented coverage, synopticity, and repetitiveness. These observations are necessarily made by remote sensors.

Although some remote sensors measure the gravitational, electrical, or magnetic force field, the vast majority of remote sensors are radiation sensors which are used to determine the distribution of the intensity of the radiational field in the vicinity of the satellite. Since this distribution is a function of interactions that have taken place between radiation and matter along the path taken by the radiant energy, scientists are able to relate the remotely sensed data to physical phenomena in the field of view of the sensor.

The citations on the following pages follow the style of the Journal of Geophysical Research.

Remote sensors may be classified as passive, active, qualitative, or quantitative. Most remote sensors are passive sensors, that is, they detect natural radiation. Sensors which provide their own illumination, such as radar sensors, are called active sensors. The difference between qualitative and quantitative remote sensors is not distinct. In general, if the output of a sensor is recorded photographically, it is a qualitative sensor. If the output of a sensor lends itself to calibration and numeration, it is a quantitative sensor.

Gases, water droplets, and other atmospheric constituents selectively absorb, scatter, and emit radiation. Scientists who desire to view surface phenomena from satellites select frequency domains in the electromagnetic spectrum (Figure 1) of maximum atmospheric transparency. These domains are called atmospheric 'windows' and are listed in Table I. These 'windows' are neither completely transparent nor sharply bound. The optical and infrared windows become opaque when clouds are in the field of view. The upper end of the radio window may become opaque over raining clouds. Some scientists may desire to study certain atmospheric phenomena using non-window regions.

In 1931, thermal radiation was first detected at radio frequencies from extra-terrestrial sources (for example, the Milky Way Galaxy) using a crude radio receiver operating at 20.5 MHz[1]

---

[1]MHz = 10^6 cycles per second (one mega-Hertz).

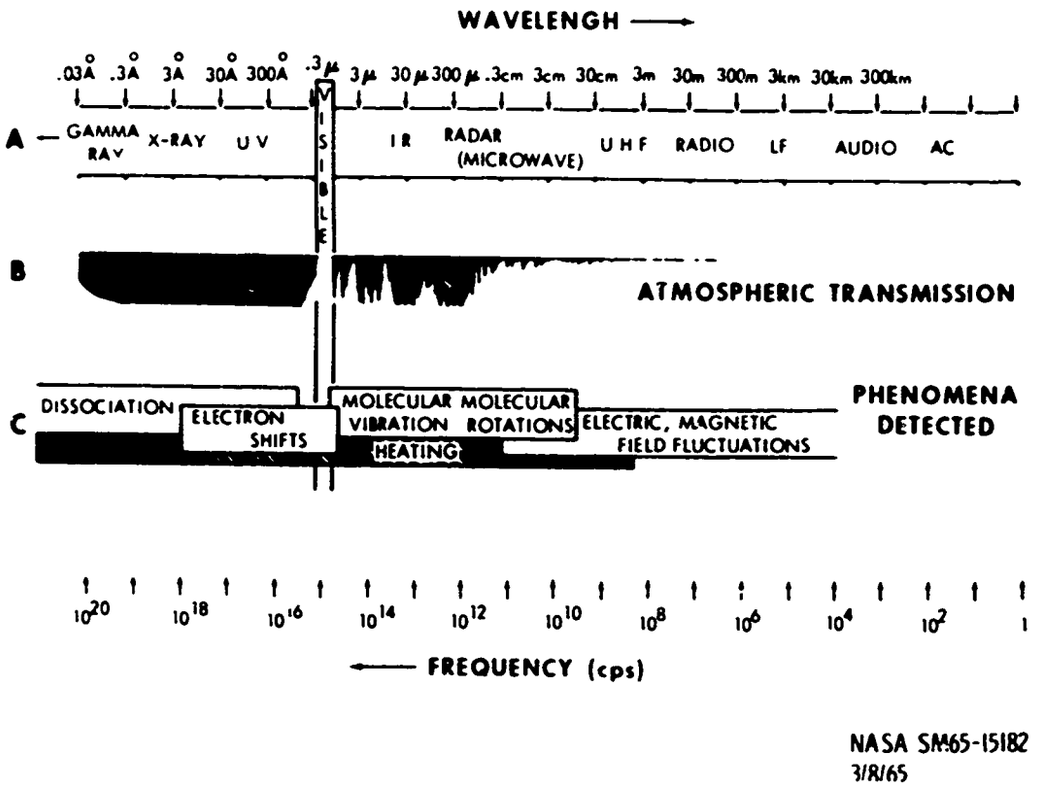

Figure 1. The electromagnetic spectrum.

Table I

Atmospheric windows in the electromagnetic spectrum

Window	Wavelength, λ	Atmospheric Gases That Absorb Radiation at the Boundaries of the Window*		Comments****
		Upper	Lower	
Optical	0.4 - 1.0 microns	All gases**	H_2O	
Near infrared	2.0 - 2.3 microns	H_2O	H_2O, CO_2	
Near infrared	3.6 - 4.0 microns	H_2O, CO_2	All gases**	
Thermal infrared	8 - 12.5 microns	All gases**	CO_2, H_2O	O_3 band (9.5 - 10 microns)
Radio	8 mm - 15 meters	O_2	Ions***	H_2O band (1.2 - 1.5 cm)

*Boundaries are not exact and are due mainly to gases listed.

**Includes only active gases and molecules.

***Ions vary in strength and number and are located in ionosphere

****Additional bands of absorption within general window region [illegible]sted.

and 30 MHz. Highly sensitive radio receivers and highly directional radio antennas were being developed. This research, coupled with intensive studies of the absorption and scattering properties of atmospheric gases and water droplets for radar propagation, led to the development of radio astronomy. Microwave radiometry evolved from the science of radio astronomy.

A microwave radiometer is a quantitative, passive remote sensor that makes precise measurements of the intensity of thermal radiation at microwave frequencies. Early receivers in microwave radiometry suffered mostly from unsteady amplification. Dicke (1946) proposed a technique to lessen errors in measurements of microwave radiance due to amplification fluctuations. By switching rapidly from the power received by the antenna system to the known power of an internal source, he was able to reduce the effect of amplification drift.

Much of the scientific community in remote sensing is presently interested in possible meteorological and oceanographic applications of radiometric measurements at microwave frequencies from spacecraft and aircraft.

The purpose of this study is to review comprehensively past developments related to microwave radiometry and to present them in a manner understandable to oceanographers and meteorologists who desire to use this remote sensor as a tool in their research.

Past Studies

During World War II, many investigations were made into problems of propagation of radar waves in the atmosphere. After the war, the results of these investigations appeared in scientific publications for the first time. Of concern to microwave radiometry are papers dealing with the absorption and scattering processes in the atmosphere, the emission of the sea surface, the electrical properties of water, and developments in the engineering of microwave radiometers.

Mie (1908) formulated the complete theory of scattering and absorption of electromagnetic waves by a homogenous dielectric sphere. Stratton (1930) computed values of attenuation in uniform clouds of water droplets using the Mie theory; however, he erroneously assumed that the imaginary part of the complex index of refraction (and hence the absorption) was zero. Franz (1940) correctly computed the attenuation of microwaves in fog; but, he did not consider rain droplets or ice crystals. Using the experimentally determined values of the complex dielectric constant of water by Saxton and Lane (1946) and the complex dielectric constant of ice by Dunsmuir and Lamb (1945), Ryde (1946) computed the absorption and scattering of microwaves by fog, cloud, rain, hail, and snow using the Mie theory as developed by Stratton (1941). He assumed the distribution of drop sizes given by Laws and Parsons (1943). Goldstein (1951) elaborated on Ryde's work. Aden and

Kerker (1951) extended the Mie theory to concentric spheres of homogeneous dielectric materials. Gunn and East (1954) presented a very complete treatment of absorption of microwaves by fogs, rain, atmospheric gases, clouds, hail, and ice. This work summarized all previous investigations and updated Ryde's calculations. Imai (1957) determined the absorption and scattering coefficients of rain drops to a great degree of accuracy. Using Aden's method for Mie theory, Stephens (1961) computed the attenuation coefficient of water droplets.

Buettner (1963, 1965) suggested that the microwave emission of a cloud could be related to its distribution of liquid water. Cummings and Hull (1966) observed large increases in sky radiance under various cloud and rain conditions and confirmed the predictions of Buettner. An increase in the intensity of upwelling radiation was observed over marine clouds during flight tests of a scanning microwave radiometer operating at 19.35 GHz over the Gulf of Mexico (Catoe et al., 1967). Kreiss (1968) computed theoretical values of the intensity of upwelling microwave radiation over clouds of various thicknesses, heights, and concentrations of liquid water. Using microwave radiometers from the ground, Decker and Dutton (1968) determined the distribution of liquid water in thunderstorms over Colorado.

Van Vleck (1947a, 1947b, 1951a), and Van Vleck and Weisskopf (1945) determined the absorption of microwaves by molecular oxygen and water vapor from quantum theory. This outstanding

work stands essentially unaltered to the present day except for a correction for microwave absorption by pressure-broadened absorption-lines in the infrared spectrum (Figure 1) of water vapor (Becker and Autler, 1946).

The absorption by molecular oxygen for wavelengths near 5 millimeters has received much attention lately. Meeks and Lilley (1963) proposed that the microwave emission from molecular oxygen in the vicinity of 5 mm could be used to determine the distribution of air temperature with height. Westwater (1965) determined profiles of air temperature by inverting measurements of the microwave radiance of the sky from ground-based microwave radiometers. A discussion of present efforts being made to invert microwave measurements of oxygen emission in the atmosphere to obtain temperature profiles in the atmosphere will not be included in this paper. One may determine the present state of these efforts by referring to Gille (1968).

The absorption by water vapor in the atmosphere is much greater than that by molecular oxygen near wavelengths of 1.35 centimeters (Van Vleck, 1947b). Thus, it should be possible to obtain information about the distribution of water vapor in the atmosphere from microwave measurements. Barrett and Chung (1962), and Staelin (1966) have studied these possibilities.

The microwave emission and reflection of the sea surface has been studied by many investigators. The reflection and emission of homogenous, flat dielectrics is well known (Jordan, 1950).

Peake (1959) defined the problem of scattering and emission from homogenous dielectrics having an irregular surface and used various models of roughness to compute the emission of various land surfaces (Chen and Peake, 1961). The theory for a smooth multi-layer dielectric was used by Pascalar and Sakamoto (1965) to compute the emission and reflection of ice sheets over water. Barath (1965) and Mardon (1965) suggested that measurements of ice distribution, ice thickness, water temperature, and sea state could be made from aloft using microwave radiometers. McAlister and McLeish (1965) proposed a method whereby the total vertical heat flow from the ocean's surface could be determined by dual-frequency microwave radiometers. Conway and Sakamoto (1965) reported on measurements of microwave radiance of various terrestrial objects at 13, 18, 35, and 70 GHz[2]. Stogryn (1967) used the Kirchhoff Approximation and the distribution of wave slopes obtained by Cox and Munk (1954a, 1954b) to determine the effects of sea state on microwave radiance of the sea at 19.4 GHz and 35 GHz.

In 1967, the U.S. Coast Guard began to use microwave scanners over the North Atlantic Ocean to detect icebergs through fog (Roeder, 1967). Sirounian (1968) and Paris (1968) determined the effect of salinity on microwave radiance at 3 GHz. Williams (1968) showed that microwave emission of foam greatly exceeds that of a

---

[2]GHz = 10^9 cycles per second (one giga-Hertz).

smooth sea surface.

Recently, measurements of microwave radiance over the Gulf of Mexico over large ranges of temperatures, salinities, and concentrations of liquid water have been furnished to the author by Blinn (1967a), Nordberg (personal communication, 1968), and the Manned Spacecraft Center. These data were taken by the MR-62 and MR-64 microwave radiometers (Blinn, 1967a) at 9.3, 15.8, 22.235, and 34.0 GHz and by a scanning 19.35 GHz microwave radiometer built by Aerojet General Corportation (Catoe et al., 1967; Tobin, 1967).

The only microwave radiometer that has been flown in a spacecraft is one dual-frequency microwave radiometer (model MR-62) carried by the Mariner II spacecraft on the Venus mission (Barath et al., 1964; Glasstone, 1965).

Although many aspects of applied microwave radiometry have been adequately considered by the above investigators, no presentation of microwave radiometry exists in the literature which comprehensively considers the total effects of water temperature, water salinity, surface roughness, foam, absorption and emission by atmospheric gases, fogs, clouds, and rain on microwave radiometric measurements.

In addition to the physical theory of microwave emission and extinction in the ocean and atmosphere, one must be aware of the capabilities and limitations of the radiometric instruments. Dicke (1946), Bracewell (1962), Ko (1964), and Barath (1967) fully

discuss these factors. Also, since microwave radiometers are very sensitive instruments and since man-made sources of microwave radiation may be many times more intense than natural sources of microwave radiation, scientists must use frequencies void of man-made interferences. In 1964, certain frequencies were set aside for use by radio astronomers. These radio astronomy bands are shown in Table II (Smith-Rose, 1964).

Table II. Microwave bands reserved for radio astronomy (after Smith-Rose, 1964).

Frequency band (GHz)	Allocations
1.4 - 1.427 (hydrogen line)	Exclusive world-wide
1.66 - 1.69 (OH line)	secondary (primary:
2.69 - 2.70	meteorological satellites
3.165 - 3.195	exclusive world-wide).
4.8 - 4.81	
4.99 - 5.00	
5.8 - 5.815	
8.68 - 8.70	
10.68 - 10.70	
15.35 - 15.4	
19.3 - 19.4	
31.3 - 31.5	
33 - 33.4	
33.4 - 34.0	Europe, Cuba and India
36.5 - 37.5	

Objective and Scope

The objective of this study is to review comprehensively past and present activities in microwave radiometry as they are related to marine applications. The development of certain physical and engineering concepts will be presented in a rigorous manner so that the nature of the simplifying assumptions can be

fully understood. This theory will be compared to measurements when appropriate and available.

The purposes of this review are to lay a firm foundation for future research in specific areas of concern to microwave radiometry and hopefully, to engender interest among other environmental scientists who may be able to use microwave radiometers as a tool in their research.

Since the problem of determining the vertical distribution of air temperature by inverting microwave measurements of oxygen emission is separate from all other aspects of applied microwave radiometry, it will not be included in the scope of this paper.

The main interests of this study, as far as applications are concerned, are techniques that are being developed for marine environmental measurements.

In Chapter II the fundamental concepts of the electrical and magnetic properties of water, ice, and air are defined; practical expressions are developed for the complex dielectric constant of water as a function of its temperature, its salinity, and the frequency of observation.

The fundamental problem of radiative transfer is discussed in Chapter III, and certain aspects of radiation in general are discussed. The concept of brightness temperature is introduced.

In Chapter IV, the extinction and emission processes in the atmosphere are discussed, and the equation of transfer is solved for various meteorological conditions.

The emission and scattering by the hydrosphere is determined in Chapter V for various conditions.

The results of Chapter IV and V are combined in Chapter VI to give expressions for the intensity of the upwelling radiation as a function of altitude, frequency, polarization, angle, and physical state.

Internal and external aspects of microwave radiometers are discussed in Chapter VII, and the effect of instrument characteristics on the measured flux of upwelling microwave radiation is determined.

Available measurements of microwave radiance are compared to theoretical values in Chapter VIII, and conclusions and recommendations are made in Chapter IX.

CHAPTER II

ELECTRIC AND MAGNETIC PROPERTIES OF MATTER

Maxwell's Equations

Maxwell (1892) generalized the laws of Ampere, Faraday, and Gauss into a set of electromagnetic field equations which can be used to describe the macroscopic properties of matter. Maxwell's equations for a chargeless medium may be expressed in the Giorgi[3] (1901) systems of units as follows:

$$\nabla \cdot \vec{E} = 0 \qquad \text{(volts/m}^2\text{)}. \qquad (1)$$

$$\nabla \cdot \vec{H} = 0 \qquad \text{(amps/m}^2\text{)}. \qquad (2)$$

$$\nabla \times \vec{E} = -\mu_o \frac{\partial \vec{H}}{\partial t} \qquad \text{(volts/m}^2\text{)}. \qquad (3)$$

$$\nabla \times \vec{H} = \sigma\vec{E} + \varepsilon'\varepsilon_o \frac{\partial \vec{E}}{\partial t} \qquad \text{(amps/m}^2\text{)}. \qquad (4)$$

$\vec{E}$ is the electric field vector (volts per meter), $\vec{H}$ is the magnetic field vector (amperes per meter), μ_o is the permeability (Henrys per meter) of a vacuum, t is time (seconds), σ is the conductivity (mhos per meter), ε' is the real relative permittivity (dimensionless), and ε_o is the permittivity (farads per meter) of a vacuum. By international consent μ_o is $4\pi \times 10^{-7}$ henrys per meter. It is assumed that the permeability of all mediums discussed in this paper is μ_o. ε_o is approximately $10^{-9}/36\pi$ farads

[3]The Giorgi system or rationalized MKS system of units uses the basic units: meter, kilogram, second, and coulomb.

per meter (Von Hippel, 1954).

It is assumed that all components of $\vec{E}$ and $\vec{H}$ are sinusoidal in nature, that is,

$$\vec{E} = \vec{E}_m \exp(j\omega t) \quad \text{(volts/m)}, \qquad (5)$$

and

$$\vec{H} = \vec{H}_m \exp(j\omega t) \quad \text{(amps/m)}, \qquad (6)$$

where $\vec{H}_m$ and $\vec{E}_m$ are the maximum values of $\vec{H}$ and $\vec{E}$, respectively, ω is the angular frequency (radians per second), and $j = \sqrt{-1}$.

According to Von Hippel, σ represents an effective conductivity which includes all dissipative effects. The customary approach has been to define a relative loss factor, ε'', such that

$$\sigma = \omega\varepsilon_o\varepsilon'' \quad \text{(mhos/m)}. \qquad (7)$$

Substitution of (5) and (7) into (4) gives:

$$\nabla \times \vec{H} = (\omega\varepsilon_o\varepsilon'' + j\omega\varepsilon'\varepsilon_o)\vec{E}$$

$$= j\omega\varepsilon_o(\varepsilon' - j\varepsilon'')\vec{E}$$

$$= \varepsilon_o(\varepsilon' - j\varepsilon'')\frac{\partial\vec{E}}{\partial t} \quad \text{(amps/m)}. \qquad (8)$$

Complex Dielectric Constant

Theory

The parenthetical expression in (8) is dimensionless and is

called the complex dielectric constant of the medium. According to Sucher and Fox (1963), ε' is associated with the ability of a material to store electric energy, and ε'' is associated with the losses that occur in the material. These losses include viscous dissipation of energy in polar liquids as well as ohmic losses. The curl of (3) is:

$$\nabla \times (\nabla \times \vec{E}) = -\mu_o \nabla \times \frac{\partial \vec{H}}{\partial t}$$

$$= -\mu_o \partial(\nabla \times \vec{H})/\partial t \qquad \text{(volts/m}^3\text{)}. \qquad (9)$$

By the use of a vector identity and (8), (9) becomes:

$$\nabla(\nabla \cdot \vec{E}) - \nabla^2 \vec{E} = -\mu_o \varepsilon_o (\varepsilon' - j\varepsilon'') \frac{\partial^2 E}{\partial t^2} \qquad \text{(volts/m}^3\text{)}. \qquad (10)$$

Since $\nabla \cdot \vec{E}$ is zero by (1),

$$\nabla^2 \vec{E} = \mu_o \varepsilon_o (\varepsilon' - j\varepsilon'') \frac{\partial^2 \vec{E}}{\partial t^2} \qquad \text{(volts/m}^3\text{)}. \qquad (11)$$

Also, the curl of (8) is:

$$\nabla \times (\nabla \times \vec{H}) = \varepsilon_o (\varepsilon' - j\varepsilon'') \partial(\nabla \times \vec{E})/\partial t \qquad \text{(amps/m}^3\text{)}. \qquad (12)$$

By the use of a vector identity and (3), (12) becomes:

$$\nabla(\nabla \cdot \vec{H}) - \nabla^2 \vec{H} = -\mu_o \varepsilon_o (\varepsilon' - j\varepsilon'') \frac{\partial^2 H}{\partial t^2} \qquad \text{(amps/m}^3\text{)}. \qquad (13)$$

Since $\nabla \cdot \vec{H}$ is zero by (2),

$$\nabla^2 \vec{H} = \mu_o \varepsilon_o (\varepsilon' - j\varepsilon'') \frac{\partial^2 H}{\partial t^2} \qquad \text{(amps/m}^3\text{)}. \qquad (14)$$

Equations (11) and (14) are the wave equations of the electromagnetic field in a chargeless medium having permeability equal to μ_c.

Without loss of generality one may assume that the electromagnetic wave described by (11) and (14) is traveling along an x-axis in space and is a plane wave. Thus,

$$\frac{\partial \vec{E}}{\partial y} = \frac{\partial \vec{E}}{\partial z} = \frac{\partial \vec{H}}{\partial y} = \frac{\partial \vec{H}}{\partial z} = 0, \tag{15}$$

and (11) and (14) reduce to:

$$\frac{\partial^2 \vec{E}}{\partial x^2} = \mu_o \epsilon_o (\epsilon' - j\epsilon'') \frac{\partial^2 \vec{E}}{\partial t^2} \quad \text{(volts/m}^3\text{)}, \tag{16}$$

and

$$\frac{\partial^2 \vec{H}}{\partial x^2} = \mu_o \epsilon_o (\epsilon' - j\epsilon'') \frac{\partial^2 \vec{H}}{\partial t^2} \quad \text{(amps/m}^3\text{)}, \tag{17}$$

respectively.

A set of solutions to (16) and (17) according to Ramo, et al., (1965) is:

$$\vec{E} = \vec{E}_o \exp(-\alpha x) \exp(-j\beta x) \quad \text{(volts/m)}, \tag{18}$$

and

$$\vec{H} = \vec{H}_o \exp(-\alpha x) \exp(-j\beta x) \quad \text{(amps/m)}. \tag{19}$$

$\vec{E}_o$ and $\vec{H}_o$ are initial values of $\vec{E}$ and $\vec{H}$, respectively, where:

$$\alpha = \omega \sqrt{(\mu_o \varepsilon_o \varepsilon'/2)\ \sqrt{1 + (\varepsilon''/\varepsilon')^2} - 1} \quad \text{(nepers)}^4, \quad (20)$$

and

$$\beta = \omega \sqrt{(\mu_o \varepsilon_o \varepsilon'/2)\ \sqrt{1 + (\varepsilon''/\varepsilon')^2} + 1} \quad \text{(nepers)}. \quad (21)$$

α is the attenuation factor (nepers), and β is the phase factor (nepers).

If ε'' is zero (and hence the medium is lossless), α is zero, and

$$\beta = \omega \sqrt{\mu_o \varepsilon_o \varepsilon'} \quad \text{(nepers)}. \quad (22)$$

Since the form of (16) and (17) is that of a wave traveling at velocity v (meter)

$$v = 1/\sqrt{\mu_o \varepsilon_o (\varepsilon' - j\varepsilon'')} \quad \text{(m/sec)}, \quad (23)$$

and since the index of refraction, m, is defined as:

$$m = c/v \quad \text{(dimensionless)}, \quad (24)$$

then:

$$m^2 = \varepsilon' - j\varepsilon'' \quad \text{(dimensionless)}. \quad (25)$$

c is the speed of propagation of electromagnetic energy in a vacuum and is given by: (26)

$$c = 1/\sqrt{\mu_o \varepsilon_o} \quad \text{(m/sec)}. \quad (26)$$

---

[4] A neper is an engineering unit which means per meter.

m is complex and may be defined as:

$$m = n + j\kappa \quad \text{(dimensionless)}. \tag{27}$$

n is the real index of refraction, and κ is the index of absorption.

From (25) and (27) we derive the relations:

$$\varepsilon' = n^2 - \kappa^2 \quad \text{(dimensionless)}, \tag{28}$$

and

$$\varepsilon'' = 2n\kappa \quad \text{(dimensionless)}. \tag{29}$$

Since it has been assumed that the permeability of all matter under study is equal to μ_o, it is only necessary to know ε' and ε'' as a function of frequency, temperature, and physical state to completely describe the electric and magnetic properties of the matter in question.

Debye (1929) suggested that the complex dielectric constant of a polar liquid such as water, could be expressed as:

$$\begin{aligned} \varepsilon' - j\varepsilon'' &= \varepsilon_\infty + (\varepsilon_s - \varepsilon_\infty)/(1 + j\omega\tau) \\ &= [\varepsilon_\infty + (\varepsilon_s - \varepsilon_\infty)/(1 + \omega^2\tau^2) \\ &\quad - j\,[(\varepsilon_s - \varepsilon_\infty)\omega\tau/(1 + \omega^2\tau^2)] \quad \text{(dimensionless)}. \end{aligned} \tag{30}$$

ε_s is the static relative permittivity, τ is the relaxation time (seconds) and ε_∞ is the relative permittivity at high frequencies. In reality, ε_∞ varies with frequency and physical state; however, since (3) is to be used only for radio and microwave frequencies, a constant value is assumed for ε_∞. In general, ε_s and τ are functions of the physical state but not of the frequency.

Lane and Saxton (1951, 1952; Saxton and Lane, 1946; Saxton and Lane, 1952), Saxton (1946a, 1946b, 1946c, 1951) and Collie, et al., (1947) have studied the electric properties of liquid water with and without sodium choloride in solution. Measurements have been made of ε' and ε'' by these investigators for frequencies of 3, 9.4, 10, 18, 24, 24.2, and 48.5 GHz, for temperatures ranging from -8° C to 50° C, and for concentrations of sodium chloride ranging up to 3N. These measurements indicate that (30) is valid for water having concentrations of sodium chloride in solution (Lane and Saxton, 1952).

The relative loss factor is quite appreciable in pure water even though the ionic conductivity of pure water is quite small. This fact indicates the importance of losses due to viscous dissipation known as Debye relaxation. The addition of sodium chloride slightly affects losses due to viscous dissipation and, of course, introduces additional losses due to the ionic conductivity as the result of the sodium and chloride ions present. It has been customary to separate these two mechanisms of loss by introducing an additional factor into the expression for ε''.

From (30), it follows that:

$$\varepsilon' = \varepsilon_\infty + (\varepsilon_s - \varepsilon_\infty)/(1 + \omega^2\tau^2) \qquad \text{(dimensionless)}, \qquad (31)$$

and

$$\varepsilon'' = \omega\tau(\varepsilon_s - \varepsilon_\infty)/(1 + \omega^2\tau^2) \qquad \text{(dimensionless)}. \qquad (32)$$

Now it is assumed that (31) and (32) are valid for pure water where ε_s and τ are functions of temperature, T, (degrees Kelvin). In the case of salt water, it can be assumed (Lane and Saxton, 1952) that:

$$\varepsilon' = \varepsilon_\infty + (\varepsilon_s - \varepsilon_\infty)/(1 + \omega^2\tau^2) \qquad \text{(dimensionless)}, \qquad (33)$$

and

$$\varepsilon'' = \omega\tau(\varepsilon_s - \varepsilon_\infty)/(1 + \omega^2\tau^2) + \sigma_i/\omega\varepsilon_0 \quad \text{(dimensionless)} \qquad (34)$$

where σ_i is the ionic conductivity of the solution (mhos per meter).

In Lane's and Saxton's papers, electrostatic units are used for ε and σ_i. Also, ε' and ε'' are the real and imaginary parts of the complex permittivity which are numerically equal to the real and imaginary parts of the dielectric constant used in this study.

In (33) and (34), ε_s, τ, and σ_i are functions of temperature and salinity only.

There now arises a problem concerning the salt concentration of a solution of pure water and sodium chloride and the salt concentration of ocean water. All previous measurements of the effects of salts in solution on the dielectric properties of water have been made using only sodium chloride. Ocean water, on the other hand, has many types of salts in solution. Table III lists the salt constituents most abundantly found in sea water and gives their percent contribution by weight (McLellan, 1965).

Table III. Principal ionic constituents of sea water (34.4 o/oo salinity) (after McLellan, 1965).

Species	Amount (g) per kg of solution	Molecular or atomic weight*	Percentage of total salt
Cations:			
Sodium	10.47	22.997	30.4
Magnesium	1.28	24.32	3.7
Calcium	0.41	40.08	1.2
Potassium	0.38	39.096	1.1
Strontium	0.013	87.63	0.05
Anions:			
Chloride	18.97	25.457	55.2
Sulfate	2.65	32.06**	7.7
Bromide	0.065	79.916	0.2
Bicarbonate	0.14	------	0.4
Borate	0.027	10.82	0.08

*D. Van Nostrand Company, Inc. (1958).
**Value for sulfur.

From Table II, one sees that 85.6 percent of the total dissolved salts are sodium and chloride. The mean molecular weight of sodium chloride in sea water is 31.0. The mean molecular weight of all cations and anions listed in Table III is 31.2. Based on this fact, it is assumed that a solution of sodium chloride and water approximates sea water as far as its electrical properties are concerned.

According to McLellan (1965) the chlorinity of a solution is the total amount of chlorine, bromine, and iodine in grams contained in one kilogram of sea water assuming the bromine and iodine

to be replaced by chlorine. Assuming that the relative proportions of the major constituents of sea water remain constant, one may relate the salinity of sea water to its chlorinity by the following expression (Cochrane, personal communication, 1967):

$$\text{salinity} = 1.80655 \times \text{chlorinity (o/oo)}. \qquad (35)$$

Practical treatment

Lane and Saxton (1952) have determined values of ε_∞, ε_s, and τ at specific values of temperatures and concentrations. They expressed concentration in terms of normal solutions. A solution that has a normality of unity contains one gram-equivalent-molecular-weight of dissolved substance per liter of solution (Chemical Rubber Co., 1959). Since the valences of sodium and chloride are unity, one normal solution contains 58.454 grams of sodium chloride per liter. The mass of one liter of solution is a function of its temperature, the pressure and the percentage of solute by weight.

The salinity of a solution may be defined as the total amount of solid material in grams contained in one kilogram of solution when all carbonate has been converted to oxide, the bromine and iodine are replaced by chlorine, and all organic matter oxidized (McLellan, 1965). This definition was formulated for sea water; it applies to sodium chloride and water. Thus, one may express the percentage of solute by weight as a salinity.

Table IV gives the specific gravity of solutions of sodium chloride and water as a function of temperature and salinity at one atmosphere of pressure (Chemical Rubber Co., 1959).

Table IV. Specific gravity of solution of sodium chloride and water as a function of temperature and salinity at one atmosphere of pressure.

Salinity, S (o/oo)	Temperature, T(°C) -8	0	4	10	20	30
0	0.99869	0.99987	1.0000	0.99973	0.99823	0.99567
10	--	--	1.0053	--	--	--
20	--	--	1.0125	--	--	--
30	--	--	--	--	--	--
40	--	--	1.0268	--	--	--

Since, in some cases, the specific gravity in Table IV is below unity, and, in some cases, it is above unity, it is assumed that the specific gravity of a solution of sodium chloride and water is approximately unity. Thus there are approximately 58.45 grams of sodium chloride per kilogram of solution for a one-normal solution, that is:

$$S = 58.45N \quad (o/oo), \tag{35}$$

where N is the concentration of the solution expressed in terms of normality.

Table V gives values of σ_s, τ, and σ_i as a function of temperature and salinity from measurement made by Saxton and Lane (1952).

Table V. Static relative permittivity (ε_s), relaxation time (τ, seconds) and ionic conductivity (σ_i, mhos per meter) of a solution of sodium chloride and water for specific values of temperature (T, °C) and salinity (S, o/oo) (after Saxton and Lane, 1952).

T	Parameter	S = 0 o/oo	S = 29.2 o/oo	S = 58.4 o/oo	S = 87.6 o/oo
0° C	ε_s	88	77	69	62
	τ	18.7×10^{-12} sec.	17.1×10^{-12} sec.	16.4×10^{-12} sec.	15.3×10^{-12} sec.
	σ_i	0.0 mho/m	2.4 mho/m	4.8 mho/m	6.1 mho/m
10° C	ε_s	84	74	66	60
	τ	13.6×10^{-12} sec.	12.2×10^{-12} sec.	11.8×10^{-12} sec.	11.3×10^{-12} sec.
	σ_i	0.0 mho/m	3.4 mho/m	6.2 mho/m	10.8 mho/m
20° C	ε_s	80	71	63	57
	τ	10.1×10^{-12} sec.	9.2×10^{-12} sec.	9.0×10^{-12} sec.	8.7×10^{-12} sec.
	σ_i	0.0 mho/m	4.4 mho/m	7.7 mho/m	10.8 mho/m
30° C	ε_s	77	68	60	55
	τ	7.5×10^{-12} sec.	7.2×10^{-12} sec.	7.1×10^{-12} sec.	6.9×10^{-12} sec.
	σ_i	0.0 mho/m	5.2 mho/m	9.2 mho/m	13.0 mho/m
40° C	ε_s	73	65	58	52
	τ	5.9×10^{-12} sec.	5.7×10^{-12} sec.	5.6×10^{-12} sec.	5.5×10^{-12} sec.
	σ_i	0.0 mho/m	6.2 mho/m	10.8 mho/m	15.1 mho/m

Using the values of ε_s, τ, and σ_i given in Table V, Huebner and McGraw of Texas A&M University formed a set of second order regression equations in temperature (T, °C) and salinity (S, o/oo) to express σ_i, ε_s, and τ. These expressions are as follows:

$$\sigma_i(T,S) = (0.08533905)S - (0.000135394)S^2 + (0.004047859111)T + (0.0000277351188)T^2 + (0.03255122)ST - (0.00000733296722)S^2T + (0.0000000549132477)S^2T^2 - (0.00000883166144)ST^2 \quad \text{(mhos/m)}. \quad (36)$$

$$\varepsilon_s(T,S) = 87.336049 - (0.34438426)S + (0.00063045524)S^2 - (0.39006802)T + (0.00068027202)T^2 + (0.0023219662)ST - (0.0000098371722)S^2T + (0.0000000995366511)S^2T^2 - (0.000012220872)ST^2 \quad \text{(dimensionless)}. \quad (37)$$

$$\tau(T,S) = 18.494012 - (0.04522073)S + (0.000082162302)S^2 - (0.54708843)T + (0.0058367346)T^2 + (0.0017348405)ST - (0.0000027579928)S^2T^2 + (0.000173711)ST^2 \text{ (sec)}. \quad (38)$$

ε_∞ is assumed to be 4.9 (Lane and Saxton, 1952).

Values of ε_s and τ determined by Collie, et al. (1948) and Hasted (1961) are very close to those given in Table V.

Electric and magnetic properties of water

The permeability of water is μ_o (4 x 10^{-7} henrys per meter) (Lane and Saxton, 1951).

Equations (36), (37) and (38) can be used together with (33) and (34) to generate values of ε' and ε'' as a function of T, S, and ν. The results are shown in Table VI.

To illustrate the variations of ε' and ε'' with temperature, salinity, and frequency, Figures 2 and 3, adapted from Saxton and Lane (1952), are presented. The salinity of 'sea water' is assumed to be 36 o/oo. The salinity of 'fresh water' is such that its ionic conductivity is about 0.01 mho per meter. The salinity of pure water is zero. Values of ε' and ε'' are plotted against frequncy for 'pure', 'fresh' and 'sea water' at 0° C and 20° C. Note that these values are identical for frequencies greater than about 10 GHz.

It will be shown later that the emissivity and reflectivity of sea water depend on its complex dielectric constant, incidence angle, polarization, and the nature of the shape of the air-sea interface. Thus, it is useful at this time to make some general comments on the behavior of the complex dielectric constant of sea water as a function of its temperature, salinity, and frequency of observation.

For all the frequencies chosen, ε' and ε'' are dependent on the temperature and salinity of the water. The dependence on salinity is very slight except for the 3 GHz radiation. ε' appears to be fairly steady with temperature at 3 GHz but increases with temperature at the other frequencies. ε'' decreases with temperature at 3 GHz and 9.3 GHz, remains steady with temperature

Table VI. Calculated values of ε' and ε'' for selected values of temperature (T, °C), salinity (S, o/oo), and frequency (ν, GHz).

Frequency = 3 GHz

T \ S	0 o/oo		10 o/oo		20 o/oo		30 o/oo		40 o/oo	
°C	ε'	ε''	ε'	ε''	ε'	ε''	ε'	ε''	ε'	ε''
0	78.4	25.6	75.8	29.1	73.2	32.6	70.7	36.0	68.2	39.2
5	78.8	22.3	76.0	26.9	73.4	31.5	70.8	35.9	68.3	40.2
10	78.7	19.2	75.9	25.0	73.2	30.6	70.5	36.0	68.0	41.3
15	78.1	16.4	75.3	23.3	72.6	29.9	70.0	36.4	67.4	42.5
20	77.3	14.1	74.5	22.0	71.8	29.6	69.1	37.0	66.6	44.1
25	76.2	12.1	73.4	21.0	70.7	29.6	68.1	37.8	65.6	45.8
30	74.9	10.6	72.2	20.4	69.5	29.9	67.0	39.0	64.5	47.8
				Frequency = 9.3 GHz						
0	42.9	41.1	42.3	41.1	41.7	41.1	41.0	41.1	40.3	41.0
5	48.1	40.2	47.2	40.4	46.2	40.6	45.4	40.8	44.5	41.0
10	53.1	38.4	51.9	38.9	50.7	39.3	49.5	39.8	43.3	40.2
15	57.5	35.8	56.0	36.6	54.5	37.4	53.0	38.2	51.5	38.9
20	61.1	32.6	59.3	33.9	57.5	35.0	55.8	36.2	54.1	37.3
25	63.6	29.3	61.6	30.9	59.7	32.6	57.7	34.1	55.9	36.6
30	65.2	26.1	63.0	28.9	60.9	30.3	58.8	32.2	56.8	34.1

Table VI (con't.)

Frequency = 15.8 GHz

S / T	0 o/oo		10 o/oo		20 o/oo		30 o/oo		40 o/oo	
°C	ε'	ε"	ε'	ε"	ε'	ε"	ε'	ε"	ε'	ε"
0	23.8	34.6	23.7	34.6	23.6	34.5	23.4	34.5	23.3	34.4
5	27.9	36.4	27.7	36.4	27.5	36.4	27.3	36.3	27.0	36.2
10	32.7	37.6	32.3	37.7	32.0	37.6	31.5	37.6	31.1	37.5
15	37.9	38.1	37.3	38.1	36.6	38.1	36.0	38.1	35.3	38.1
20	43.1	37.5	42.2	37.7	41.3	37.8	40.3	37.9	39.4	38.0
25	47.8	36.1	46.6	36.4	45.4	36.7	44.4	36.9	43.0	37.2
30	51.5	34.1	50.1	34.6	48.6	35.1	47.2	35.6	45.8	36.0

Frequency = 19.35 GHz

0	18.5	30.6	[illegible].5	30.6	18.5	30.6	18.4	30.5	18.4	30.5
5	21.9	32.9	21.8	32.9	21.7	32.9	21.6	32.8	21.4	32.7
10	25.9	34.8	25.7	34.8	25.5	34.8	25.6	34.7	25.0	34.7
15	30.6	36.3	30.2	36.2	29.8	36.2	29.4	36.1	28.9	36.0
20	35.5	36.9	34.9	36.9	34.3	36.9	33.7	36.8	33.0	36.7
25	40.4	36.6	39.5	36.7	38.6	36.7	37.7	36.7	36.8	36.7
30	44.6	35.6	.5	35.7	42.3	35.9	41.2	36.0	40.0	36.1

Table VI (con't.)

Frequency = 22.235 GHz

T °C \ S	0 o/oo		10 o/oo		20 o/oo		30 o/oo		40 o/oo	
	ε'	ε"	ε'	ε"	ε'	ε"	ε'	ε"	ε'	ε"
0	15.6	27.7	15.6	27.8	15.6	27.8	15.6	27.7	15.6	27.7
5	18.5	30.1	18.4	30.2	18.4	30.2	18.3	30.1	18.2	30.1
10	21.9	32.4	21.8	32.4	21.7	32.4	21.5	32.3	21.3	32.8
15	26.1	34.3	25.8	34.3	25.5	34.2	25.2	34.1	24.9	34.0
20	30.7	35.7	30.2	35.6	29.7	35.5	28.3	35.4	28.7	35.3
25	35 4	36.1	34.7	36.1	34.0	36.0	33.3	35.9	32.5	35.8
30	39.7	35.8	38.7	35.8	37.8	35.8	36.8	35.7	35.9	35.7

Frequency = 34.0 GHz

0	9.9	19.6	9.9	19.7	9.9	19.7	9.9	19.7	9.9	19.7
5	11.3	21.8	11.3	21.9	11.3	21.9	11.3	21.9	11.3	21.9
10	13.2	24.2	13.2	24.2	13.1	24.2	13.1	24.3	13.1	24.2
15	15.6	26.7	15.6	26.6	15.5	26.6	15.4	26.5	15.3	26.5
20	18.6	29.0	18.5	28.9	18.3	28.8	18.1	28.7	17.9	28.6
25	22.0	31.0	21.7	30.9	21.4	30.7	21.1	30.5	20.8	30.3
30	25.6	32.4	25.1	32.2	24.9	32.0	24.1	31.8	23.6	31.5

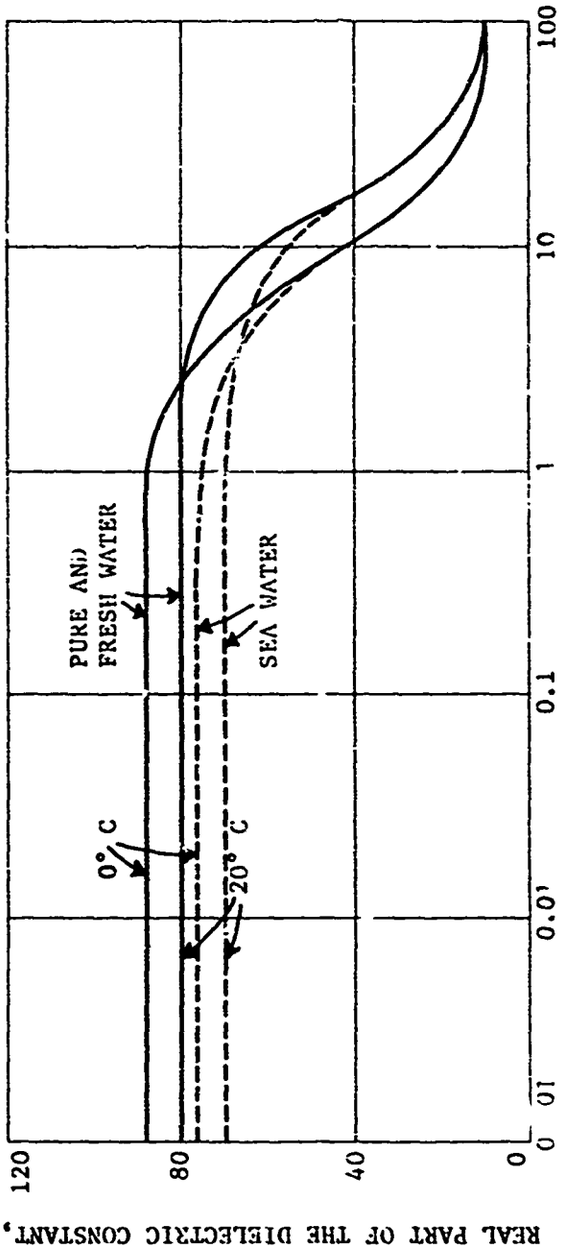

Figure 2. Real part of the complex dielectric constant of pure, fresh and sea water versus frequency for 0° C and 20° C.

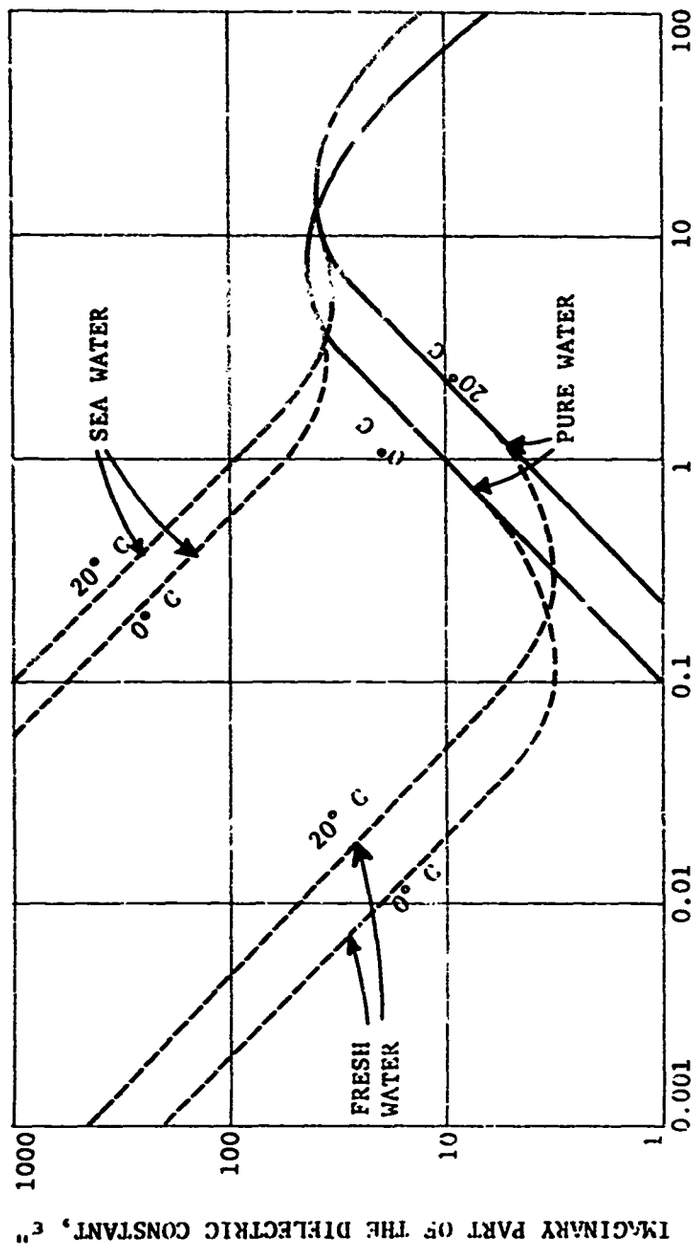

Figure 3. Imaginary part of the complex dielectric constant of pure, fresh and sea water versus frequency for a water temperature of 0° C and 20° C.

at 15.8 GHz and 19.35 GHz, and increases with temperature at 22 235 GHz and 34.0 GHz. The marked change in ε'' with salinity at the warmer temperatures at 3 GHz shows that ionic conductivity is a dominant factor in (34). Apparently, Debye relaxation dominates at other frequencies (Debye, 1929).

The polynomial expressions used above are based on measurements made for a wide range of salinity and cover salinities which are much larger than those observed in the World Ocean. These measurements should be repeated for actual sea water for many values of salinity between 0 o/oo and 40 o/oo.

Electric and magnetic properties of ice

The permeability of ice is $\mu_o(4\pi \times 10^{-7}$ henrys per meter).

According to Gunn and East (1954), the dielectric constant of ice is not a function of frequency in the microwave range. Table VII shows the values of ε' and ε'' for ice for various temperatures.

Table VII. Dielectric constant of ice (after Gunn and East, 1954).

Temperature, T (°C)	ε'	ε''
0	3.165	0.00855
-10	3.165	0.00281
-20	3.165	0.00196

The permittivity of ice is assumed to be constant over the range of temperatures and frequencies considered in this paper and equal to $\varepsilon_o(3.165 - j\ 0.003)$ farods per meter.

The large difference between the complex permittivities of water and ice lead to large differences between the emission of ice and water. It will be shown later how this can be used to detect ice/ocean boundaries and possibly to infer ice thickness.

CHAPTER III

RADIATIVE TRANSFER

Elementary Radiation

Intensity

In this study, the word intensity denotes the specific intensity of electromagnetic radiation. Consider the flow of radiant energy as shown in Figure 4. The intensity, $I(\nu,P,\vec{a},t)$ is defined by:

$$I(\nu,P,\vec{a},t) = \frac{dE}{d\Omega\, dA\, d\nu\, dt} \qquad (\text{watts/m}^2\text{steradian/Hz}), \quad (39)$$

where dE is the amount of radiant energy (joules) that passes through an element of area (dA, m^2) in an interval of time (dt,sec). This energy travels along a direction indicated by the unit vector $\vec{a}$, and is contained with an element of solid angle, $d\Omega$, surrounding $\vec{a}$. This energy is carried by electromagnetic waves having frequencies in the range from ν to $\nu + d\nu$ (Hertz). I is a function of frequency, position, direction, and time. The use of differential notation in (39) implies that I exists only if the limit exists. For practical cases, one must use finite areas, solid angles, times, and bandwidths. The actual energy that flows is the integrated intensity. It is convenient to retain the concept of a monochromatic intensity since it will be necessary to weigh the intensity field by the gain pattern of the antenna system used

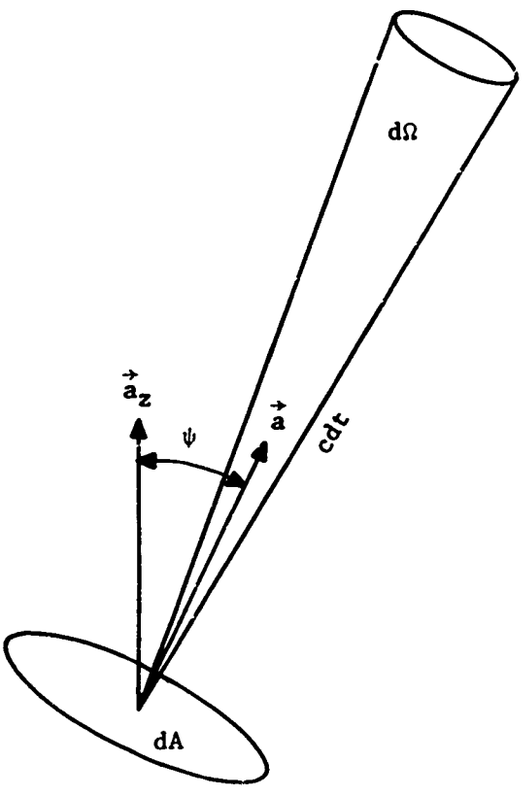

Figure 4. Geometry of intensity.

by a given microwave radiometer. Thus, the intensity gives the rate of flow of energy per unit time per unit solid angle per unit area and per unit frequency band width.

Poynting's theorem

The relationship between the time varying electromagnetic field and the corresponding electromagnetic radiational intensity can be deduced from Maxwell's equations in a manner first shown by Poynting. This development will be outlined here using concepts established in Chapter II.

Suppose one takes the dot product of (8) and $\vec{E}$, that is:

$$\vec{E} \cdot \nabla \times \vec{H} = \varepsilon_o(\varepsilon' - j\varepsilon'') \vec{E} \cdot \frac{\partial \vec{E}}{\partial t} \qquad (\text{watts/m}^3). \qquad (40)$$

By a vector identity,

$$\vec{E} \cdot \nabla \times \vec{H} = \vec{H} \cdot \nabla \times \vec{E} - \nabla \cdot (\vec{E} \times \vec{H}) \qquad (\text{watts/m}^3). \qquad (41)$$

Also,

$$\frac{}{\partial t} (\vec{E} \cdot \vec{E}) = \frac{\partial |\vec{E}|^2}{\partial t} = 2\vec{E} \cdot \frac{\partial \vec{E}}{\partial t} \qquad (\text{volts}^2/\text{m}^2 \text{ sec}), (42)$$

and

$$\frac{\partial}{\partial t} (\vec{H} \cdot \vec{H}) = \frac{\partial |\vec{H}|^2}{\partial t} = 2\vec{H} \cdot \frac{\partial \vec{H}}{\partial t} \qquad (\text{amps}^2/\text{m}^2 \text{ sec}). \quad (43)$$

Substitution of (41), (42), (43), and (3) into (40) yields the expression:

$$\nabla \cdot (\vec{E} \times \vec{H}) = - \omega\varepsilon_o\varepsilon''\vec{E} \cdot \vec{E} - \frac{\partial}{\partial t} (\varepsilon_o\varepsilon' |\vec{E}|^2/2 + \mu_o|\vec{H}|^2/2) \qquad \text{(watts/m}^3\text{)}. \qquad (44)$$

The first term on the right-hand side of (44) represents the power lost in the medium; the second term represents the power stored in the electric and magnetic field. If one integrates over a volume V and uses the divergence theorem, one obtains the expression:

$$\cdot \oint_A (\vec{E} \times \vec{H}) \cdot d\vec{A} = - \iiint_V \omega\varepsilon_o\varepsilon''\vec{E}\cdot\vec{E}\, dV$$

$$- \frac{\partial}{\partial t} \iiint_V (\varepsilon_o\varepsilon' |\vec{E}|^2/2 + \mu_o|\vec{H}|^2/2)\, dV \qquad \text{(watts)}, \qquad (45)$$

where A encloses V and $d\vec{A}$ is the outward normal vector to the surface A. From the form of (45) one must conclude that $\vec{E} \times \vec{H}$ is the power flowing across A since energy must be conserved. The first term on the right-hand side of (45) represents all the losses occurring in V, and the second term represents the time rate of change of the energy stored in the electric and magnetic fields in V.

One defines Poynting's vector $\vec{P}$ such that:

$$\vec{P} = \vec{E} \times \vec{H} \qquad \text{(watts/m}^2\text{)}. \qquad (46)$$

Polarization

Measurements of microwave intensity are accomplished by using a radiometer whose antenna is sensitive to only part of the radiational field. Also, microwave power is received and integrated over periods of one second or longer due to the low intensities involved. The intensity field consists of statistically independent waves. Microwave radiometers are usually sensitive to one plane of electrical polarization. It is convenient, therefore, to divide the intensity field into two components -- those waves whose electric vectors lie in the vertical plane and those waves whose electric vectors lie in the plane perpendicular to the vertical plane. Consider the radiation traveling along the direction indicated by $\vec{a}$. There is an infinite number of planes containing $\vec{a}$. The plane which contains both $\vec{a}$ and $\vec{a}_z$, the vertical unit vector, is called the vertical plane and is denoted by the subscript v. The plane containing $\vec{a}$ that is perpendicular to the vertical plane is commonly called the 'horizontal plane', and is denoted by the subscript h. The horizontal plane is rarely level, that is tangent to the geoid; but, this is the common reference made to this plane in the literature.

The intensity may be thought of as being the sum of the horizontally polarized and vertically polarized components of the intensity, that is,

$$I = I_h + I_v \qquad (\text{watts/m}^2\text{/steradian/Hz}). \qquad (47)$$

I_h and I_v are, in general, not equal. It is assumed that I_h and I_v are mean values integrated over some finite time period which is many times longer than the time period of the radiation. Also, I_h and I_v bear no phase relationship to each other and are independent of each other. Thus, the time dependences in (39) are only those slowly varying changes associated with overall changes in mean intensity.

The resolution of the intensity field into its horizontally polarized and vertically polarized components results in the necessity of expressing many of the following equations as couplets, that is, one would need one equation for horizontal polarization and one equation for vertical polarization. To reduce the number of equations in the remaining pages of this paper, the subscript p is used when either horizontal or vertical polarization is applicable, that is, p = h or v. In cases where cross polarization effects are under study, this shorthand notation will be dropped.

Blackbody radiation

Consider the intensity field within a constant temperature enclosure. A constant temperature enclosure is necessarily in a state of thermodynamic equilibrium. Consider a small area dA within this enclosure on the walls of the enclosure. Let

$B(\nu,T)$ be the intensity of the radiation emitted by an area dA where

$$dE = B(\nu,T)\ dA\ d\nu\ dt\ d\Omega \qquad \text{(joules)}. \qquad (48)$$

One major discovery of recent time was the form of $B(\nu,T)$ by Planck (1906) where:

$$B(\nu,T) = 2h\nu^3/c^2\ [\exp(h\nu/kT) - 1] \qquad \text{(watts/m}^2\text{/steradian/Hz)}. \qquad (49)$$

T is the temperature (degrees Kelvin, °K) of the medium, h is Planck's constant (6.623×10^{-34} joule-seconds), c is the speed of light in a vacuum (2.9979×10^8 meters per second), and k is Boltzman's constant (1.380×10^{-23} joules per degree Kelvin).

In the case of frequencies less than 100 GHz and for temperatures more than 200° K, $(h\nu/kT)$ is very much less than unity. A Maclaurin expansion of the bracketed quantity in (49) is:

$$\exp(h\nu/kT) - 1 = h\nu/kT + h^2\nu^2/2k^2T^2 + \ldots \qquad \text{(dimensionless)}. \qquad (50)$$

Equation (49) reduces to

$$B(\nu,T) = (2k\nu^2/c^2)T \qquad \text{(watts/m}^2\text{/steradian/Hz)} \qquad (51)$$

when higher order terms in (50) are neglected. Equation (51) is the Rayleigh - Jeans Radiation Law and is valid for considerations

in this paper.

Suppose one removes the emitting matter from the enclosure without changing its physical state. Will the emission function still be the same as it was in the enclosure? Goody (1964) says that it is doubtful that radiation laws valid inside a constant temperature enclosure would be valid outside the enclosure due to the existence of stimulated emission. He goes on to prove that the form of Planck's Law (and thus Rayleigh-Jean's Law) is valid as long as local thermodynamic equilibrium is maintained or as long as the matter is excited predominantly through collisions (as opposed to photon excitment).

It is assumed that Rayleigh-Jean's Law is valid for all purposes in this paper.

A perfect radiator is called a blackbody since it absorbs completely all radiation incident upon its surface. Natural objects may approximate blackbodies at least for some range of frequencies. The emission from a blackbody is completely random, and; therefore, the polarized intensity of emissions (B_p, watts/m^2/steradian/Hz) can be expressed as:

$$B_p = (k\nu^2/c^2)T \qquad \text{(watts/m}^2\text{/steradian/Hz)} \qquad (52)$$

since one-half the total intensity of emission would exist in each plane of polarization.

A natural body is less efficient than a perfect emitter

(blackbody). It is assumed that the form of the emission is the same as that of a blackbody or enclosed body, and that the polarized intensity of emission is given by:

$$I_p^e = \xi_p B_p \qquad \text{(watts/m}^2\text{/steradian/Hz)} \qquad (53)$$

where ξ_p is the polarized emissivity.

Brightness Temperature

In (52) there is a linear relationship between the physical temperature of a perfect emitter and its polarized intensity of emission. This convenient relationship led to the common practice in microwave physics of referring to any given intensity as an apparent temperature or brightness temperature. This practice results in a simplification of resulting transfer equations and the units used in microwave radiometry.

All investigators have used (51) to relate an intensity to a brightness temperature. Since microwave radiometers are sensitive to only one component of the natural field of radiation, it is erroneous to employ a polarized brightness temperature that relates to the total intensity of emission of a blackbody. This incorrect definition of polarized brightness temperature is corrected by these same investigators by erroneously assuming that the natural radiation field is unpolarized and random.

The natural field of radiation is usually biased toward one particular plane of polarization, that is, the vertical

component may be statistically more intense than the horizontal component. One would expect, however, that the emission from a blackbody is unpolarized and completely random. Thus, one should use (52) to define polarized brightness temperature. Suppose the natural field of microwave radiation is defined by I_p, the polarized intensity. Then T_p, the polarized brightness temperature (degrees Kelvin), is given by:

$$T_p = (c^2/k\nu^2)\ I_p \qquad (°K). \qquad (54)$$

It is convenient to refer to certain components of the total polarized field of intensity as certain types of polarized brightness temperature.

Cosmic temperature

The polarized intensity I_p^c of the radiation impingent upon the top of the atmosphere may be referred to as T_p^c, the polarized cosmic temperature where:

$$T_p^c = (c^2/k\nu^2)\ I_p^c \qquad (°K). \qquad (55)$$

Sky temperature

The polarized intensity (I_p^{sky}) of the microwave radiation incident upon the solid or liquid surface of Earth is referred to as T_p^{sky}, the polarized sky temperature which is given as:

$$T_p^{sky} = (c^2/k\nu^2)\ I_p^{sky} \qquad (°K). \qquad (56)$$

Emissive temperature of the surface

The polarized intensity I_p^e of the radiation emitted by a natural surface such as land or water may be refered to as T_p^e, the polarized emissive temperature where:

$$T_p^e = (c^2/k\nu^2)\ I_p^e \qquad (°K). \qquad (57)$$

Using (52) and (53) in (57), one obtains the expression:

$$T_p^e = \xi_p T \qquad (°K), \qquad (58)$$

where T is the effective temperature of the surface or the actual temperature of the surface emitting layer if the temperature is isothermal throughout the emitting layer.

Reflective temperature

If I_p^r is the polarized intensity of the radiation reflected or scattered by the surface, then T_p^r, the reflective temperature, is given by:

$$T_p^r = (c^2/k\nu^2)\ I_p^r = r_p\ T_p^{sky} \qquad (°K). \qquad (59)$$

Equations of Transfer

The following developments of the equations of radiative transfer follow closely that given by Chandrasekhar (1950) and Goody (1964).

Extinction and emission

Radiation traveling along a particular path in space and existing in one particular plane of polarization is called a pencil of radiation. A pencil of radiation may be weakened through extinction processes and strengthened through emission processes as it travels through a medium. According to Goody (1964) the fundamental law of extinction is Lambert's Law which states that the extinction processes are linear and independent of the intensity of radiation and in the amount of matter provided that the physical state is held constant. This law is assumed to be valid for the purposes of this paper.

Lambert's Law may be stated mathematically as:

$$dI_p = eI_p d\ell \qquad \text{(watts/m}^2\text{/steradian/Hz)}, \quad (60)$$

where I_p is the intensity of the polarized radiation under study, $d\ell$ is the differential path length (meters), and e is the volume extinction-coefficient (nepers). e is a function of the physical properties of the matter and the frequency. It is assumed that e is isoplaner, that is, it does not depend upon the particular plane of polarization under consideration.

The optical path length $\Lambda(\ell,\ell')$ is defined as:

$$\Lambda(\ell,\ell') = \int_{\ell'}^{\ell} e(u)du \qquad \text{(dimensionless)}. \quad (61)$$

Extinction consists of absorption (conversion of energy to internal thermal energy) and scattering (redistribution of energy with direction and/or frequency). Since all extinction processes are linear one may say that

$$e = \alpha + s \qquad \text{(nepers)}, \qquad (62)$$

where α is the volume absorption-coefficient (nepers) and s is the volume scattering-coefficient (nepers).

It is now assumed that extinction processes are isotropic for a differential volume in the atmosphere or ocean. On the other hand, the distribution of the intensity of the scattered radiation is a function of direction.

Formally one may state that dI_p, the differential change in polarized intensity due to emission processes, is given by:

$$dI_p = eJ_p d\ell \qquad \text{(watts/m}^2\text{/steradian/Hz)}, \qquad (63)$$

where J_p is the polarized source function having units of intensity.

General equation of transfer

The total differential change in polarized intensity is the result of the processes defined by (60) and (63) and is given by:

$$dI_p = (I_p - J_p)\, d\Lambda \qquad \text{(watts/m}^2\text{/steradian/Hz)}, \qquad (64)$$

which is known as Schwarzschild's Equation of Radiative Transfer.

The nature of the polarized source function is crucial to

problems of radiative transfer. The simplest case is that of local thermodynamic equilibrium. In this case, the polarized source function is Planckian (Goody, 1964) and is given by:

$$J_p \text{ (emission)} = (k\nu^2/c^2)\ T \qquad \text{(watts/m}^2\text{/steradian/Hz)}. \quad '65)$$

Conversely, the source of radiation may be due to the total amount of scattered radiation, that is,

$$J_h \text{ (scattering)} = \int_{4\pi} [\Gamma_{hv} (\vec{a}, \vec{a}_\Omega)\ I_v (\vec{a}_\Omega) + \Gamma_{hh} (\vec{a}, \vec{a}_\Omega)\ I_h (\vec{a}_\Omega)]d\Omega \qquad \text{(watts/m}^2\text{/steradian/Hz)} \quad (66)$$

and

$$J_v \text{ (scattering)} = \int_{4\pi} [\Gamma_{vv} (\vec{a}, \vec{a}_\Omega)\ I_v (\vec{a}_\Omega) + \Gamma_{vh} (\vec{a}, \vec{a}_\Omega)\ I_h (\vec{a}_\Omega)]d\Omega \qquad \text{(watts/m}^2\text{/steradian/Hz)} \quad (67)$$

where Γ_{hv}, Γ_{hh}, Γ_{vv}, and Γ_{vh} are the coefficients of scattering in the medium, I_v and I_h are the polarized intensities of the incident field of radiation, and $\vec{a}_\Omega$ is a unit vector which is allowed to vary over the entire hemisphere. The integrations are performed over 4π steradians. Now $I_v (\vec{a}_\Omega)$ and $I_h (\vec{a}_\Omega)$ are difficult to assess in a practical situation since they are also the result of extinction and emission in the space around the differential volume under question. Most investigators avoid this problem by assuming that scattering is negligible. This assumption is adopted in the present paper. When cases arise for

which this assumption seems to be significantly in error, the effects of scattering will be discussed in a qualitative manner. The author intends to pursue the case of a scattering and thermally emitting medium in future research. Thus, with this assumption,

$$e = \alpha \qquad \text{(nepers)}, \tag{68}$$

and

$$J_p \text{ (scattering)} = 0. \tag{69}$$

Transfer equation in a non-scattering medium under local thermodynamic equilibrium in terms of brightness temperatures

Consider the transfer of microwave radiation that occurs in a horizontally uniform atmosphere overlying a uniform ocean as shown in Figure 5. The polarized intensities of the microwave radiation incident upon the air-sea interface are the result of two processes. Polarized cosmic radiation is partially extincted throughout the atmosphere and reaches the surface. The atmosphere emits radiation which is partially extincted by the atmosphere between that level and the surface. It follows from equation (64) and (65) that the polarized intensity I_p^{sky} of the sky radiation is given by:

$$I_p^{sky} = I_p^c \exp(-\Lambda_m \sec\psi) + (k\nu^2/c^2) \sec\psi \int_0^{\Lambda_m} \cdot T(\Lambda') \exp(-\Lambda' \sec\psi) d\Lambda \quad \text{(watts/m}^2\text{/steradian/Hz)}, \tag{70}$$

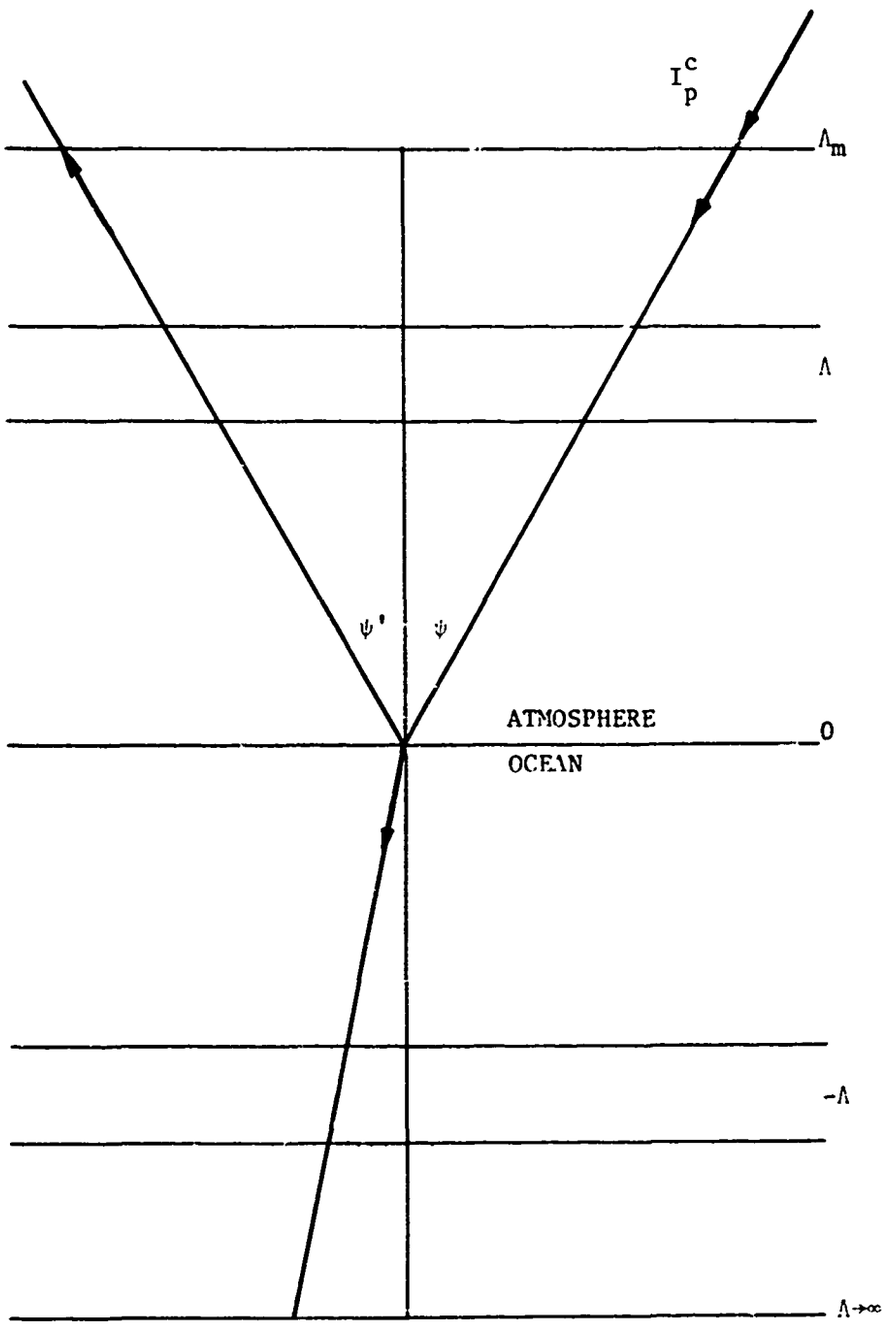

Figure 5. Geometry of radiative transfer in a horizontally uniform, plane, parallel atmosphere.

where:

$$\Lambda_m = \int_0^\infty \alpha(z)\, dz \qquad \text{(dimensionless)}, \qquad (71)$$

$$\Lambda' = \int_0^z \alpha(z)\, dz \qquad \text{(dimensionless)}, \qquad (72)$$

and

$$d\Lambda' = \alpha(z)\, dz \qquad \text{(dimensionless)}. \qquad (73)$$

z is the distance (meters) above the air-sea interface.

If the intensities are expressed as polarized brightness temperatures according to (55) and (56), then:

$$T_p^{sky} = T_p^c \exp(-\Lambda_m \sec\psi) + \sec\psi \int_0^{\Lambda_m} T(\Lambda') \exp(-\Lambda' \sec\psi) d\Lambda' \qquad (°K). \qquad (74)$$

In most cases the contribution from cosmic sources can be ignored when compared to emission from the atmosphere. Solar cosmic radiation cannot be ignored since the sun radiates with an effective temperature of 11,000° K in the microwave region (Barrett and Chung, 1962). The attenuation of solar microwave radiation by atmospheric gases has been measured by Staelin (1966), Dicke (1946), and other investigators to determine the distribution of water vapor, oxygen, and temperature in the atmosphere.

Extinction and emission at the air-sea interface

At the air-sea interface some microwave radiation is reflected or scattered into the atmosphere and the rest enters the hydrosphere. In the hydrosphere additional extinction takes place.

Unless the depth of water is extremely small, all of the microwave energy entering the hydrosphere is absorbed.

If the air-sea interface is flat, the reflected pencil of radiation will emerge along a direction inclined at ψ' which is equal to ψ and is opposite to ψ (see Figure 5). The incident and reflected pencils lie in a vertical plane. If the air-sea interface is smooth but is not flat the reflected pencil lies along an angle coangular to the incident angle with respect to the normal of the inclined smooth surface. A surface is defined to be smooth if the radius of curvature of the surface at a point is many times larger than the wavelength of the microwave radiation (Peake, 1959). Since microwave wavelengths are typically one to one-hundred centimeters, the assumption applies only to long wavelength ocean swells. In most cases, the sea surface is rough and must be treated from the standpoint of physical optics.

Peake (1959) has defined a set of quantities known as the bistatic scattering coefficients per unit area which give the scattering properties of an interface separating two homogenous dielectrics. Let I_h^i and I_v^i be the polarized intensities of radiation incident upon the scattering surface along a direction indicated by $\vec{a}_i$, a unit vector. Let I_v^s and I_h^s be the polarized intensities of radiation scattered along a direction indicated by $\vec{a}_s$ from the scattering interface. Let D be the radial distance from the point of observation and A be the area of the

scatterer. The scattering coefficients per unit area are defined by Peake (refer to Figure 6) as:

$$\gamma_{hh} = \lim_{\substack{A\to\infty \\ R\to\infty}} \left[4\pi D^2 \; I_h^s / A\cos\psi_i \; I_h^i \right], \; (m^{-2}). \tag{75}$$

$$\gamma_{hv} = \lim_{\substack{A\to\infty \\ R\to\infty}} \left[4\pi D^2 \; I_v^s / A\cos\psi_i \; I_h^i \right], \; (m^{-2}). \tag{76}$$

$$\gamma_{vv} = \lim_{\substack{A\to\infty \\ R\to\infty}} \left[4\pi D^2 \; I_v^s / A\cos\psi_i \; I_v^i \right], \; (m^{-2}). \tag{77}$$

$$\gamma_{vh} = \lim_{\substack{A\to\infty \\ R\to\infty}} \left[4\pi D^2 \; I_h^s / A\cos\psi_i \; I_v^i \right], \; (m^{-2}). \tag{78}$$

where ψ_i is the angle between $\vec{a}_i$ and $\vec{a}_z$.

Consider the transfer of radiation through a homogenous slab of dielectric material. The polarized intensity of the radiation entering the material is less than I_p^i, the polarized intensity of the radiation incident upon the slab. If the surface of the slab is a smooth surface, then I_p^o, the polarized intensity of the radiation entering the slab, is given by:

$$I_p^o = (1 - r_p) \; I_p^i \qquad (\text{watts}/m^2/\text{steradian}/H) \tag{79}$$

where r_p is the polarized reflectivity. If the surface is a scattering surface, I_p^o is dependent upon the distribution of γ's. According to Peake, the polarized albedos of a surface per unit solid angle is given by:

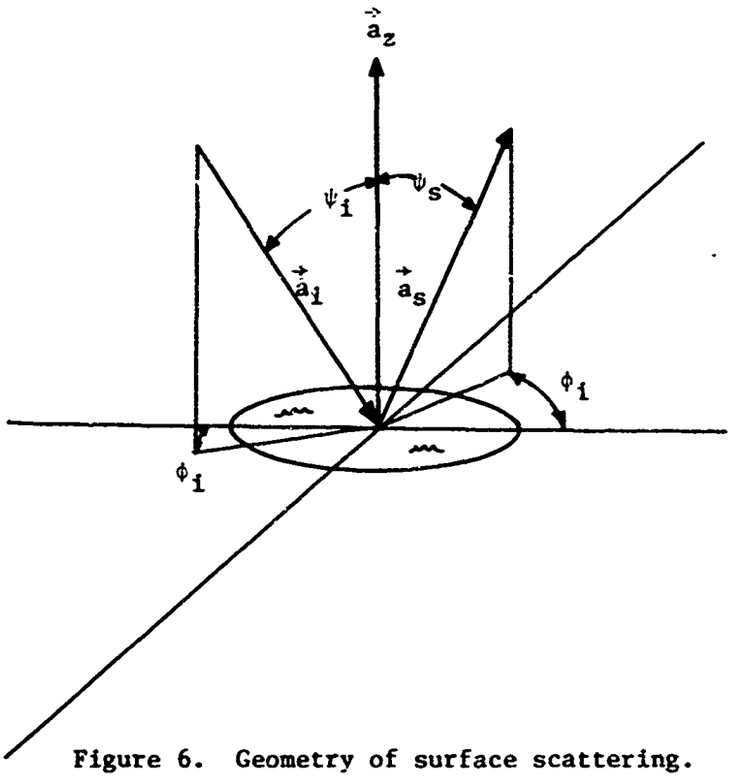

Figure 6. Geometry of surface scattering.

$$\beta_h = (1/4\pi) \int_{2\pi} [\gamma_{hh}(\vec{a}_i, \vec{a}) + \gamma_{hv}(\vec{a}_i, \vec{a})] d\Lambda \qquad (m^{-2}), \qquad (80)$$

and

$$\beta_v = (1/4\pi) \int_{2\pi} [\gamma_{vh}(\vec{a}_i, \vec{a}) + \gamma_{vv}(\vec{a}_i, \vec{a})] d\Lambda \qquad (m^{-2}), \qquad (81)$$

where β_h and β_v are the polarized albedos.

Thus,

$$I_p^o = (1 - \beta_p) I_p^i \qquad \text{(watts/m}^2\text{/steradian/Hz)}. \qquad (82)$$

The entering radiation will suffer some attenuation as it travels in the dielectric slab and will gain some energy due to emissions in the slab. The polarized intensity I_p^t of the resulting transmitted energy is

$$I_p^t = I_p^o \exp\left(-\int_o^\chi \alpha dx\right) + (k\nu^2/c^2)\int_o^x \alpha T \cdot \exp\left(-\int_o^\chi \alpha dx\right) dx \qquad \text{(watts/m}^2\text{/steradian/Hz)}. \qquad (83)$$

therefore,

$$I_p^t = I_p^o \exp(-\alpha\chi) + (k\nu^2/c^2)T\,[1 - \exp(-\alpha\chi)], \qquad \text{(watts/m}^2\text{/steradian/Hz)}, \qquad (84)$$

where α is the absorption coefficient of the slab, T is the slab temperature, and χ is the slab thickness. The term, $\exp(-\alpha\chi)$, is the polarized transmissivity of the medium. The amount of radiation absorbed is $I_p^o\,[1 - \exp(-\alpha\chi)]$ since energy must be conserved. The second term of the righthand side of (84) is

$T[1 - \exp(-\alpha\chi)]$, and this form suggests that the bracketed multiplier takes on the role of a polarized emissivity for the entire slab; however, the same term gives us the expression for the absorptivity. This equivalence of absorbtivity and emissivity is the result of the assumption that local thermodynamic equilibrium is maintained as was first stated by Kirchhoff. If χ is increased to such an extent that the transmissivity is practically zero, then one may draw certain conclusions about the relationships between the scattering, absorbing and emissive properties of the air-sea interface, and these are as follows:

For a smooth surface:

$$\xi_p = 1 - r_p \qquad \text{(dimensionless)}, \tag{85}$$

and for a rough surface:

$$\xi_p = 1 - \beta_p \qquad \text{(dimensionless)}. \tag{86}$$

Upwelling microwave radiation

Consider the intensity of the upwelling microwave radiation at some point Λ'' above the surface of the sea. The expression for T_p, polarized brightness temperature, in a horizontally uniform atmosphere is

$$T_p(\Lambda'',\theta) = \{(1 - r_p)\, T_{sea} + r_p \left[\sec\psi \int_o^{\Lambda_m} T(\Lambda') \cdot \exp(-\sec\psi\Lambda')d\Lambda' + T_p^c \exp(-\sec\psi\Lambda_m)\right]\} \cdot \exp(-\sec\psi\Lambda'') + \sec\psi \int_o^{\Lambda''} T(\Lambda''') \exp(-\sec\psi\Lambda''')d\Lambda''' \quad (°K), \tag{87}$$

where:

$$\Lambda_m = \int_0^\infty \alpha(z)dz \qquad \text{(dimensionless)}, \qquad (88)$$

$$\Lambda' = \int_0^z \alpha(z)dz \qquad \text{(dimensionless)}, \qquad (89)$$

$$\Lambda'' = \int_0^{h_o} \alpha(z)dz \qquad \text{(dimensionless)}, \qquad (90)$$

and

$$\Lambda''' = \int_z^{h_o} \alpha(z)dz \qquad \text{(dimensionless)}. \qquad (91)$$

In the above equation, h_o is the height of the observer above sea level in meters and z is the height of a level under consideration. The computations in (87) through (91) can be performed by various finite difference schemes on the electronic computer if d(z) and T(z) are known. $\alpha(z)$ is usually dependent upon temperature, density, pressure, and type of absorbing medium.

In the microwave region the atmospheric gases of molecular oxygen and water vapor and the atmospheric constituents of liquid water droplets and ice are the principal absorbers. Their relative and absolute values are the subject of Chapter IV.

CHAPTER IV

EXTINCTION AND EMISSION IN THE ATMOSPHERE

General

Atmospheric gases and other atmospheric constituents selectively absorb, scatter, and emit microwave radiation as it travels through the atmosphere. Molecular oxygen and water vapor are the primary absorbing gases in the atmosphere in the microwave region of the electromagnetic spectrum (Van Vleck, 1951a). Droplets of liquid water in clouds and rain strongly absorb and scatter microwave radiation. As a consequence of Kirchhoff's Law, molecular oxygen, water vapor, and droplets of liquid water are the primary sources of emitted microwave energy in the atmosphere. All investigators in microwave radiometry have assumed that scattering is negligible as an extinction process as well as an emission process. This assumption greatly simplifies the solutions to radiative transfer since it is necessary to know the entire field of intensity throughout the volume being considered if one is to treat a scattering atmosphere.

Since this study is a review of the present state of investigations in microwave radiometry, qualitative speculation of the effects of scattering under actual atmospheric conditions will be offered along with quantitative results from other investigations that treat the atmosphere as a non-scattering medium in local thermodynamic equilibrium.

Previous studies of the absorption coefficient and scattering coefficient of molecular oxygen, water vapor, and liquid water were often presented from the standpoint of applications to radar. Consequently, the total attenuation coefficient or extinction coefficient is usually discussed in these papers. Thermal emission of rain clouds is of little concern to radar studies since the intensities involved in radar are several orders of magnitude larger than the intensity of thermal emission. For the purposes of the present paper, a knowledge of the absorption characteristics of the atmosphere is needed as opposed to the total attenuation characteristics.

One other point of semantics needs clarification before going into detailed discussion of absorption and emission in the atmosphere. Most investigators have used absorption coefficients which are expressed in terms of decibels per kilometer[5] (db/km). In Chapter III, α is expressed in nepers. Let I_p^o be the polarized intensity of a pencil of radiation at some point along its path, $x = 0$, and let I_p^x be the polarized intensity of this pencil at x. Let α_{db} be the absorption coefficient along x in terms of decibels per kilometers, and let α be the absorption coefficient along x in terms of nepers. Then,

$$I_p^x/I_p^o = \exp(-\alpha x) \qquad \text{(dimensionless)}, \qquad (92)$$

---

[5] Lengths may be expressed as centimeters (cm), meters(m) or kilometers (km) in various expressions in the following developments.

or

$$-10 \log_{10} (I_p^x / I_p^o) = 10^{-3} \alpha_{db} x \quad \text{(db)}. \tag{93}$$

Equation (92) follows from (60), and (93) follows from the definition of a decibel where x is in meters in both cases.

From (92) it follows that:

$$-\ln (I_p^x / I_p^o) = \alpha x \quad \text{(dimensionless)}, \tag{94}$$

or

$$-10 \log_{10} (I_p^x / I_p^o) = 4.3429\, \alpha x \quad \text{(db)}. \tag{95}$$

Thus, from (93) and (95), it follows that:

$$\alpha_{db} = 4342.9\alpha \quad \text{(db/km)}. \tag{96}$$

Conversely,

$$\alpha = 0.00023026\, \alpha_{db} \quad \text{(nepers)}. \tag{97}$$

If α_{db} is expressed as decibels per meter, then

$$\alpha = 0.23026\, \alpha_{db} \quad \text{(nepers)}. \tag{98}$$

Atmospheric Gases

Molecular oxygen

The oxygen molecule (O_2^{16}) absorbs microwaves because it possesses a permanent magnetic moment. Van Vleck (1947a) made

predictions of the absorptive characteristics of molecular oxygen from quantum theory. As a result of collisions with neighboring molecules, the energy levels of the oxygen molecule are broadened, and a statistical distribution of allowable transitions results. Van Vleck used the broadening distribution developed by Van Vleck and Weisskopf (1945).

The general quantum mechanical expression for α_{ox}, the absorption coefficient of molecular oxygen, is quite complicated. Oxygen has a series of absorption lines near 60 GHz. Outside this resonance region, one may assume that one central resonance line exists and may predict absorption based on broadening of this line. Van Vleck (1947a) gives a simplified expression for α_{ox} for a temperature of 293° K and for a pressure of 1013.25 millibars (mb)[6] that is applicable for frequencies less than 35 GHz; this expression is:

$$\alpha_{ox} = 0.34\ (\nu^2/c^2)\left[\frac{\Delta\nu/c}{[2-(\nu/c)]^2+(\Delta\nu/c)^2} + \frac{\Delta\nu/c}{[2+(\nu/c)]^2+(\Delta\nu/c)^2} + \frac{\Delta\nu/c}{(\nu/c)^2+(\Delta\nu/c)^2}\right] \text{(db/km, (99)}$$

where:

c = speed of light (cm/sec),

ν = frequency (GHz),

$(\Delta\nu/c)$ = line breadth constant (cm^{-1}).

---

[6] In the rationalized MKS system of units 1 millibar (mb) = 100 newtons per square meter (nt/m^2).

The value of $(\Delta\nu/c)$ has to be determined from experimental data since the nature of the cross-section for collisions between atmospheric gases is poorly understood. Van Vleck selected a value for $(\Delta\nu/c)$ of 0.02 cm^{-1} and made calculations of α_{ox} based on equation (99). These values are given in Table VIII along with similar values based on the quantum expression for α_{ox} for frequencies above 35 GHz.

Table VIII. Theoretical values of the absorption coefficient of molecular oxygen (α_{ox}, db/km) at a pressure of 1013.25 mb and a temperature of 293.0° K (after Van Vleck, 1951).

ν (GHz)	α_{ox} (db/km)	ν (GHz)	α_{ox} (db/km)	ν (GHz)	α_{ox} (db/km)
0.3	0.0014	30	0.014	64.5	5.0
1.0	0.0050	45	0.077	69	0.51
3.0	0.0066	51	0.32	75	0.19
10	0.0072	54	1.99	150	0.03
20	0.0089	60	14.0		

The values of α_{ox} given in Table VIII are for standard conditions (p = 1013.25 mb; T = 293° K). These values served a useful purpose as far as horizontal propagation of microwave energy in the atmosphere is concerned. Vertical and slant-range propagation is of concern in this study. For other pressures and other temperatures, the expression given in (99) is altered in two ways.

First, the line-breadth constant is affected by temperature and pressure. This dependence is not well established. Van Vleck (1947a) states that:

$$(\Delta\nu/c) \propto pT^{-1/2}. \tag{100}$$

Meeks and Lilley (1963) stated that measurements by Hill and Gordy (1954) indicate that:

$$(\Delta\nu/c) \propto pT^{-0.85}. \tag{101}$$

Falcone (1966) confirmed (101) through measurements of sky radiance where the value of $(\Delta\nu/c)$ at 1013.25 mb and 293° K was taken to be 0.025 cm^{-1}. There may be some non-linearity in $(\Delta\nu/c)$ in regard to its dependence on p. Zimmer and Mizushima (1961) report that the slope of $\Delta\nu$ versus p is 2 MHz per mm of mercury at very low pressures and is 0.8 MHz per mm of mercury at one atmosphere.

Broadening also results from Zeeman splitting and thermal agitation (Doppler broadening). Above 40 kilometers, the Zeeman effect becomes a major factor; above 80 kilometers, Doppler broadening is the main cause of broadening (Meeks and Lilley, 1963). The effect of these causes can be accounted for by adding a line breadth constant for Doppler $(\Delta\nu_d/c)$ and Zeeman $(\Delta\nu_z/c)$ effects.

In addition to the effects of pressure and temperature on the line-breadth constant in (99), the constant term of (99) is affected by pressure and temperature.

Water vapor

The molecule of water (H-O-H) in its gaseous state absorbs microwaves due to its permanent electric dipole. Van Vleck (1947b) determined its absorptive characteristics from quantum theory in a manner similar to that used to determine α_{ox}. In the case of water vapor, there is a single absorption line at 22.235 GHz. Since water vapor is electrically polar, strong absorption occurs at infrared frequencies. Broadening of infrared absorption lines results in some additional absorption in the microwave region which is called residual absorption. Becker and Autler (1946) have shown that the contribution to α_w, the absorption coefficient for water vapor, due to residual absorption was about five times larger than that predicted by Van Vleck. The quantum mechanical expression for α_w developed by Van Vleck can be simplified and corrected for the observed residual absorption. The resulting expression given by Staelin (1966) is:

$$\alpha_w = 140.71 \exp(-644/T)\nu^2 p\rho_w T^{-3.125} (1 - 0.0147 \rho_w T/p)$$
$$\cdot \{1/[(\nu - 22.234)^2 + (\Delta\nu)^2] + 1/[(\nu + 22.234)^2 + (\Delta\nu)^2]\}$$
$$+ 0.01107 \rho_w^2 \Delta\nu T^{-1.5} \quad \text{(db/km)}, \qquad (102)$$

where:

ν = frequency (GHz)

T = temperature (°K)

p = total pressure (mb)

ρ_w = density of water vapor (g/m^3)

and

$$\Delta\nu = 2.58 \times 10^{-3}\, p(1 + 0.0147\rho_w T/p)\, (T/318)^{-0.625}\ (cm^{-1}).$$

Van Vleck (1951) has calculated α_w at 1013.25 mb pressure and for a temperature of 293° K. These calculations are given in Table IX.

Total gaseous absorption

Dicke, et al., (1946) determined α_w through measurements of sky radiance at 20 GHz, 24 GHz, and 30 GHz. These values are 0.014, 0.026, and 0.011 (db/km per g/m^3), respectively, and they agree closely with the corrected theoretical values given in Table IX.

The density of water vapor depends somewhat on the temperature of the air and varies over a large range throughout the year. At sea level, saturated air at a temperature of 20° C contains about 17 grams of water vapor per cubic meter (Chemical Rubber Co., 1959). Thus, ρ_w may be 17 g/m^3 or less under these conditions. In model atmospheres, it has been popular to assume that ρ_w is 7.5 grams per cubic meter at sea level. In Table X, values of α_{ox} and α_w have been calculated for a pressure of 1013.25 mb, for a temperature of 293° K, and ρ_w equal to 3, 7.5, and 17 g/m^3. It can be seen in Figure 7 that water vapor is the principal absorber for frequencies between 8 GHz and 50 GHz. Water vapor is quite

Table IX. Theoretical values of the absorption coefficient of water vapor (α_w, db/km) per unit of water-vapor density (ρ_w, g/n^3) at a pressure of 1013.25 mb and a temperature of 293° K (after Van Vleck, 1951).

Frequency ν (GHz	$\alpha_w(22.234)/\rho_w$(db/km per g/m^3)	α_w(Res)/ρ_w* (db/km per g/m3)	α_w(Res)/ρ_w** (db/km per g/m^3)	α_w(total)/ρ_w w/o correction (db/km per g/m^3)	α_w(total)/ρ_w w/correction (db/km per g/m^3)
3.0	0.0000133	0.000013	0.0000650	0.0000263	0.0000783
10.0	0.00256	0.00013	0.000650	0.000386	0.000906
15.0	0.00136	0.00029	0.00145	0.00165	0.00281
20.0	0.01010	0.00052	0.00260	0.01062	0.01270
21.0	0.1470	0.00057	0.00285	0.01527	0.01755
22.235	0.01930	0.00064	0.00320	0.01994	0.02250
24.0	0.01680	0.00074	0.00370	0.01754	0.02050
27.0	0.00820	0.00095	0.00475	0.00915	0.01295
30.0	0.00470	0.00116	0.00580	0.00586	0.01050
45.0	0.00150	0.00262	0.013120	0.00412	0.01460
60.0	0.00107	0.00470	0.02350	0.00577	0.02457

* Values based on theory

** Theoretical values times five

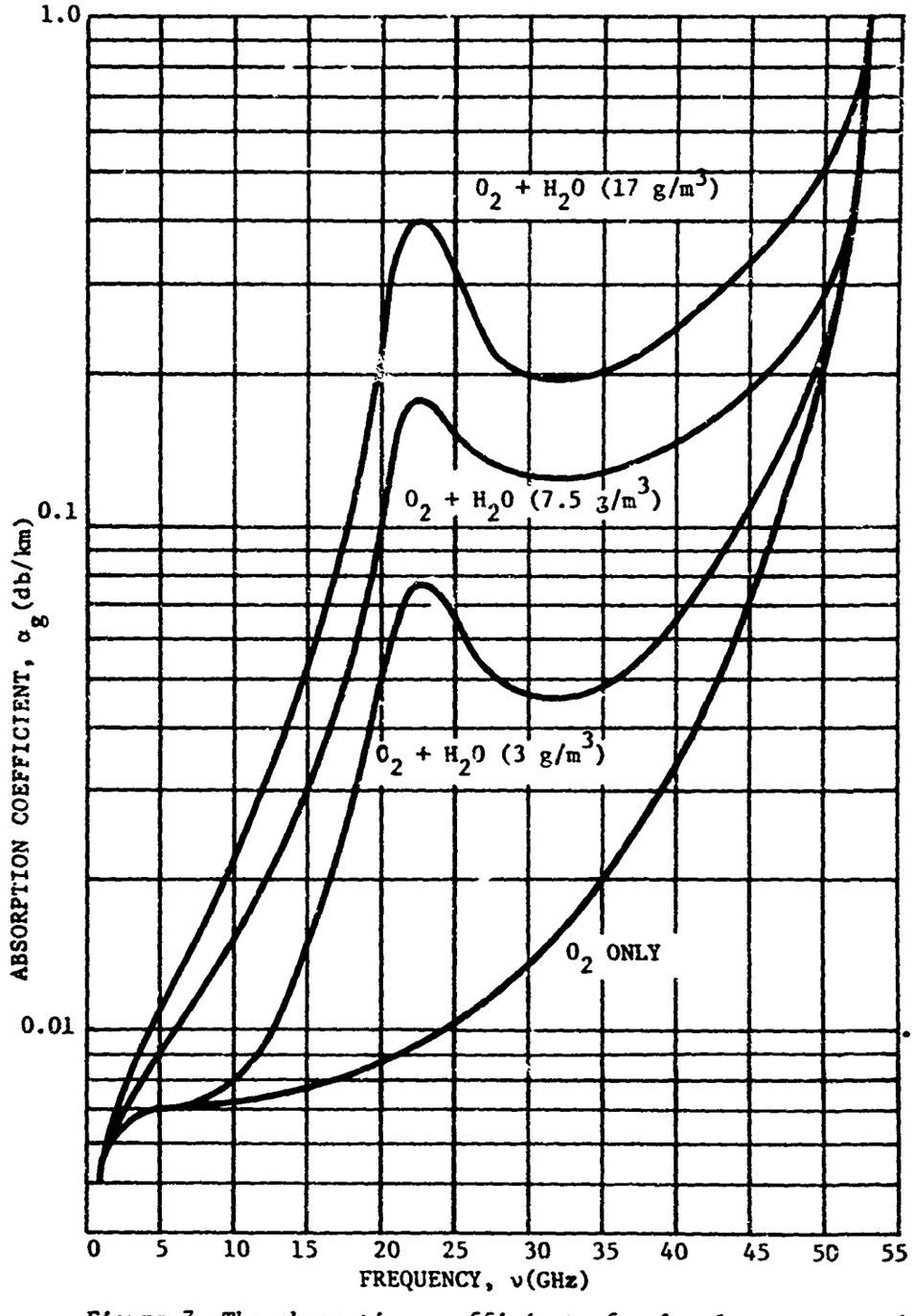

Figure 7. The absorption coefficient of molecular oxygen and water vapor at sea level versus frequency for a temperature of 293° K and for water-vapor densities of 0, 3, 7.5, and 17 grams per cubic meter.

Table X. Total absorption coefficient for molecular oxygen and water vapor (α_g, db/km) for a pressure of 1013.25 mb, for a temperature of 293° K and for water-vapor densities of 3, 7.5 and 17 g/m^3.

Frequency (GHz)	α_{ox} (db/km)	α_g (db/km) $\rho_w = 3$ (g/m^3)	$\rho_w = 7.5$ (g/m^3)	$\rho_w = 17$ (g/m^3)
3	0.0066	0.0068	0.0072	0.0079
10	0.0072	0.0075	0.014	.0226
15	0.0078*	0.0162	0.029	.0556
20	0.0089	0.047	0.104	.2248
21	0.0092	0.063	0.141	.308
22.235	0.0096*	0.077	0.178	.392
24	0.0102	0.072	0.164	.359
30	0.014	0.046	0.125	.193
45	0.077	0.121	0.187	.325

* Value is estimated from plot of α_{ox}.

variable in the atmosphere in amount and distribution with height. In most cases the amount and distribution of water vapor distribution tion in the atmosphere is not well known. Thus, one would endeavor to use frequencies less than 8 GHz if one wishes to view surface phenomena. However, if one is interested in measuring remotely some aspect of the field of water vapor, then frequencies near 22.235 GHz seem appropriate.

Tables VIII through X and Figure 7 present data for sea level pressure and temperature only. Since the transmission of microwave energy through the atmosphere along vertical and slanting paths is of concern to this study, the effects of pressure and temperature on α_g must be considered. Perhaps the best way to proceed now is to examine the results of past calculations of sky

radiance and total atmospheric transmission for a cloudless atmosphere. Most investigators have calculated sky radiance or total attenuation by assuming a model atmosphere and by using Van Vleck's formulas for α_{ox} and α_{w}.

Total atmospheric attenuation for a clear atmosphere

If $\alpha(z)$ is known, then L_g, the total zenith attenaution of microwave radiation, is:

$$L_g = \int_0^\infty \alpha_g(z)dz \qquad \text{(db)}, \qquad (103)$$

where:

L_g = total zenith attenuation (db),

α_g = attenuation coefficient for molecular oxygen and water vapor (db/km),

and

z = altitude (km).

Equation (103) may be evaluated by finite differences or any other approximation scheme.

Using the distribution of pressure and temperature given by the 1960 ARDC model atmosphere, Meeks and Lilley (1963) calculated L_g for oxygen only over the range of frequencies from 1 GHz to 120 GHz. In the range from 1 GHz to 10 GHz, L_g was approximately 0.04 db.

Stogryn (1967) calculated values of the fractional absorption of a 1960 ARDC model atmosphere for various values of altitude and

frequencies of 19.4 GHz and 35 GHz. He assumed that the vertical distribution of water vapor was given by:

$$\rho_w(z) = 9.35 \exp(-0.5z) \quad (g/m^3), \qquad (104)$$

where z is the altitude (km).

In terms of decibel loss, the attenuation due to absorption by oxygen and water vapor in a layer of atmosphere extending from the surface to altitude z(km) is:

$$L_g(z) = 4.3429 \int_0^z \alpha(z)\, dz \quad (db), \qquad (105)$$

where $\alpha(z)$ is in nepers and z is in meters. Stogryn gives values for the integral in (105). Table XI gives these values of $L_g(z)$ expressed in decibels. The majority of the loss is incurred in the lower five kilometers of the atmosphere. This emphasizes the dependence of α_{ox} and α_w on pressure. The total loss throughout the entire vertical path is 0.346 and 0.326 decibels at 19.4 GHz and 35 GHz, respectively. This is approximately one order of magnitude higher than the loss at frequencies less than 10 GHz.

Calculations of L_g have also been made by Peake (1967) and Marandino (1967). These publications did not include information about the exact atmospheric model used. Wulfsberg (1967) measured the total attenuation of solar microwave energy by the atmosphere over a six-month period at 15 GHz and 35 GHz.

Hogg (1959) computed values of L_g based on the distribution of temperature, pressure and water-vapor given by the International

Table XI. Zenith attenuation ($L_g(z)$, db) in a 1960 ARDC model atmosphere with a density of water vapor of 9.35 exp (-5z) grams per cubic meter versus altitude (z, km) (after Stogryn, 1967).

z (km)	L(z) 19.4 GHz	L(z) 35 GHz	z (km)	L(z) 19.4 GHz	L(z) 35 GHz	z (km)	L(z) 19.4 GHz	L(z) 35 GHz
0	0	0	5	0.3765	0.3518	10	0.436	0.4108
1	0.1398	0.1398	6	0.3982	0.3713	15	0.4443	0.426
2	0.2354	0.2284	7	0.413	0.3856	20	0.446	0.4299
3	0.3010	0.2866	8	0.4234	0.396	25	0.4466	0.4304
4	0.3461	0.3257	9	0.4308	0.4043	30	0.4466	0.4304

Standard Atmosphere, that is, he assumed that:

$$T(z) = 255 + 5.5\ (10 - z) \qquad (°K), \qquad (106)$$

$$\rho_w(z) = 2\ (5 - z) \qquad (g/m^3), \qquad (107)$$

for $(0 \leq z \leq 5\ km)$,

$$\rho_w(z) = 0 \qquad (g/m^3) \text{ for } (z \geq 5\ km), \qquad (108)$$

and

$$p(z) = 1039.91\ (-0.014z) \qquad (mb), \qquad (109)$$

where z is the altitude in kilometers.

The results of these calculations and observations of L_g are presented in Table XII.

The calculated values in Table XII agree among themselves quite well and agree closely to the mean total attenuation observed by Wulfsberg (1967). His observations also show that L_g is very sensitive to the distribution of ρ_w for frequencies near the resonance absorption line for water vapor. The values of L_g for frequencies less than 10 GHz are quite low and indicate that radiation at these frequencies would suffer a loss of about one percent when traveling either outward from the surface or vice versa.

Sky temperature

If $\alpha(z)$ and T(z) are known, then T_p^{sky}, the polarized sky temperature, may be calculated from (74). Several investigators

Table XII. Summary of calculated and observed values of total zenith attenuation (L_g, db).

Frequency ν, (GHz)	Calculated values of L_g(db) Hogg (1959)	Meeks Lilley (1963)	Peake (1967)	Marandino (1967)	Stogryn (1967)	Observed L_g(db) Wulfsberg, 1967 T_G = -2°C ρ_w = 14 g/m^3	T_G = -2°C ρ_w = 1.2 g/m^3	Six-month average
1.4	- - -	0.036*	- - -	0.038	- - -	- - -	- - -	- - -
6	- - -	0.04*	- - -	0.042	- - -	- - -	- - -	- - -
10	0.05	0.043*	- - -	0.06	- - -	- - -	- - -	- - -
15	0.09	0.046*	0.11	0.096	- - -	0.1	0.06	0.94
20	0.35	0.05*	0.41	0.27	0.346**	- - -	- - -	- - -
22.235	0.70	0.053*	0.70	-.62	- - -	- - -	- - -	- - -
35	0.27	0.15	0.22	0.30	0.326	0.32	0.21	0.28

* Molecular oxygen only

** Calculated for ν = 19.4 GHz

T_G = surface air-temperature

have calculated T_p^{sky} under specific conditions of assumed model atmospheres. Several other investigators have measured the sky radiation with ground-based microwave radiometers. The results of these calculations and observations will be reviewed now in order to understand better the magnitude and variability of this parameter.

Hogg (1959) calculated values of T_p^{sky}, under the conditions given in (106) - (109) for a stratified atmsophere

Weger (1960) calculated values of T_p^{sky} under slightly different assumptions. He assumed that the atmosphere was horizontally uniform and that the surface of Earth was flat. He considered absorption above the tropopause to be negligible. Using Van Vleck's calculations of α_g for a pressure of 1013.25 mb, for a temperature of 293° K and for ρ_w equal to 7.5 g/m^3, he formulated expressions for α_{ox} and α_w as follows:

$$\alpha_{ox} = \alpha_{ox}\,(1013.25\ \text{mb},\ 293^\circ\ \text{K}, \nu)\ \exp\,(-0.183z) \quad (\text{km}^{-1}) \quad (110)$$

and

$$\alpha_w = \alpha_w\,(1013.25\ \text{mb},\ 293^\circ\ \text{K},\ 7.5\ \text{g/m}^3, \nu) \cdot \exp\,(-0.5z) \quad (\text{km}^{-1}), \quad (111)$$

where z is the altitude in kilometers. The surface values of α_{ox} and α_w may be taken from Van Vleck (1951a).

Croom (1965) calculated values of T_p^{sky} by assuming an I.C.A.O.

Standard Atmosphere with:

$$\rho_w = 10 \exp(-0.58z) \quad (g/m^3), \quad (112)$$

where z is the altitude in kilometers ($0 \leq z \leq 20$ km). In addition to this distribution of water vapor, he assumed that a layer of water vapor existed in the stratosphere which was 5 km thick and which contained 0.01 grams of water vapor per cubic meter. The result of stratospheric water is most pronounced at 22.235 GHz.

Stogryn (1967) calculated values of T_p^{sky} at 19.4 GHz and 35 GHz based on his model of the atmosphere previously given.

Hogg and Semplak (1963a) have calculated values of T_p^{sky} based on "dry, average, and humid" weather. These values are given by Peake (1967) without explanation of the precise model employed by Hogg and Semplak. Marandino (1967) also gives values of T_p^{sky} for 15.8 GHz, 22.2 GHz, and 34 GHz.

Wulfsberg (1964) has approached the problem of calculating T_p^{sky} from an engineering and empirical point of view. If one considers the atmosphere as a whole, then τ_o, the transmissivity, is given by:

$$\tau_o = \exp(-\sec\psi \int_0^\infty \alpha(z)\, dz) \quad \text{(dimensionless)}. \quad (113)$$

If one assumes furthermore that the atmosphere is non-reflecting then the absorptivity, a_o, is given as:

$$a_o = (1 - \tau_o) \quad \text{(dimensionless)}. \quad (114)$$

By Kirchhoff's Laws, the emissivity is equal to the absorptivity and, thus, the sky temperature is given by

$$T_p^{sky} = T_m \left[1 - \exp\left(-\alpha_o \sec\psi\right)\right] \quad (°K), \qquad (115)$$

where

$$\alpha_o = \int_0^\infty \alpha(z)dz \quad \text{(dimensionless)} \qquad (116)$$

and T_m = effective temperature (°K) of the atmosphere. Without proof, Wulfsberg (1964) and Peake (1967) have given the following empirical expression for T_m:

$$T_m = 1.12\, T_g - 50 \quad (°K), \qquad (117)$$

where T_g = the temperature of the air at the surface (°K).

Kreiss (1968) assumed that T_m could be given by the hypsometric equation for a layer, and he calculated values of T_p^{sky} by dividing the atmosphere into fourteen layers and applying an equation similar to (115) to each layer and summing over all the layers accordingly. Wulfsberg (1967) stated that (117) could be used in place of a more rigorous expression to give correct values of T_n to within 2° K.

Conway and Sakamoto (1965), Cummings and Hull (1966), and Decker and Dutton (1968) have measured T_p^{sky} of the real atmosphere at various frequencies.

Table XIII presents a summary of some of the calculated and

measured values of polarized sky temperature determined by the aforementioned investigators for various zenith angles.

It will be shown later that approximately two-thirds of the microwave radiation incident upon the sea surface is reflected or scattered back into the atmosphere. Also, the intensities measured by a downward looking radiometer are typically 200° K in terms of brightness temperature. From Table XIII, it is seen that T_p^{sky} is usually less than 30° K for frequencies below about 16 GHz. Thus, approximately 20° K or less of the total brightness temperature is due to reflected sky radiation for frequencies less than 16 GHz. In most cases this contribution to the total radiation is quite small for these low frequencies. Also, the effect of natural variations in water vapor is very small for these frequencies. However, the amount of reflected sky radiation is quite large for frequencies above 16 GHz. The calculations by Kreiss (1968) illustrate the pronounced effect of water vapor on sky temperature at frequencies near the absorption line of water-vapor. The natural variability of water vapor in the atmosphere can cause variations in the microwave radiance of the sea of 10 to 30° K for frequencies ranging from 19 GHz to 25 GHz.

If the atmosphere is horizontally uniform over any particular area, then one might be able to make meaningful measurements of microwave radiance by using relative measurements.

Table XIII. Summary of calculated and observed values of polarized sky temperature (T_p^{sky}, °K).

Investigator	Zenith Angle	Frequency, ν (GHz)							
		1.4	6	9.3	15.8	19.4	22.235	24	35
Hogg*, 1959	0°	2	3	3.5	6	17	42	30	18
	60°	2	5.5	7	11	30	70	60	40
Weger*, 1960	0°	-	-	3	7	-	-	27	19
	30°	-	-	4	8	-	-	47	21
	45°	-	-	5	9	-	-	38	28
	60°	-	-	6	12	-	-	53	28
Wulfsberg*, 1962	0°	-	-	-	3.2	-	-	-	9.6
	30°	-	-	-	3.7	-	-	-	11
	60°	-	-	-	6.4	-	-	-	19
Marandino*, 1967	0°	-	-	-	6	-	36	-	17
	30°	-	-	-	8	-	41	-	19
	45°	-	-	-	10	-	50	-	24
	60°	-	-	-	11	-	67	-	33
Peake*, 1967	0°	2	3	3.5	10	23	40	30	15
	60°	4	5.8	5.8	15	35	75	50	25
Peake*, 1967	0°	2.2	4.5	7.5	25	60	100	80	55
	60°	4.5	9	15	40	95	160	130	100
Stogryn*, 1967	0°	-	-	-	-	26.7	-	-	25.6
	30°	-	-	-	-	30.5	-	-	29.4
	45°	-	-	-	-	38.5	-	-	36.5
	60°	-	-	-	-	50.8	-	-	48.9

Table XIII. (con't)

Investigator	Zenith Angle	Frequency, ν (GHz) 1.4	6	9.3	15.8	19.4	22.235	24	35
Kreiss*, 1968	0°	-	-	-	7-18	9-43	14-106	10-90	-
Conway & Sakamoto** 1965	0°	-	-	-	50	-	-	-	-
	30°	-	-	-	50	-	-	-	-
	45°	-	-	-	50	-	-	-	-
	60°	-	-	-	60	-	-	-	-
Cummings & Hull** 1966	0°	-	-	-	-	-	-	30	30
	45°	-	-	-	-	-	-	47	40
Decker & Dutton** 1968	0°	-	-	5	-	-	-	-	-
	30°	-	-	6	-	-	-	-	-
	45°	-	-	8	-	-	-	-	-
	60°	-	-	9	-	-	-	-	-
Wulfsberg**, 1964	0°	-	-	-	3-8	-	-	-	10-30
	30°	-	-	-	3-9	-	-	-	10-30
	45°	-	-	-	4-10	-	-	-	10-30
	60°	-	-	-	5-11	-	-	-	10-30

*theory

** measurement

Hydrometeors

General

Droplets of liquid water in clouds and rain absorb, scatter, and emit microwave radiation. In some cases, the scattering of microwaves can be neglected when compared to processes of absorption and thermal emission. Several investigators have calculated the polarized sky temperature under various conditions of rain and clouds (Servey, 1964; Edison, 1966). The consideration of this general problem as it concerns applied microwave radiometry has just begun. Recently, Kreiss (1968) calculated theoretical values of microwave radiance over marine clouds by assuming that scattering is negligible and that α_c, the absorption coefficient of cloud droplets, is proportional to M, the liquid water content of the cloud (grams per cubic meter), and the square of the electromagnetic frequency. Comparison of these theoretically derived values to aircraft measurements of microwave radiance over clouds in the Gulf of Mexico shows that scattering can be neglected in all cases except where the maximum drop sizes are large.

Due to the freezing of the rotational motion of water in ice, absorption of microwaves by ice is quite low. This leads to a correspondingly low thermal emission for ice clouds. Flights of microwave radiometers in aircraft have shown that ice clouds are essentially transparent to microwave radiation and do not significantly emit microwave radiation.

Mie theory

Mie (1908) developed the rigorous solution to the problem of predicting the absorption and scattering of electromagnetic harmonic waves by a homogenous dielectric sphere of radius a and complex index of refraction m.

Since the absorption and scattering of microwaves by clouds of liquid water are caused by a finite number of individual droplets, it is convenient to introduce the concept of effective cross-sections as used in radar meteorology. Suppose the W_I is the power density (watts per square meter) of radiation incident upon a particular droplet of liquid water. The rate of extinction of energy by scattering (P_S, watts) or by absorption (P_A,watts) can be given in terms of an effective scattering cross section (Q_S, square meters)or an effective absorption cross section (Q_A, square meters), respectively. The effective cross section may bear little relationship to the actual cross-sectional area of the water droplet. The energy passing through these effective cross sections is the energy absorbed or scattered, that is:

$$C_A = P_A/W_I \qquad (m^2), \qquad (118)$$

and

$$Q_S = P_S/W_I \qquad (m^2). \qquad (119)$$

The rate at which energy is removed from a pencil of

radiation (P_T, watts) can be given in terms of Q_T the total extinction cross-section (m^2), where:

$$Q_T = Q_S + Q_A \qquad (m^2). \qquad (120)$$

The backscattering of microwave energy by water droplets is of importance to radar meteorology and may be important to microwave radiometry. According to Battan (1959), Q_B, the backscattering cross section, is "the area intercepting that amount of power, which, if scattered isotropically, would return to the receiver an amount of power equal to that actually received." Backscattering of solar microwave radiation by clouds and rains may be an important part of the microwave radiance of clouds as viewed from above during daytime.

Q_S, Q_A, and Q_B are functions of a, the drop radius, ν, the frequency of the radiation, and T, the temperature of the drop.

Aden (1952) gives the following expressions for Q_T, Q_S and Q_B from the Mie theory:

$$Q_T = -(\pi a^2/\delta^2) \sum_{n=1}^{\infty} (4n + 2)\ \mathrm{Re}\ (a_n + b_n) \qquad (m^2), \qquad (121)$$

$$Q_S = (\pi a^2/\delta^2) \sum_{n=1}^{\infty} (4n + 2)(|a_n|^2 + |b_n|^2) \qquad (m^2), \qquad (122)$$

and

$$Q_B = (\pi a^2/\delta^2) \left| \sum_{n=1}^{\infty} (-1)^n\ (2n + 1)(a_n - b_n) \right|^2 \qquad (m^2), \qquad (123)$$

where:

$$\delta = 2\pi a/\lambda = 2\pi a\nu/c \qquad (124)$$

and λ is the wavelength (meters).

a_n and b_n are the complex scattering-amplitude coefficients and are expressed in terms of spherical Bessel functions of the first and third kind of order n. See Stephens (1960) for exact expressions for a_n and b_n.

The absorption or scattering per meter is dependent upon n(a), the number of water droplets per unit volume of radius a, that is:

$$e_d(\nu) = \int_0^{a_m} n(a)\, Q_T\, (a,\nu,T)da \qquad \text{(nepers)}, \quad (125)$$

$$\alpha_d(\nu) = \int_0^{a_m} n(a)\, Q_A\, (a,\nu,T)da \qquad \text{(nepers)}, \quad (126)$$

and

$$s_d(\nu) = \int_0^{a_m} n(a)\, Q_S\, (a,\nu,T)da \qquad \text{(nepers)}, \quad (127)$$

where a_m is the maximum droplet radius found in the cloud and where the subscript d denotes phenomena associated with water droplets only. The expressions (125) - (127) might be understood best as the cross section (m^2) per unit volume (m^3).

The Mie expressions for Q_T, Q_S and Q_B are quite complicated, and only a few calculations of these quantities have been made and reported in the literature.

Approximations to the Mie theory

Ryde (1946) was able to compute values of attenuation of

microwave energy by clouds and rain based on accurate determinations of complex dielectric constant of water by Saxton. He assumed that the distribution of drop sizes was that given by Laws and Parsons (1943). Unfortunately, he only discussed Q_T and Q_B.

In the case of small water droplets ($r \leq 0.05$), Ryde (1946) found that:

$$e_c = \alpha_c = 0.000832\ C_1 M\nu/c\rho_L \quad \text{(nepers)}$$

$$= 4.093\ C_1 M\nu/c_L \quad \text{(db/km)}, \quad (128)$$

where M is the mass concentration of liquid water (grams of liquid water per cubic meter of air), ρ_L is the water density (grams per cubic centimeter), c is the speed of light (centimeter per second), ν is the frequency (Hz) and C_1 is dependent upon the temperature and frequency. Note that scattering is negligible in this case and that α_d is proportional to M. Values of α_c/M for temperatures of 0° C and 20° C were computed by Ryde and are given in Table XIV. The subscript c refers to cloud droplets.

Table XIV. The attenuation coefficient of non-raining clouds and for (α_c, db/km) per unit concentration of liquid water (M, g/m^3) for temperatures of 0° C and 20° C and for frequencies of 3, 6, 10, 15, and 30 GHz (after Ryde, 1946).

Frequency (GHz)	3	6	10	15	30
α_c/M at 0° C (db/km per g/m^3)	0.009	0.036	0.099	0.22	0.87
α_c/M at 20° C (db/km per g/m^3)	0.0045	0.018	0.05	0.11	0.44

Goldstein (1951) reasoned that one could neglect quadrupole and higher oscillations in the water droplet and consider only the scattering and absorption that results from dipole interactions. Thus, all scattering amplitude coefficients except a_1, b_1, and b_2 could be assumed to be zero. For small drop sizes ($\delta < 0.1$), one can express the Bessel functions as infinite series in terms of ascending powers of δ. Truncating terms involving δ^3 or higher, he found that:

$$Q_T = (c^2\delta^3/2\pi\nu^2)\ (C_2 + C_3\delta^2 + C_4\delta^3) \qquad (m^2), \qquad (129)$$

where c is the speed of light (m/sec) and ν is the frequency (Hz). The constants C_2, C_3 and C_4 are given by:

$$C_2 = 6\varepsilon''/[(\varepsilon' + 2) + \varepsilon''^2] \qquad \text{(dimensionless)}, \qquad (130)$$

$$C_3 = (\varepsilon''/15)\left[\frac{3(7\varepsilon'^2 + 4\varepsilon' - 20 + 7\varepsilon''^2)}{[(\varepsilon' + 2)^2 + \varepsilon''^2]^2} + 25/[(2\varepsilon' + 4\varepsilon''^2] + 1\right] \qquad \text{(dimensionless)}, \qquad (131)$$

and

$$C_4 = \frac{4}{3}\left[\frac{(\varepsilon'-1)^2(\varepsilon'+2)^2 + \varepsilon''^2(2(\varepsilon'-1)(\varepsilon'+2)-9)+\varepsilon''^4}{[(\varepsilon'+2)^2 + \varepsilon''^2]^2}\right] \qquad \text{(dimensionless)}. \qquad (132)$$

If $\varepsilon'' = 0$, C_2 and C_3 are equal to zero,

$$C_4 = \frac{4}{3}\frac{(\varepsilon' - 1)^2}{(\varepsilon' + 2)^2} \qquad \text{dimensionless}), \qquad (133)$$

and

$$Q_T \simeq Q_S = (2\pi^2\delta^6/3\pi\nu^2) \left|(\varepsilon' - 1)/(\varepsilon' + 2)\right|^2 \quad (m^2), \qquad (134)$$

which is the expression for the scattering cross-section according to Battan (1959).

If $\delta<<1$, then the terms of (129) involving C_3 and C_4 may be neglected and

$$Q_T \simeq Q_A = 4\pi^2\nu C_2\, a^3/c \qquad (m^2). \qquad (135)$$

Equation (135) is known as the Rayleigh Approximation for the absorption cross-section.

The volume of a spherical droplet of radius a is $(4\pi a^3/3)$ cubic meters. Regardless of the distribution of drop sizes in one cubic meter of atmosphere, if there are M grams of liquid water per cubic meter, then it follows that:

$$Q_A = 4.093\, MC_1\nu/c \qquad (m^2). \qquad (136)$$

According to Goldstein (1951), C_1 is proportional to frequency and

$$\alpha_c = 0.000487\, M\nu^2 \qquad (db/km), \qquad (137)$$

where ν is the frequency (GHz) and M is the liquid water content (g/m^3).

Values of α_c/M (db/km per g/m^3) calculated by Goldstein are presented in Table XV for 18° C.

Table XV. Absorption coefficient of non-raining clouds and fog (α_c, db/km) per unit concentration of liquid water (M, g/m^3) for a temperature of 18° C (after Goldstein, 1951).

Frequency, ν (GHz)	α_c/M (db/km per g/m^3)
3	0.0045
6	0.0178
10	0.05
15	0.112
24	0.28
30	0.438
42.9	0.876
60	1.65
150	7.14

The liquid water content of fog may be as high as one gram per cubic meter. Comparison of values of α_c in Table XV to values of α_g the absorption coefficient of molecular oxygen and water vapor given in Table X, shows that absorption and emission by clouds and fog are higher than absorption and emission of atmospheric gases for frequencies of 10 GHz or higher and for surface pressure and a temperature of 18° C.

Goldstein (1952) gives a set of correction factors for α_c for cases where the temperature is not equal to 18° C. Let F_1 (T) be such that:

$$\alpha_c(T) = \alpha_c(18°C)\ F_1\ (T) \qquad \text{(db/km)}. \quad (138)$$

Values of F_1 (T) are given in Table XVI.

Table XVI. Correction factor, $F_1(T)$ (dimensionless), for α_c in Table XV (after Goldstein, 1952).

Frequency, ν(GHz)	8° C	10° C	18° C	20° C	30° C	40° C
3	2.0	1.25	1.0	0.95	0.67	0.59
9.4	1.98	1.30	1.0	0.95	0.7	0.56
24	1.93	1.29	1.0	0.95	0.73	0.57
60	1.59	1.2	1.0	0.95	0.73	0.59

Goldstein discusses the attenuation by raindrops and calculates values of e_R, the extinction coefficient for raindrops, for various rates of precipitation (R, millimeter per hour) based on the distribution of drop sizes given by Laws and Parsons. Some of his values are listed in Table XVII.

From Table XVII, one can see that very substantial attenuation takes place for heavy rains and for high frequencies. Scattering is the dominant extinction process for raindrops having large diameters and for high frequencies (Goldstein, 1951).

Gunn and East (1954) have made calculations of e_R based on distributions of drop sizes other than that given by Laws and Parsons (1943). Again, no distinction was made between scattering and true absorption. Other investigators who have calculated Q_T or e_R using the Mie theory are Imai (1957) and Stephens (1961).

Emission of clouds and rain

According to Deirmendjian (1963),

Table XVII. Extinction coefficient for raindrops (e_R, db/km) for various precipitation rates (R, mm/hr) for a temperature of 18° C (after Goldstein, 1951).

Precipitation Rate, R (mm/hr)	Extinction coefficient, e_R (db/km) Frequency, (GHz)							
	3	9.4	10	19.35	24	30	50	60
0.25	0.00001	0.0019	0.00224	0.014	0.0215	0.037	0.106	0.16
1.00	- - - -	- - -	- - - -	0.062	- - -	- - -	- - -	- - -
1.25	0.00042	0.0117	0.0161	0.096	0.136	0.228	0.549	0.72
2.5	0.0079	0.0388	0.0388	0.208	0.298	0.492	1.08	1.34
4.0	- - - -	- - -	- - - -	0.32	- - -	- - -	- - -	- - -
12.5	0.00364	0.285	0.285	1.28	1.77	2.73	4.72	5.36
16.0	- - - -	- - -	- - - -	1.7	- - -	5.47	- - -	- - -
25.0	0.00728	0.656	0.656	2.70	3.72	10.7	8.59	9.49
50.0	0.0149	1.26	1.46	6.60	7.67	20.0	15.3	16.6
100.0	0.0311	3.24	3.24	11.3	15.3	28.8	27.0	29.0
150.0	0.0481	4.97	4.97	13.0	22.8	- - -	37.9	40.5

$$\alpha_c = 1.11 \times 10^{-7} \, M\nu^2 \qquad \text{(nepers)}, \quad (139)$$

where ν is the frequency (GHz) and M is the liquid water content of the cloud (g/m^3). Equation (139) is valid only for non-precipitating clouds. This relationship is similar to (137).

Following a suggestion by Buettner (1963, 1965), Kreiss (1968) used (139) to compute values of polarized sky temperature under various conditions of cloud thicknesses, cloud heights and concentrations of liquid water. Kreiss considered forty-two cases which are listed in Table XVIII. See his paper for more details. Space does not permit the presentation of his complete tabulations, but some values are presented in Table XIX. His curves give T_p^{sky} versus ν for (15 GHz $\leq \nu \leq$ 30 GHz).

The values of polarized sky temperature in Table XIX show how drastically T_p^{sky} is affected by various meteorological conditions. Since the sea reflects approximately two-thirds of the microwave radiation incident upon its surface at the nadir angle, it is easy to see that much of the upwelling radiation at the frequencies shown in Table XIX originates from thermal emission by atmospheric constituents. Also, tall cumulus clouds act nearly as black bodies for even moderate values of M. One should notice that the polarized sky temperature is not linearly proportional to M, the liquid water content, although α_c is proportional to M.

Decker and Dutton (1968) were able to map the liquid water

Table XVIII. List of cases considered by Kreiss (1968).

Case Numbers	Temperature	Humidity	Type of Cloud	Base of Cloud m	Top of Cloud m	Thickness of Cloud m	Liquid-water content (g/m^3)
1	S	D	N	N	N	N	N
2	S	S	N	N	N	N	N
3	S	W	N	N	N	N	N
4	H	D	N	N	N	N	N
5	H	S	N	N	N	N	N
6	H	W	N	N	N	N	N
7	C	D	N	N	N	N	N
8	C	S	N	N	N	N	N
9	C	W	N	N	N	N	N
10	S	S (SIC)	N*	628	1457	829	N*
11	S	S (SIC)	N*	628	7185	6557	N*
12-13	S	S (SIC)	F	SFC	280	280	0.0625, 1.0
14-16	S	S (SIC)	F	SFC	629	629	0.0625, 0.5, 1
17-22	S	S (SIC)	ST	628	1457	829	0.0625, 0.25, 0.5, 1, 2, 4
23-29	S	S (SIC)	ST	628	1949	1321	0.0625, 0.125, 0.25, 0.5, 1, 2, 4
30-36	S	S (SIC)	TST	628	3012	2384	0.0625, 0.12, 0.25, 0.5, 1, 2, 4
37-42	S	S (SIC)	TC	628	7185	6557	0.0625, 0.125, 0.25, 0.5, 1, 4

Table XVIII, (con't)

S - Standard temperature or humidity profile

H - Temperature profile for hot atmosphere**

C - Temperature profile for cold atmosphere**

D - Dry atmosphere**

W - Wet atmosphere**

SIC - Humidity 100% in cloud

F - Fog

ST - Stratus cloud

TC - Tall cumulus cloud

* Computed for water vapor and oxygen only

** See Kreiss (1968) for specific distributions of temperature and humidity.

Table XIX. Some values of polarized sky temperature (T_p^{sky}, °K) under various meteorological conditions (from Kreiss, 1968).

Case number from Table XVIII	Brief description of case	Frequency (GHz) 15.8	19.35	22.235
6	Hot, wet, cloudless	18	43	105
2	Standard temperature and humidity, cloudless	10	22	56
7	Cold, dry, cloudless	7	9	14
10	Standard, cloudless, saturated from 628-8457 m	12	27	64
11	Standard, cloudless, saturated from 628-6557 m	13	29	73
15	Standard, fog, 629 m thick, M = 0.5 g/m^3	19	37	73
16	Standard, fog, 629 m thick, M = 1 g/m^3	26	48	85
19	Standard, stratus from 628-1457 m, M = 0.5	21	40	77
20	Standard, stratus from 628-1457 m, M = 1.0	31	52	90
22	Standard, stratus from 628-1457 m, M = 4.0	80	118	160
40	Standard, tall cumulus from 628-7185 m, M = 0.5	190	230	255
41	Standard, tall cumulus from 628-7185 m, M = 1.0	250	265	275
42	Standard, tall cumulus from 628-7185 m, M = 4.0	280	280	280

content of thunderstorms over Colorado using a microwave radiometer operating at 10.7 GHz. They assumed that scattering was negligible and thus computed values of M times column length that are unrealistically high.

Cummings and Hull (1966) measured sky radiance at 23 GHz and 35 GHz under various meteorological conditions. These values are shown in Table XX using their word descriptions of the meteorological conditions existing at the time of the observations.

Table XX. Average values of measured vertically polarized sky temperatures (T_v^{sky}, °K) at Columbus, Ohio, for frequencies of 23 GHz and 35 GHz taken in the summers of 1964 and 1965 (after Cummings and Hull, 1966).

Meteorological condition	23 GHz		35 GHz	
	ψ^* = 0°	ψ = 45°	ψ = 0°	ψ = 45°
Clear sky	30	47	30	40
Fog	--	--	40	42
Light cloud cover	40	60	35	50
Moderate dark cloud cover	45	100	40	65
Dark cloud cover	140	160	50	70
Light rain	200	200	90	90
Heavy rain	255	255	120	120

*ψ is the zenith angle.

Comparing measured values in Table XX to theoretical values in Table XIX, one sees that the atmosphere was slightly cooler and dryer than the 1962 Standard Atmosphere assumed by Kreiss. The values of measured sky temperature agree very well with calculated values.

Weger (1960) also has calculated values of sky temperature for various conditions of cloud cover and rain using a simplified

engineering approach. Table XXI shows the results of his calculations. He assumed that the ARDC Model Atmosphere is valid and that relations given in (110) and (111) are valid.

Table XXI. Values of vertically polarized sky temperature (T_v^{sky}, °K) by Weger (1960) for various meteorological conditions.

Meteorological Conditions	Frequency, ν(GHz) 10	16.7	24	34.9
Clear sky	4	8	27	19
Uniform cloud, 900-1800 m M = 0.3 g/m^3	4	9	32	29
Uniform rain, 0-900 m R = 4 mm/hr	8	20	57	77

Weger's values differ greatly from Kreiss' values in Table XIX. This is probably a reflection of the simplified approach used by Weger.

Wulfsberg (1964) measured sky temperatures under various conditions of cloudiness and rain. His results are given in Table XXII.

Wulfsberg's measured values agree closely with Weger's theoretical values at near 17 GHz, but, they differ at 35 GHz.

Summary

From the preceeding tables, one can see that the presence of liquid water in the atmosphere can greatly affect the intensity

Table XXII. Measured values of polarized zenith sky temperature by Wulfsberg (1964) for various meteorological conditions.

Meteorological Condition	Frequency, ν (GHz) 15	17	35
Cold, dry, clear atmosphere	3	4	10
Hot, wet, clear atmosphere	8	12	29
Overcast clouds	13	--	57
Light rain (1 mm/hr)	14	20	41
Moderate rain (4 mm/hr)	31	26	112

of downward radiation from the atmosphere. All of the quantitative calculations have been made with the assumption that clouds do not scatter significantly and that the atmosphere is horizontally uniform in a state of local thermodynamic equilibrium. The extinction in rain is largely due to scattering (Deirmendjian, 1963) for centimeter wavelengths (3-30 GHz). One is prompted to ask the question: How does scattering affect the relationship between the environment and the intensity of microwave radiation?

Solar microwave radiation is a major source of extra-terrestrial microwave radiation. Forward scattering and back-scattering of solar radiation could result in a significant addition to the thermally emitted sky radiation. Side scattering of microwave radiation impinging upon a cloud from horizontal directions is another possible source of emission by scattering. On the other hand, one must consider the greatly increased

extinction that results in clouds due to scattering. If multiple scattering is dominant, one would expect the scattered radiation to be isotropic and equal to the average flux per unit solid angle of the radiation intercepted by the cloud. Before this matter can be pursued further, one must determine the polarized intensity of microwave radiation emerging from the surface. This is the subject of Chapter V.

CHAPTER V

EXTINCTION AND EMISSION IN THE HYDROSPHERE

General

When microwave radiation encounters the air-sea interface, it is partially reflected or scattered back into the atmosphere. The remaining radiation enters the hydrosphere and is quickly absorbed since sea water is a very absorptive material. The hydrosphere also emits microwave radiation into the atmosphere.

One may use certain models of the hydrosphere to predict its emissive and reflective characteristics. As a first approximation, one may assume that the air-sea interface is perfectly flat and that the active surface layer is homogenous in its temperature and dielectric properties. The active surface layer of the hydrosphere is that part of the hydrosphere in which the microwave energy from the atmosphere is absorbed and the thermally emitted microwave radiation originates. The active surface layer is usually no thicker than a few multiples of the wavelength of the microwave radiation under consideration. In the case of two homogenous dielectric materials separated by a flat boundary, one may use Fresnel's Laws of Reflection to predict the polarized reflectivities of the interface. Through thermodynamic considerations, one may relate the polarized emissivities of the hydrosphere to its polarized reflectivities by use of

(58) and (59).

The actual air-sea interface is not flat; indeed, it is quite rough. In fact, it is sometimes impossible to define a single air-sea interface under conditions of high shearing stress when bubbles and foam form on the sea surface. Blown salt spray may also complicate the problem.

One may add a certain degree of reality to the case of a perfectly flat sea surface by assuming that the air-sea interface has an irregular shape which is smooth. According to Beckman and Spizzichino (1963), a surface may be treated as a smooth surface if its radius of curvature is many times larger than the wavelength of the radiation under consideration. These assumptions hold very well for the actual sea surface when infrared and visible radiation are under consideration. In the case of microwave radiation, only gravity waves have radii of curvature suitable to the condition of smoothness required. At any rate, one may assume that Fresnel's law of reflection is valid at a particular point on the surface, and one may compute mean polarized emissivities by integrating over the slope distribution (Buettner et al., 1968).

Finally one may treat the sea surface as a scattering surface. A knowledge of γ, the bistatic scattering cross section per unit area, is needed in this case. Scientists have been unable to determine the form of γ from purely theoretical grounds. Thus, they resort to making educated guesses as to the form of γ

for the sea and other natural surfaces.

Peake et al., (1966) have suggested several forms for γ for land surfaces. Stogryn (1967) and Janza (1968) have proposed models for γ for the sea surface.

The purpose of this chapter is to review the problem of predicting the polarized reflective and emissive temperatures of the sea for the three cases of a flat surface, an irregular smooth surface, and a rough surface of the sea.

Flat Sea Surface

Fresnel's Laws of Reflection

The polarized electric reflection coefficients for two homogenous dielectrics separated by a flat boundary are given by Jordon (1950) as:

$$\rho_v = \frac{(\varepsilon_2/\varepsilon_1)\cos\psi - \sqrt{(\varepsilon_2/\varepsilon_1) - \sin^2\psi}}{(\varepsilon_2/\varepsilon_1)\cos\psi + \sqrt{(\varepsilon_2/\varepsilon_1) - \sin^2\psi}} \quad \text{(dimensionless)}, \quad (140)$$

and

$$\rho_h = \frac{\cos\psi - \sqrt{(\varepsilon_2/\varepsilon_1) - \sin^2\psi}}{\cos\psi + \sqrt{(\varepsilon_2/\varepsilon_1) - \sin^2\psi}} \quad \text{(dimensionless)}, \quad (141)$$

where:

ρ_v = vertically polarized reflection coefficients for the electric field (dimensionless),

ρ_h = horizontally polarized reflection coefficients for the electric field, (dimensionless),

ε_1 = the complex dielectric constant of the first medium (dimensionless),

ε_2 = the complex dielectric constant of the second medium (dimensionless),

and

ψ = angle of incidence.

The radiation is assumed to be plane polarized radiation coming from medium 'one' toward medium 'two'. In the case of a homogenous layer of sea water overlain by air, ε_1, is equal to unity, and ε_2 is equal to $\varepsilon' - j\varepsilon''$ as given in Chapter II for sea water.

The polarized reflectivity is equal to the square of the polarized electric reflectivity. Thus:

$$r_v = \left| \frac{(\varepsilon' - j\varepsilon'')\cos\psi - \sqrt{(\varepsilon' - j\varepsilon'') - \sin^2\psi}}{(\varepsilon' - j\varepsilon'')\cos\psi + \sqrt{(\varepsilon' - j\varepsilon'') - \sin^2\psi}} \right|^2 \quad \text{(dimensionless)}, \qquad (142)$$

and

$$r_h = \left| \frac{\cos\psi - \sqrt{(\varepsilon' - j\varepsilon'') - \sin^2\psi}}{\cos\psi + \sqrt{(\varepsilon' - j\varepsilon'') - \sin^2\psi}} \right|^2 \quad \text{(dimensionless)}. \qquad (143)$$

Reflective temperature of a flat sea surface

Values of ε' and ε'' were computed in Chapter II and were given for specific values of temperature, salinity, and frequency in Table VII as obtained from equations (33), (34), (36), (37), and (38). Using these equations, one may compute r_p as a function

of ν, S, and T for any given ψ and polarization. If T_p^{sky} is also known, then:

$$T_p^r (\nu,S,T,\psi) = r_p (\nu,S,T,\psi)\, T_p^{sky} (\nu,\psi) \qquad (°K) \qquad (144)$$

Emissive temperature of a flat sea surface

When a flat sea surface is under conditions of local thermodynamic equilibrium, the polarized emissivities of that surface are given as:

$$\xi_p = 1 - r_p \qquad \text{(dimensionless)}. \qquad (145)$$

From (58) and (145) it follows that:

$$T_p^e = (1 - r_p)\, T_{sea} \qquad (°K), \qquad (146)$$

where T_p^e is the polarized emissive temperature of the sea.

Brightness temperature of a flat sea surface

The term polarized brightness temperature (T_p, °K) is now defined as the effective blackbody temperature associated with the total polarized upwelling microwave radiational intensity. T_p is a function of height and other variables. Now, it may be stated that:

$$T_p (z = 0) = r_p T_p^{sky} + (1 - r_p) T_{sea} \qquad (°K). \qquad (147)$$

For purposes of illustration, values of $T_p(0)$ have been

computed for an incidence angle of 0°. Table XXIII shows values of r_p, ξ_p, T_p^e, T_p^r, and T_p for frequencies of 1, 6, 9 3, 15.8, 19.35, 22.235, and 34 GHz, for temperatures of 10° C and 20° C, and for salinities of 10 and 35 o/oo. The assumed values of T_p^{sky} were taken from Table XXIII for average meteorological conditions.

Measurements of the microwave radiance of the sea are available for incidence angles near 0° and for frequencies of 9.3, 15.8, 19.35, 22.235, and 34 GHz. From Table XXIII, it is seen that T_p does not change more than 3° K for a change in sea temperature from 10° C to 20° C at these frequencies. This is due, in part, to the fact that the polarized emissivity of the sea decreases with increasing temperature; consequently, the polarized emissive temperatures of the sea remain fairly constant. In fact, for a frequency of 34 GHz, the sea emits less radiation when the temperature is 20° C than when it is 10° C!

The frequency domain below 8 GHz is of interest because of the low attenuation by the atmosphere and the small values of polarized sky temperature. The values in Table XXIII for frequencies of 1 GHz and 6 GHz show many interesting features about the emission and reflection of the sea surface for these low microwave frequencies. The effect of changes in salinity on T_p at 1 GHz is quite large. For a water temperature of 20° C, a change in salinity from 10 o/oo to 35 o/oo results in a decrease of T_p by 18.9° K. There is also a pronounced effect on T_p due to

Table XXIII. Reflectivity, emissivity, emissive temperature, reflective temperature, and brightness temperature of a flat sea surface for various frequencies, temperature, and salinity and for an incidence angle of 0°.

Frequency ν, (GHz)	Sea Temp. T_{sea} (°C)	Salinity S (o/oo)	Polarized Reflectivity r_p	Polarized Emissivity $\xi_p = 1-r_p$	Polarized Emissive Temp. T_p^e (°K)	Polarized Sky Temp. T^{sky} (°K)	Polarized Reflective Temp. T_p^r (°K)	Polarized Brightness Temp. T_p (°K)
1	10	10	0.650	0.350	99.1	12	7.8	106.9
1	10	35	0.697	0.303	85.7	12	8.4	94.1
1	20	10	0.649	0.351	102.8	12	7.8	110.6
1	20	35	0.717	0.283	83.1	12	8.6	91.7
3	10	10	0.642	0.358	101.5	7.0	4.5	106.0
3	10	35	0.647	0.353	100.1	7.0	4.5	104.6
3	20	10	0.637	0.363	106.4	7.0	4.5	110.9
3	20	35	0.647	0.353	103.4	7.0	4.5	107.9
4	10	10	0.640	0.360	102.1	6	3.8	105.9
4	10	35	0.641	0.359	101.7	6	3.8	105.5
4	20	10	0.636	0.364	106.9	6	3.8	110.7
4	20	35	0.640	0.360	105.6	6	3.8	109.4

Table XXIII. (con't.)

Frequency ν, (GHz)	Sea Temp. T_{sea} (°C)	Salinity S (o/oo)	Polarized Reflectivity r_p	Polarized Emissivity $\xi_p = 1-r_p$	Polarized Emissive Temp. T_p^e (°K)	Polarized Sky Temp. T_p^{sky} (°K)	Polarized Reflective Temp. T_p^r (°K)	Polarized Brightness Temp. T_p (°K)
6	10	10	0.634	0.366	103.5	4.0	2.5	106.1
6	10	35	0.634	0.366	103.6	4.0	2.5	106.1
6	10	10	0.632	0.368	107.8	4.0	2.5	110.3
6	10	35	0.632	0.368	107.8	4.0	2.5	110.3
9.3	10	10	0.623	0.377	106.7	3.5	2.2	108.9
9.3	35	35	0.622	0.378	107.1	3.5	2.2	109.3
9.3	10	10	0.625	0.375	109.9	3.5	2.2	112.1
9.3	35	35	0.624	0.376	110.4	3.5	2.2	112.6
15.8	10	10	0.596	0.404	114.3	10.0	6.0	120.3
15.8	10	35	0.595	0.405	114.6	10.0	6.0	120.6
15.8	10	10	0.608	0.392	115.1	10.0	6.0	121.7
15.8	10	35	0.605	0.395	115.7	10.0	6.0	134.4

Table XXIII. (con't.)

Frequency ν, (GHz)	Sea Temp. T_{sea} (°C)	Salinity S (o/oo)	Polarized Reflectivity r_p	Polarized Emissivity $\xi_p = 1-r_p$	Polarized Emissive Temp. T_p^e (°K)	Polarized Sky Temp. T_p^{sky} (°K)	Polarized Reflective Temp. T_p^r (°K)	Polarized Brightness Temp. T_p (°K)
19.35	10	10	0.581	0.419	118.7	27	15.7	134.4
19.35	10	35	0.580	0.420	119.0	27	15.7	134.7
19.35	20	10	0.596	0.404	118.3	27	16.1	134.4
19.35	20	35	0.594	0.406	118.9	27	16.0	134.9
22.235	10	10	0.568	0.432	122.3	56	31.8	154.1
22.235	10	35	0.567	0.433	122.5	56	31.8	154.3
22.235	20	10	0.587	0.413	121.0	56	32.9	153.9
22.235	20	35	0.585	0.415	121.6	56	32.8	154.4
34.0	10	10	0.520	0.480	136.0	26	13.5	149.5
34.0	10	35	0.520	0.480	136.0	26	13.5	149.5
34.0	20	10	0.549	0.451	132.1	26	14.3	146.4
34.0	20	35	0.548	0.452	132.6	26	14.2	146.8

temperature at this frequency.

Figure 8 shows a plot of T_p^e versus T_{sea} for frequencies of 1, 5.4, 9.3, 15.8, 19.35, 22.235, and 34 GHz and for various values of salinity. The effect of salinity is negligible for frequencies higher than 5.4 GHz. The curves in Figure 8 show that the same emissive temperature may be the result of two different values of sea temperature for frequencies of 15.8, 19.35 and 22.234 GHz. At 5.4 GHz, there is no salinity effect, and it appears that the emissivity is practically constant with temperature. The pronounced effect of salinity at 1 GHz is obvious from Figure 8. Also, it should be recalled from Chapter IV that the polarized sky temperature for these frequencies is small and fairly constant since it is mostly the result of pressure broadening oxygen emission. The natural variability of water vapor has little effect at these frequencies.

It is proposed, therefore, that the temperature and salinity of sea water could be measured remotely by use of a dual-channel microwave radiometer operating near 5.4 GHz and 1 GHz. The first step would be to determine the temperature of the water through measurements at 5.4 GHz, and, having determined the temperature, one could infer the salinity of the water from the measurements at 1 GHz. The accuracy of these environmental measurements is of course, dependent upon the accuracy of the remote measurements. Also, the existance of foam on the sea surface would invalidate these measurements.

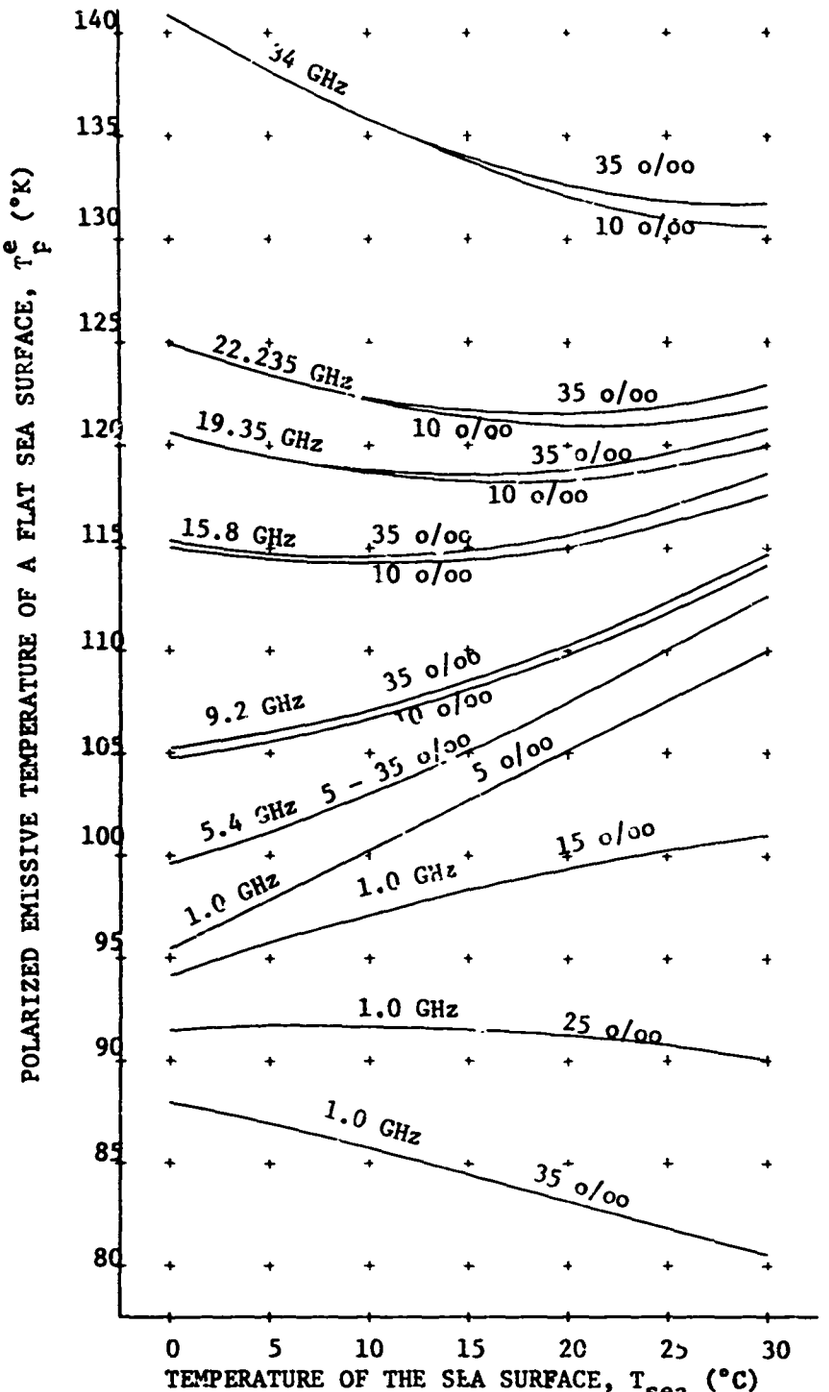

Figure 8. The polarized emissive temperature of a flat sea surface versus the thermometric temperature of the sea surface for frequencies of 1, 5.4, 9.2, 15.8, 19.35, 22.235, and 34 GHz and for various salinities.

Any further discussion of these possibilities will be postponed until roughness effects and instrument effects have been considered.

Marandino (1967) studied the brightness temperature of the sea as a function of sea temperature and frequency. For ocean water, he determined ΔT_p^e, the change in polarized emissive temperature (°K), that results when the temperature of the sea surface is changed from 273° K to 300° K. His results are shown in Figure 9.

He found that the polarized emissive temperature is most sensitive to changes in temperature at 5 to 6 GHz and is least sensitive to temperature at 1.4 GHz.

Sirounian (1968) studied the effect of salinity on T_p^e at a frequency of 3 GHz. He found that the effect of salinity was largest for incidence angles near zero and that a salinity change from 6.7 o/oo to 32 o/oo resulted in a decrease of T_p^e of 3 to 4° K for a sea temperature of 25° C and for an angle of incidence of zero. These results agree with the values obtained by Paris (1968).

Smooth Irregular Sea-Surface

Buettner, et. al. (1968) have considered the effect of roughness on T_p for centimeter wavelengths. They assumed that the sea surface acts as a specular reflector for any given facet of the surface and determined the effective emissivity by

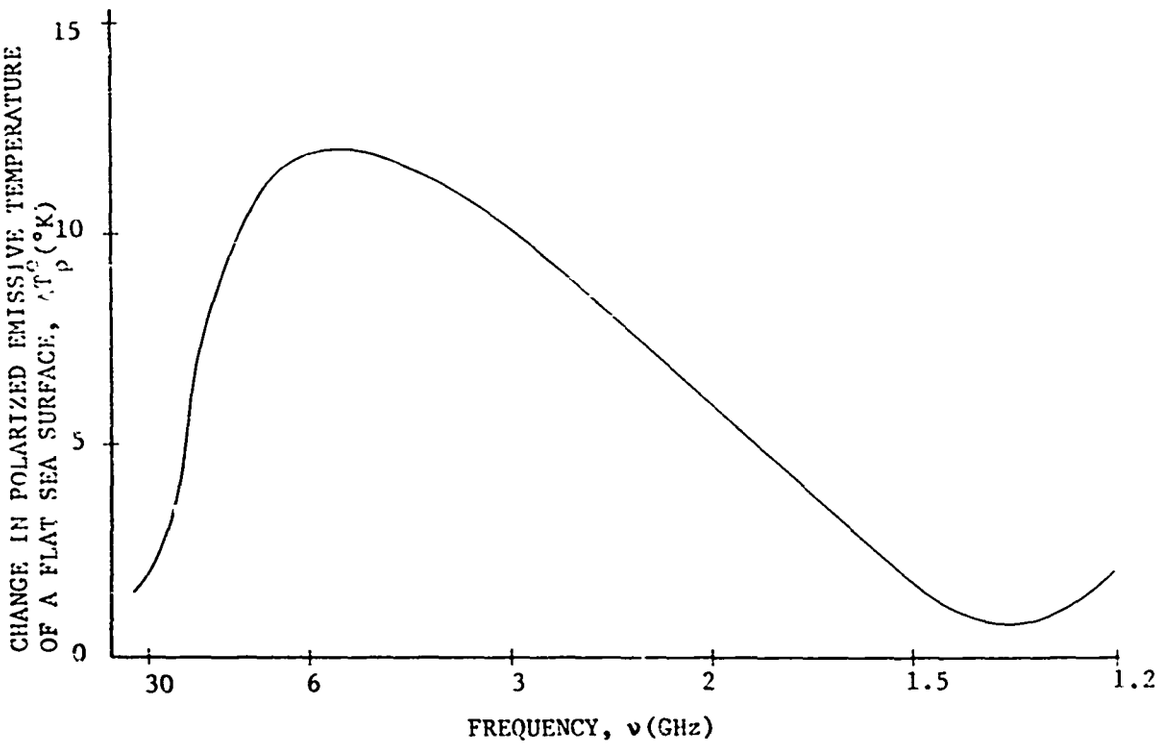

Figure 9. The change in polarized emissive temperature of a flat sea surface due to a change in water temperature from 273° K to 300° K versus frequency (after Marandino, 1967).

integrating over the distribution of sea slopes given by Cox and Munk (1954a, 1954b). Their estimates show that the emissivity increases with increasing roughness; but, the increase is largest at large incidence angles of observation. In fact, the emissivity does not appear to be a function of roughness for incidence angles near zero. This is probably due to the fact that the reflectivity of a flat sea surface is fairly constant with angle for incidence angles near zero (Saxton and Lane, 1952)

In addition to the change in the effective emissivity of the sea surface with roughness, one should consider the effect of roughness on the reflected radiation. Two effects are present in this regard. First, the effective reflectivity or albedo changes with the distribution of slopes to a slight extent. Second, the source of the reflected radiation changes since sky radiation at all incidence angles is reflected, to some extent, in a given direction by the irregular surface. The sky temperature is highly dependent upon incidence angle for any given atmospheric condition since the path length increases with increasing incidence angle. From Table XIII, one can see that the sky temperature may be 60° K higher for incidence angles of 60° than for incidence angles near zero for frequencies near the absorption line of water vapor. This effect is not so severe for frequencies less than 10 GHz. In addition to other effects, one effect of roughness is to increase the amount of reflected radiation for frequencies near 22.235 GHz.

Rough Sea Surface

General

The actual sea surface is rough and scatters microwave energy. To determine the value of the polarized brightness temperature of a rough surface, one must know its bistatic scattering coefficients per unit area, as defined by (75) through (78) and T_p^{sky}, the polarized sky temperatures as a function of incidence angle. Peake (1959) shows that:

$$T_h^r = (1/4\pi)\iint\left[T_h^{sky}\ \gamma_{hh} + T_v^{sky}\ \gamma_{hv}\right] d\Omega \qquad (°K), \qquad (148)$$

and

$$T_v^r = (1/4\pi)\iint\left[T_v^{sky}\ \gamma_{vv} + T_h^{sky}\ \gamma_{vh}\right] d\Omega \qquad (°K), \qquad (149)$$

where the integrations indicated in (148) and (149) are performed over the upper hemisphere. From (58), (80), (81), (86), the polarized emissive temperatures, T_h^e and T_r^e, are expressed as:

$$T_h^e = T_{sea}\ \{1 - (1/4\pi)\int\ [\gamma_{hh} + \gamma_{hv}]d\Omega\} \qquad (°K), \qquad (150)$$

and

$$T_v^e = T_{sea}\ \{1 - (1/4\pi)\int\ [\gamma_{vv} + \gamma_{vh}]d\Omega\} \qquad (°K), \qquad (151)$$

where the integration is performed over the upper hemisphere.

The definitions of bistatic cross section per unit area

give no indication of the physics of scattering as such. The problem of scattering of electromagnetic waves by an irregular surface cannot be approached in a rigorous fashion. Some approximations have been developed.

Kirchhoff approximation

Stogryn (1967) reasoned that the Kirchhoff approximation can be used to give the scattering coefficients per unit area for a very rough surface. He assumed that the distribution of wave slopes given by Cox and Munk (1954a, 1954b) is valid and that the root-mean-squared wave slopes (g_x and g_y) depend on the wind speed (w, m/sec) at 41 feet above the mean sea-surface, that is:

$$g_x^2 = 0.003 + 1.92 \times 10^{-3} w, \tag{152}$$

and

$$g_y^2 = 3.16 \times 10^{-3} w, \tag{153}$$

where the x-axis lies cross wind and the y-axis lies parallel to the wind.

The exact expressions for γ_{hh}, γ_{vv}, γ_{hv}, and γ_{vh} are quite complex. The reader is referred to the compact expression of these quantities in Stogryn's paper since it is impossible to obtain any analytic information from these expressions explicitly. The results of his studies agree, in general, with the results of the previous case of a smooth irregular surface. In general,

the horizontally polarized brightness temperature increases with increasing wind speed for incidence angles between zero and 70° at all frequencies in the microwave domain. This increase is largest for incidence angles near 50°.

Qualitatively, it appears that the horizontally polarized brightness temperature may be increased by as much as 20° K due to increased roughness. The vertically polarized brightness temperature of the sea is not noticeably affected by roughness (Stogryn, 1967).

Any further discussion of the roughness effect will be postponed until Chapter VI where the extinction and emission of the intervening atmosphere between the aircraft or spacecraft and the sea will be considered.

Foam, Bubbles, and Ice

General

In each of the three cases treated previously, it was assumed that a single liquid-gas interface existed between these two homogenous dielectrics. This surface was allowed to be quite irregular and rough. In the case of the real air-sea boundary, large surface shearing stresses often result in the formation of bubbles and foam on the sea surface. In this case, one cannot use equations developed for a single boundary between two homogenous dielectrics. There is no physical theory that is adequate to describe the

effective dielectric constant of this domain consisting of multiple layers of water films and air spaces of random orientation and thickness.

Also, in some parts of the World Ocean, the surface of the hydrosphere is covered to some extent by ice of various thickness and shape. The great difference between the dielectric constant of ice and of sea water has been noted in Chapter II. This difference should result in a large difference between the polarized brightness temperature of sea water and that of sea ice on the water.

Foam and bubbles

The only information in the literature on the effects of foam on the polarized brightness temperature of the sea is the experiment performed by Williams (1968). Using the microwave radiometers on the Convair 240A operated by NASA, he made measurements of the antenna temperature[7] of water in a large portable swimming pool placed in front of the aircraft while it was parked on the runway of the Miami International Airport in June 1967. Measurements were made of the reflected sky radiation, a smooth water surface, a surface of bubbles, and a surface of foam. His values are shown in Table XXIV.

---

[7] This quantity is discussed in detail in Chapter VII.

Table XXIV. Results of ground measurements of the emission of the sky, smooth water, bubbles, and foam by Williams (1968).

Condition	Antenna temperature, T_a (°K) 9.4 GHz	15.8 GHz	22.235 GHz	34 GHz
Reflected Sky	90	120	150	170
Smooth Water	170	190	218	224
Bubbly water	185	210	240	260
Foamy Water	295	280	285	310

Serious doubt must be cast on the absolute accuracy of these measurements due to the fact that the measurements were made in the near field of the radiometers. Note the unusually high values of reflected sky temperature.

It is evident from values in Table XXIX that the emissivity of foam approaches unity. Thus, as Williams proposed, one should be able to measure the amount of foam coverage on the sea surface by observing the increase in the antenna temperature that results when a large area is viewed by a microwave radiometer in which there exists some foam covered areas and some open areas. The percentage of coverage by foam is related to the surface wind speed (Munk, 1947; Blanchard, 1963). Foam appears to raise the apparent brightness temperature of the sea surface significantly for all frequencies, polarizations, and incidence angles.

Ice

There have been many excellent papers written on the microwave emission of ice. The paper by Pascalar and Sakamoto (1965) is quite representative. Two cases will be considered. First, predictions are made of the polarized brightness temperature of a large ice domain such as that of an iceberg. Secondly, the brightness temperature of horizontal sheets of ice overlying water is studied.

In the first case, one may consider the problem of determining the reflectivity of a homogenous dielectric having a flat surface. The dielectric constant of ice can be taken to be 3.165-j0.003 (see Chapter II). Using (143), one finds that the reflectivity of ice is 0.08 for ψ equal to zero. Therefore, the emissivity of ice for incidence angles near 0° is about 0.92. If one considers the difference between the emission of ice at a temperature of 273° K and the combined emission and reflection of sea water at a temperature of 273° K and for a frequency of 9.2 GHz, for example, then one finds that the polarized brightness temperatures are 251° K and 107° K, respectively. The difference between these two values is 144° K and is easily measured by microwave radiometers in use today. In fact, scanning microwave radiometers operating near 13 GHz are being used by the U.S. Coast Guard to survey icebergs in the North Atlantic Oceans (Roeder, 1967). In the field, the microwave radiometers do not 'see' as large a

brightness temperature difference as indicated above since the iceberg does not occupy the entire field of view of the sensor. The size of the increase in brightness temperature is used, qualitatively, to distinguish between large and small icebergs.

Since the imaginary part of the dielectric constant of ice is small, one would expect ice to be nearly lossless. This property of ice can be used to measure remotely the thickness of horizontally uniform ice sheets overlying water. The reflectivity, r_p^i, of an ice sheet of thickness ℓ over water for normal incident is easily deduced from standard text books on electromagnetic theory (for example, Ramo, et.al., 1965) and may be expressed as:

$$r_p^i = \left|(Z_L - Z_1)/(Z_L + Z_1)\right|^2 \qquad \text{(dimensionless)}, \qquad (154)$$

where Z_1 is the impedence of air (377 ohms) and where:

$$Z_L = Z_i \frac{Z_w \cos(2\pi\ell/\lambda_i) + jZ_i \sin(2\pi\ell/\lambda_i)}{jZ_i \cos(2\pi\ell/\lambda_i) + jZ_w \sin(2\pi\ell/\lambda_i)} \qquad \text{(ohms)}, \qquad (155)$$

$$Z_w = \sqrt{\mu_o/\varepsilon_o(\varepsilon_w' - j\varepsilon_w'')} \qquad \text{(ohms)}, \qquad (156)$$

$$Z_i = \sqrt{\mu_o/\varepsilon_o\varepsilon_i} \qquad \text{(ohms)}, \qquad (157)$$

$$\lambda_i = c/\nu\sqrt{\varepsilon_i} \qquad \text{(meters)}, \qquad (158)$$

$\varepsilon_w' - j\varepsilon_w''$ is the complex dielectric constant of water, and ε_1 is the dielectric constant of ice (about 3.165).

One should note that the arguments of the trigonometric functions in (155) involve the thickness of the ice and the wavelength of the electromagnetic wave in the ice (λ_i, meters). Since these functions are periodic, one would expect that r_p^i is periodic in ℓ. Thus, the polarized brightness temperature is not single valued with respect to the ice thickness. It does not appear that measurements of ice thickness could be made by a single channel microwave radiometer. This could be done, however, with a multi-frequency radiometer since λ_i would change with frequency.

CHAPTER VI

INTENSITY OF UPWELLING MICROWAVE RADIATION

General

The purposes of this chapter are to illustrate the intensity field of upwelling microwave radiation for several general cases as a function of appropriate physical parameters of the hydrosphere and atmosphere and to discuss the relative advantages and disadvantages of using various polarizations, incidence angles, and microwave frequencies to study, remotely, certain aspects of this marine environment. One should recall at this point that intensity is a quantity that is, strictly speaking, impossible to determine with practical sensors. Regardless, the concept of intensity must be retained until the next chapter where the effects of the antenna characteristics of the microwave radiometer used to measure microwave radiation will be considered. Then, the intensity field may be weighted by the gain pattern of the antenna to predict theoretical values of actual measurements by microwave radiometers.

This chapter is concerned only with the upwelling microwave radiation that is passing through some point above the surface of Earth in the atmosphere where aircraft may operate or in 'free' space where an Earth satellite may operate.

Let $T_p\ (h_o,\psi)$ be the polarized brightness temperature of the

upwelling microwave radiation at height, h_o (meters), and for an incidence angle of ψ. In Chapter V, $T_p\ (0,\psi)$ was discussed. In the case of a non-scattering, horizontally uniform atmosphere, it follows from (87) that:

$$T_p\ (h_o,\psi) = T_p\ (0,\psi)\ \exp[-\sec\psi \int_o^{h_o} \alpha(z)\ dz]$$

$$+ \sec\psi \int_o^{h_o} \alpha(z)\ \ T(z)\ \exp[-\sec\psi \int_z^{h_o} \alpha(z)\ dz]dz$$

$$(°K). \qquad (159)$$

The first term of (159) refers to the portion of the emitted and reflected microwave radiation that reaches height, h_o, after partial extinction. The second term of (159) refers to the direct contribution from the atmosphere between h_o and the surface.

One may immediately describe two special cases. In the first case, h_o is above 20 kilometers. In this case, the radiometer is above most of the radiating part of the atmosphere. Due to the high transmissivity of the atmosphere, one may assume that the atmosphere emits upward at the same intensity that it emits downward for the same incidence angle. The author has computed the brightness temperature of upwelling microwave radiation at 19.4 GHz using Stogryn's (1967) values for fractional absorption and found that it differs by only a few hundreths of a degree from the sky-temperature calculated for the same incidence angles. Thus, for a clear atmosphere, it is assumed that:

$$T_p^{air}\ (\nu,\psi,h_o \geq 20\ \text{km}) = T_p^{sky}\ (\nu,\psi) \qquad (°K), \qquad (160)$$

where T_p^{air} represents the second term of (159) in terms of an apparent brightness temperature (°K), and where T_p^{sky} is the polarized sky temperature as used in Chapter IV. The angle, ψ, represents both the incidence angle and angle of observation since they are equal interior angles.

In the second case, h_o is very small (less than one kilometer). In this case, one may treat the intervening atmosphere as an isothermal, homogenous layer and compute its emission by:

$$T_p^{air}(\psi, h_o \leq 1 \text{ km}) \quad \bar{T}\,[1 - \exp(-\bar{\alpha} h_o] \qquad (°K), \qquad (161)$$

where $\bar{T}$ is the mean temperature of the layer (°K) and where $\bar{\alpha}$ is the mean value of the absorption coefficient of the layer.

Five special cases will be considered in the next sections. These cases are listed in Table XXV. The purpose in presenting these cases is to illustrate the effect of salinity, temperature, roughness, incidence angle, polarization, frequency, humidity, clouds, and altitude on the field of brightness temperature at some point above Earth. The effect of temperature as a variable has been considered before in Chapter V (see Figure 8).

Salinity Effect

One of the most important parameters of the hydrosphere is its salinity. The salinity of the surface layer of the sea is usually 34 to 37 o/oo. Near coastlines, the salinity may vary between 5 o/oo and 37 o/oo due to the influence of coastal runoff of precipitation

Table XXV. List of special cases considered in Chapter VI.

Case Name	Frequencies ν(GHz)	Temperature of the Sea T_{sea} (°C)	Salinity of the Sea S (o/oo)	Angles of Observation ψ (degrees)	Humidity	Clouds	
						Type	Liquid Water Content
Salinity Effect	1,5.4,9.3, 15.8,19.35, 22.235,34	10	0 - 36	0	Standard	Clear	0
Salinity Effect	1,5.4,9.3. 15.8,19.35, 22.235,34	30	0 - 36	0	Standard	Clear	0
Effect of Water Vapor	19.35, 22.235	15	36	0	3,7.5,17 (g/m^3)	Clear	0
Effect of Roughness	19.4, 35	17	36	0 - 50	Standard		
Effect of Liquid Water	35,19.35	25	36	0	Standard (saturated in clouds)	Stratus Tall Cumulus	0.0625 4(g/m^3)

or river outflow. Temperatures in the ocean are usually between -1° C and 30° C. To illustrate the effect of changes in salinity on the polarized brightness temperature, the following environmental conditions have been assumed:

1. Let the temperature of sea water be held at 10 °C.

2. Assume that the sea surface is flat, smooth, and non-foamy.

3. Let the incidence angle, ψ, be zero so that the maximum effect of salinity may be ascertained (Sirounian, 1968). The previous studies of the effect of roughness show that the emissivities of a rough and smooth surface for near zero degrees are practically identical as long as there is no foam on the surface.

4. Assume that there are no clouds present in the atmosphere and that the atmosphere is in a standard state as far as its temperature, humidity, and pressure dependence or height are concerned.

5. Let the height of the observer be one kilometer.

6. Let the salinity, S, vary from 0 o/oo to 36 o/oo.

Figure 10 shows plots of T_p ($\nu, h_o = 1, \psi = 0$, S, T = 10 C°) versus S for frequencies of 1, 5.4, 9.3, 15.8, 19.35, 22.235, and 34 GHz. The polarized sky temperatures have been taken from Table XIII. The specific values used in the calculations are given in Table XXVI. The mean temperature of the layer of atmosphere between the surface and one kilometer is taken to be 283° K. The absorption coefficient for molecular oxygen and water vapor

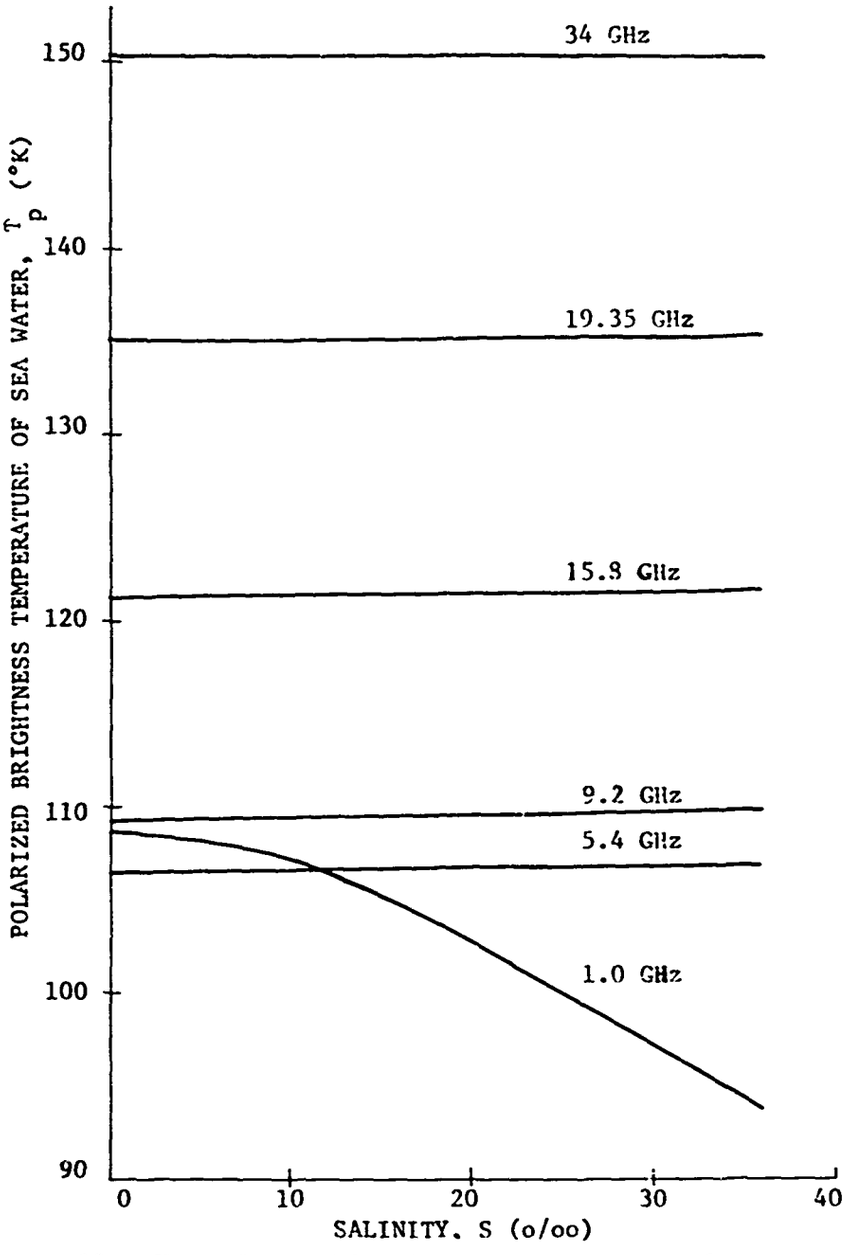

Figure 10. The polarized brightness temperature of sea water versus salinity for a water temperature of 283° K, for an incidence angle of 0°, for frequencies of 1, 5.4, 9.2, 15.8, 19.35, and 34 GHz and for an altitude of 1 km.

are taken from Table X for a density of water vapor of 7.5 grams per cubic meter. These values are also shown in Table XXVI. The values of the transmissivity and emissivity of the layer of atmosphere from the surface to a height of kilometer are also shown in Table XXVI as they are derived from the mean absorption coefficient.

It can be seen from Figure 10 that salinity affects the polarized brightness temperature significantly for a frequency of 1 GHz and insignificantly at the other frequencies shown.

Calculations were made of the polarized brightness temperature under the same conditions as above with two exceptions: the temperature of the sea water was assumed to be 30° C, and the mean temperature of the layer from the surface to one kilometer was assumed to be 294° K. The values of sky temperature also were increased to more representative values for humid, summertime conditions over the tropical ocean. The results of the calculations for this case are shown in Figure 11.

One can see that the salinity effect at 1 GHz is much greater for a water temperature of 30° C than for a temperature of 10° C. Again, the polarized brightness temperatures for the other frequencies shown in Figure 11 are practically constant with salinity. Thus, it appears that one may be able to determine the temperature and salinity of the sea surface to some degree of accuracy by measuring the intensity of microwave radiation at 5.4 GHz and 1.0

Table XXVI. Assumed atmospheric parameters and derived quantities used in calculating values of brightness temperature given in Figure 10.

Frequency, ν(GHz)	1.0	5.4	9.3	15.8	19.35	22.235	34
Zenith sky temperature T_p^{sky} (°K)	12	5	3.5	10	22	56	20
Mean absorption coefficient from 0 to 1 km	0.0016	0.0023	0.0032	0.0069	0.0239	0.041	0.0299
Transmissivity of surface layer of atmosphere	0.9984	0.9977	0.9968	0.9932	0.9770	0.9607	0.9702
Emissivity of surface layer of atmosphere	0.0016	0.0023	0.0032	0.0068	0.023	0.0393	0.0298

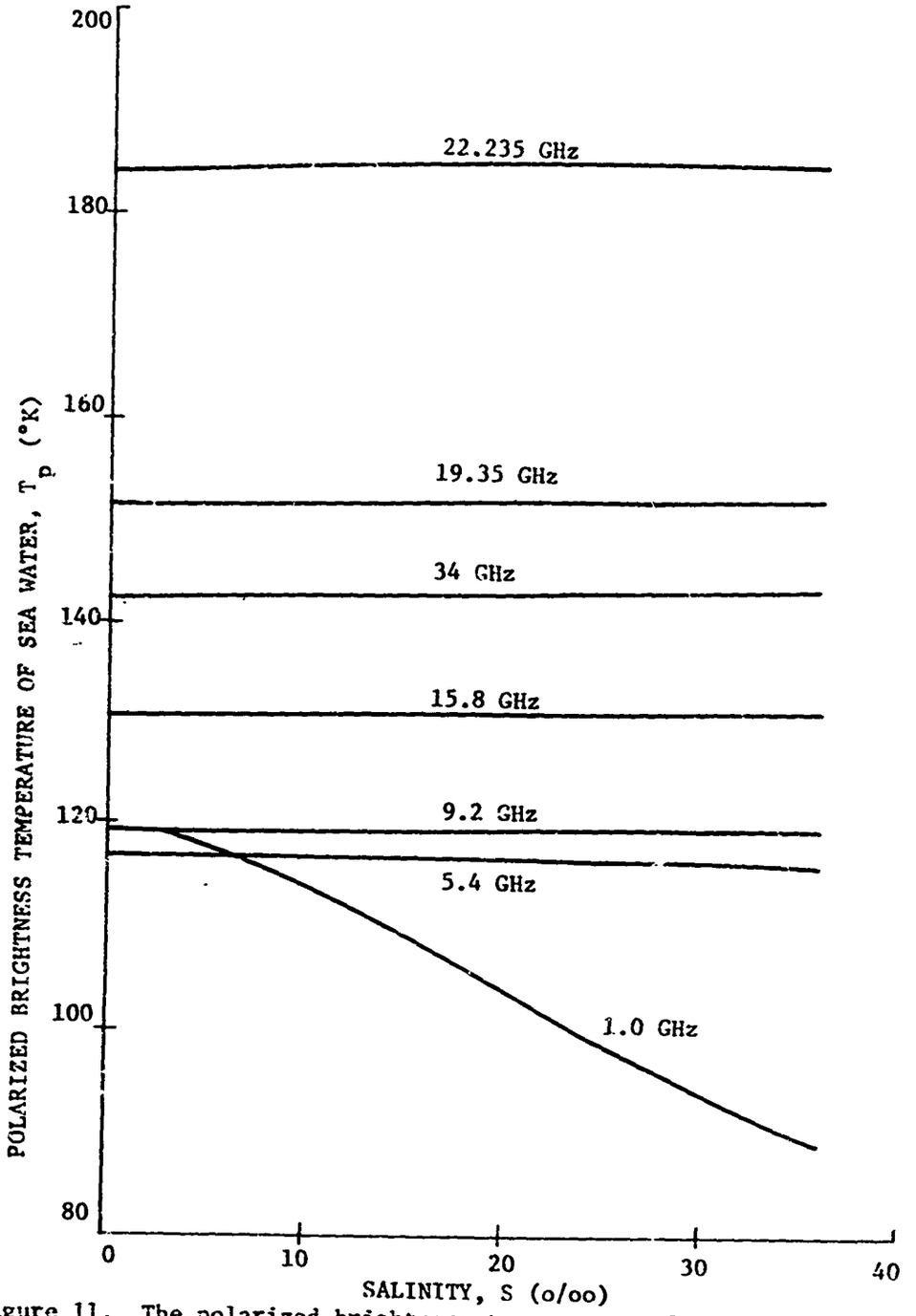

Figure 11. The polarized brightness temperature of sea water versus salinity for a water temperature of 303° K, for an incidence angle of 0°, for frequencies of 1, 5.4, 9.2, 15.8, 19.35, 22.235, and 34 GHz, and for an altitude of 1 km.

GHz. The existence of significant foam cover and rain would negate this possibility.

Effect of Water Vapor

The contribution of thermal emission by water vapor in the atmosphere to the overall polarized brightness temperature is quite large for frequencies near the resonance line of water vapor. If one assumes a certain form for the distribution of water vapor with height, it is possible to compute values of polarized brightness temperature for an incidence angle of zero degrees for various conditions of humidity.

Suppose one wishes to measure the total amount of precipitable water (W,cm) in the marine atmosphere. It has been shown in Chapter V that the emissive temperature of sea water is practically constant for the usual ranges of temperature and salinity for frequencies of 19.35 GHz and 22.235 GHz. It is assumed that T_p^e is 120° K and 122° K, respectively. The reflectivities for these frequencies are approximately 0.60 and 0.59, respectively. Kreiss (1968) shows that the zenith sky temperature ranges from 9 to 43° K for 19.35 GHz and from 14 to 106° K for 22.235 GHz under various meteorological conditions. Thus, the overall brightness temperature of upwelling microwave radiation may change by as much as 147° K due to changes in the emission of water vapor in the atmosphere.

Kreiss (1968) gives values of T_p^{sky} for an incidence angle of

0° for several conditions of temperature and humidity in the atmosphere (see Table XIX). Using his values of precipitable water for these conditions of temperature and humidity, one may plot T_p ($\nu, h_o \geq z_o$ km, $\psi = 0$) versus W for frequencies of 19.35 GHz and 22.235 GHz as shown in Figure 12 (circles). An independent calculation by Staelin (personal communication, 1967) is also included in Figure 12 (triangles).

There appears to be a simple correlation between these polarized brightness temperatures and the total amount of precipitable water in the atmosphere. The values given by Kreiss were computed for nine conditions of temperature and humidity in the atmosphere; however, the effect of temperature does not appear to be significant. This fortunate circumstance probably is due to the fact that the amount of moisture present in the atmosphere is highly dependent upon its temperature profile. The values shown in Figure 12 are for h_o above 20 kilometers. As the observer decends to lower altitudes, the polarized brightness temperature decreases proportionately. Even at the surface, one still would be able to distinguish between various conditions of precipitable water due to the facet that the surface of the water reflects about
upon it.

Effect of Roughness

Stogryn (1967) has presented a very complete treatment of the

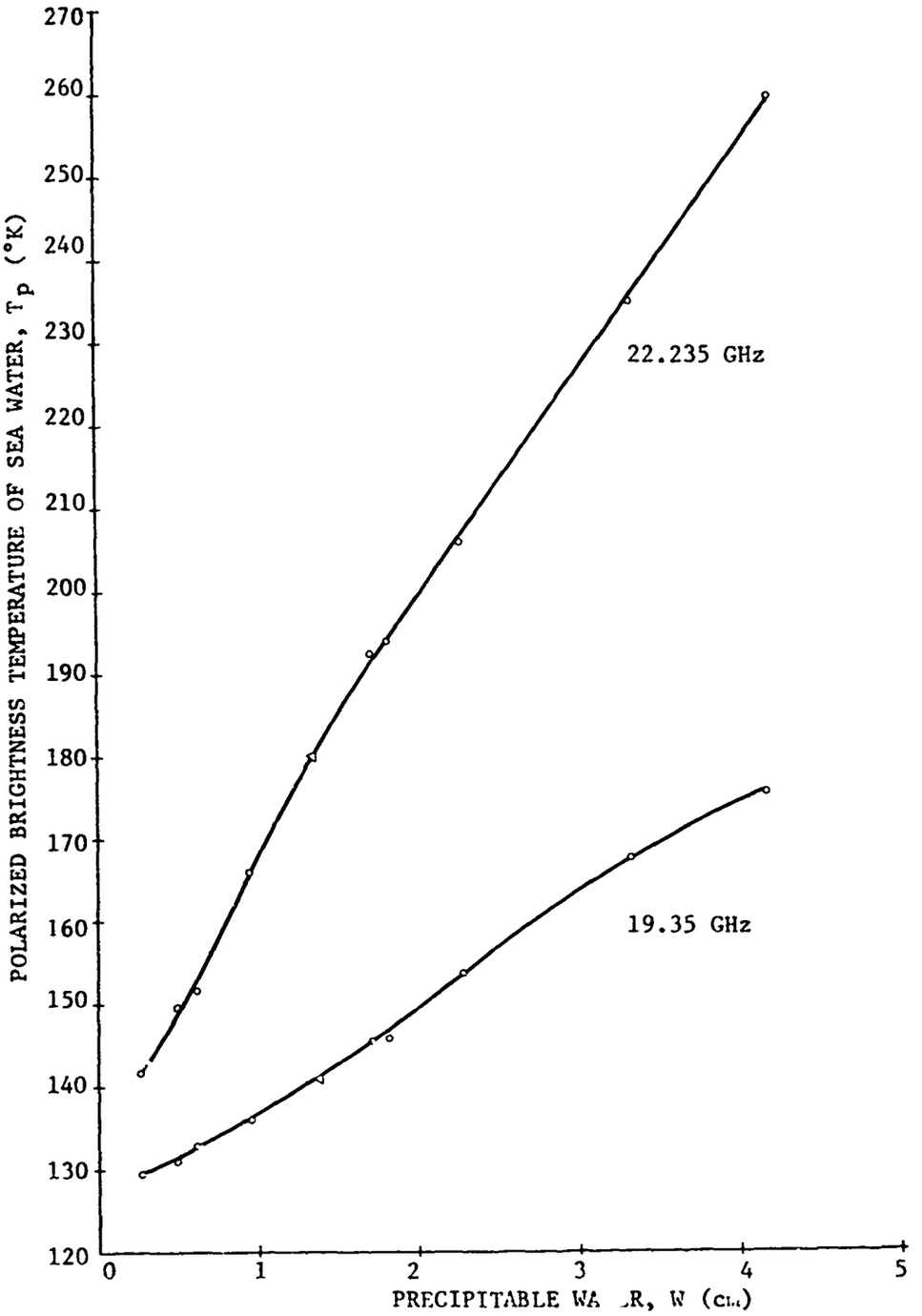

Figure 12. The polarized brightness temperature of sea water versus precipitable water in the atmosphere for frequencies of 19.35 GHz and 22.235 GHz, for an incidence angle of 0°, and for an altitude in excess of 20 km.

effects of a distribution of wave slopes on the polarized brightness temperature. Figure 13 shows the plots of polarized brightness temperature versus incidence angle for horizontally and vertically polarized radiation at 19.4 GHz for the following conditions:

1. The temperature of the sea water is held constant at 17° C, and the salinity of the sea water is assumed to be 36 o/oo. One may say that these conditions are representative of the average surface state of the ocean in mid-latitudes. It can be seen in Figure 8 that the emissive temperature of the sea is fairly constant with temperature and salinity at 19.4 GHz.

2. The temperature profile of the atmosphere was assumed to be that of the ARDC standard atmosphere.

3. The density of water vapor was assumed to vary with altitude as given by (104).

4. The Kirchhoff Approximation was assumed to be valid, and the slope statistics developed by Cox and Munk (1954a, 1954b) were adopted.

Values of T_h and T_v are plotted in Figure 13 versus ψ for h_o equal to one kilometer and for w equal to 0, 4, 8, and 14 meters per second.

Figure 13 shows that the roughness effect is greatest for horizontal polarization and for incidence angles near 50°. The main cause of this phenomenon is the change in the source of the reflected sky radiation that results when the surface is roughened

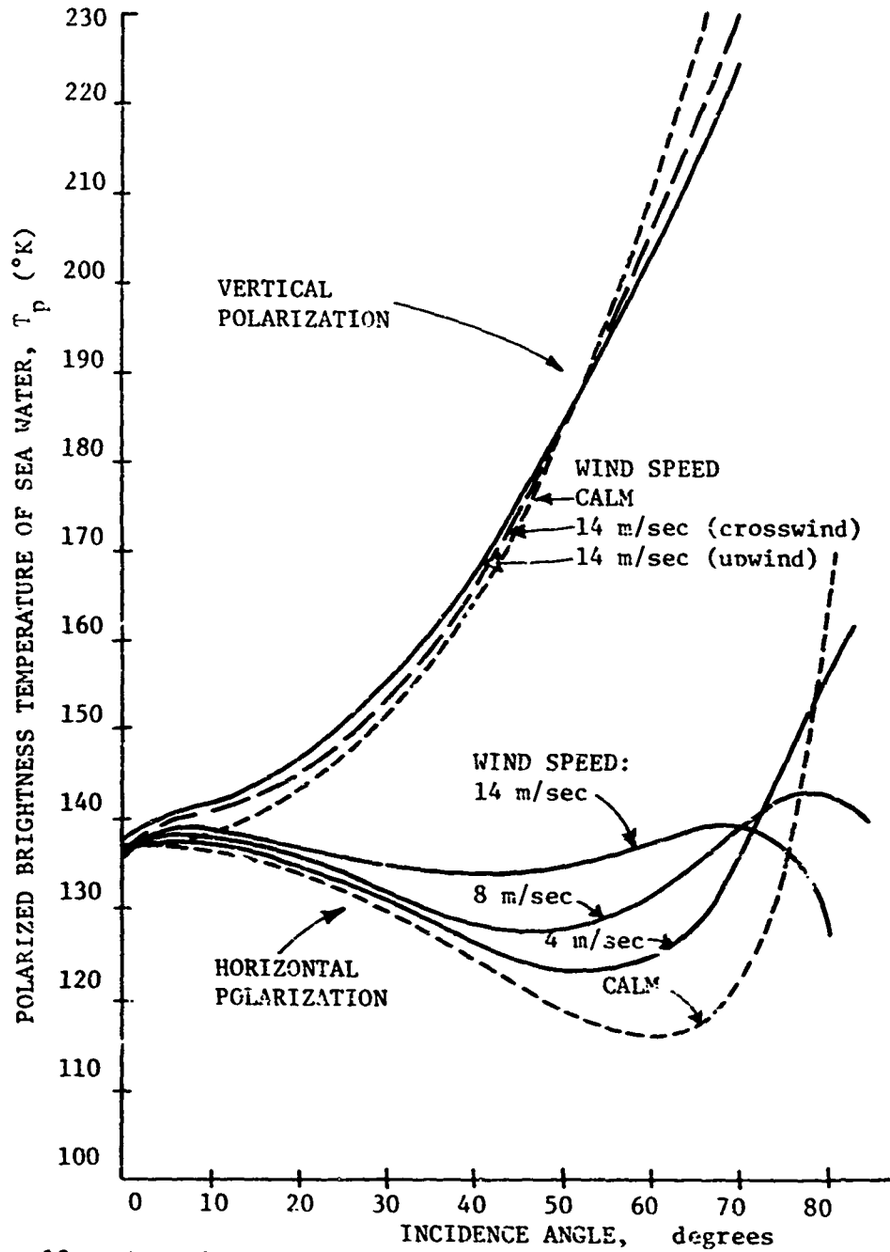

Figure 13. The polarized brightness temperatures of sea water versus incidence angle for horizontal and vertical polarization, for fully developed sea driven by surface winds of 0, 4, and 14 m/sec, for an altitude of 1 km, and for a frequency of 19.4 GHz (after Stogryn, 1967).

(Stogryn, 1967).

It has been noted before that the root-mean-squared slopes, g_x and g_y, of the sea surface are related to wind speed by (152) and (153). Saunders and Wilkens (1968) say that if the sun is overhead, the angular radii (radians) of the sun's glitter pattern as seen in photographs are approximately $2g_x$ and $2g_y$ along directions cross wind and upwind, respectively. Thus, one may use photographs of the sun's glitter pattern to provide 'ground truth' about the roughness of the sea surface (Cox and Munk, 1954a, 1954b).

Table XXVII shows the difference between horizontally polarized brightness temperatures for incidence angles of 0° and 45°.

These theoretical values of T_p as a function of roughness are valid only if there is no foam on the sea surface. For surface winds above seven meters per second, one would expect some finite area of the sea surface to be covered by foam and bubbles.

Table XXVII. Difference between the horizontally polarized brightness temperature of sea water at an incidence angle of 0° (T_h (0°)) and that of sea water at an incidence angle of 45° (T_p (45°)) for a frequency of 19.4 GHz versus the speed of the wind at 41 feet above sea level (w, m/sec) for a fully developed sea.

Wind speed, w, (m/sec)	T_h (ψ = 0) - T_h (ψ = 45°)
0	19° K
4	14° K
8	8° K
14	1° K

Effect of Liquid Water

Kreiss (1968) has computed values of the polarized brightness of upwelling microwave radiation over various types of clouds containing various concentrations of liquid water (M, g/m^3). These computations are presented in his paper for specific cases and values of M as T_p ($\nu, h_o > 30$ km, $\psi = 0$) versus ν for ν between 15 GHz and 30 GHz. It may be more convenient to present his data in a slightly different manner.

Consider the following case:

1. The frequency is 19.35 GHz.

2. Standard temperature and humidity profiles as given by Kreiss (1968) are assumed to be valid. In addition, the relative humidity is assumed to be 100% in clouds.

3. Equation (139) is assumed to be valid.

4. The cloud bases are assumed to be 688 meters above the sea surface.

5. Cloud tops are assumed to be at 1949 meters for 'stratus', 3012 meters for 'thick stratus' and 7185 meters for 'tall cumulus' clouds.

Figure 14 shows plots of T_p (19.35 GHz, $h_o > 20$ km, $\psi = 0$) versus M for 'stratus', 'thick stratus', and 'tall cumulus' clouds.

Figure 15 shows a plot of T_p versus the product of M times the thickness of the cloud. This latter product may be called the concentration of liquid water per unit horizontal area.

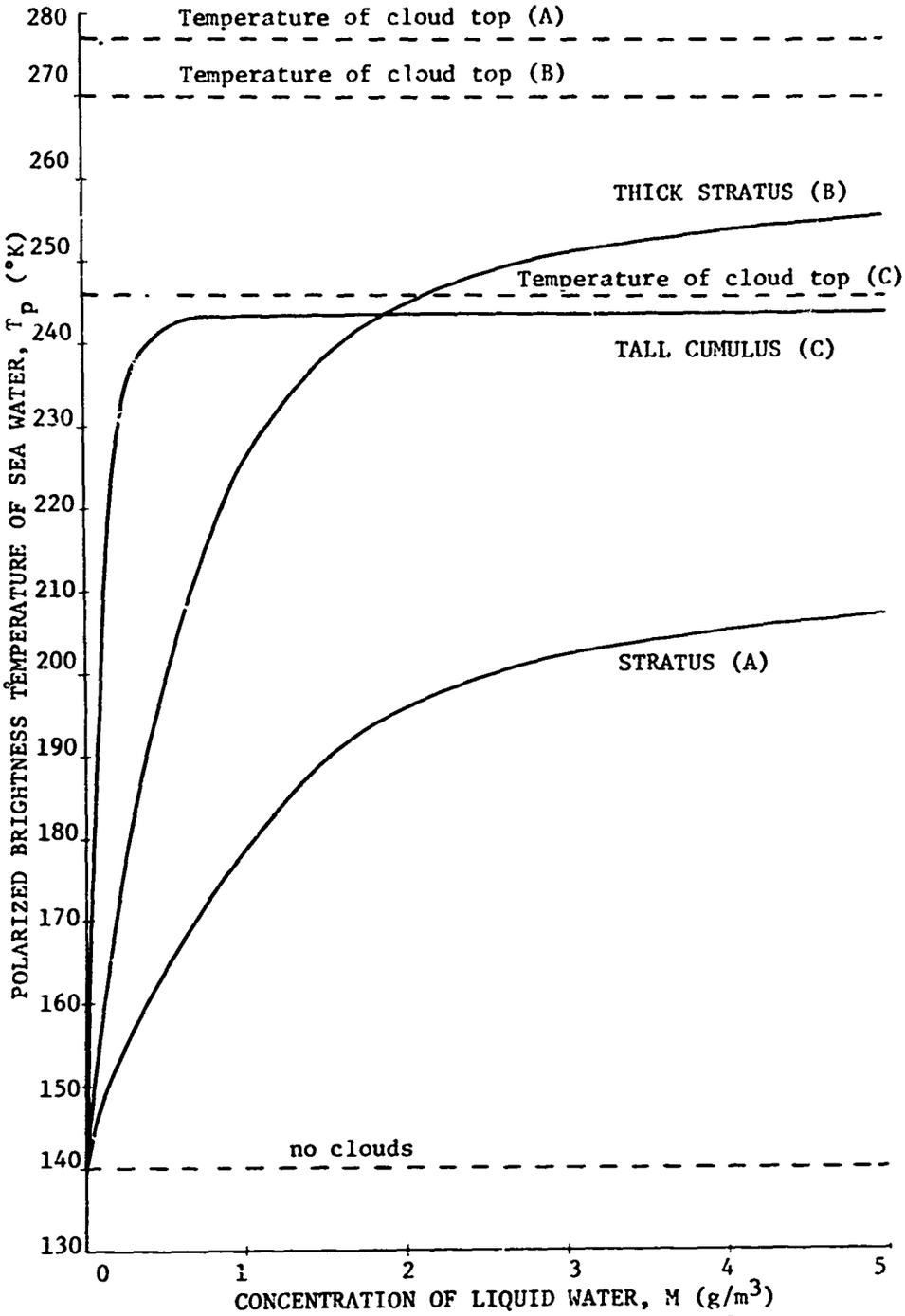

Figure 14. The polarized brightness temperature of sea water versus the concentration of liquid water in intervening clouds for a frequency of 19.35 GHz and for an incidence angle of 0°.

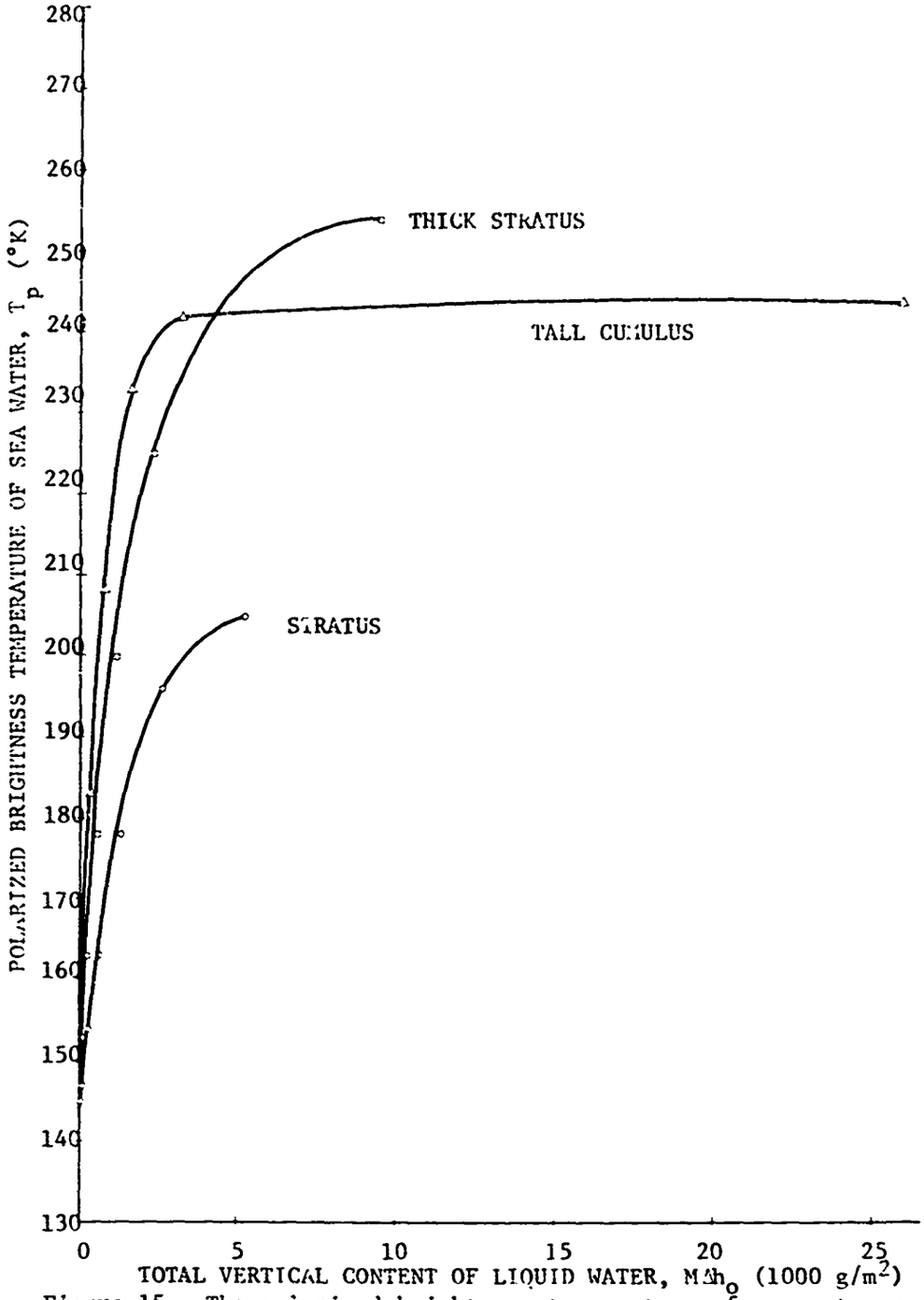

Figure 15. The polarized brightness temperature of sea water versus the product of the thickness of intervening clouds and their concentration of liquid water for a frequency of 19.35 GHz and for an incidence angle of 0°.

The dashed lines in Figure 14 indicate the temperature of the top layers of the stratus (A), thick stratus (B), and tall cumulus (C). It is apparent from Figure 14 that the polarized brightness temperature over clouds for a frequency of 19.35 GHz depends on the type of cloud and its concentration of liquid water. The plots in Figure 15 indicate, furthermore, that the temperature of the cloud is very important in determining the microwave radiance over the cloud. In this figure, the effects of total vertical water content are normalized by using M times Δh_o as the independent variable.

Of course, if one knew the thickness and height of the clouds being viewed, one could use curves in Figure 14 to ascertain its mean value of M from measurements of the brightness temperature. It appears that one may be able to determine the height of the topmost clouds in the atmosphere by measuring the infrared radiational intensity near wavelengths of 10 microns as by measurements of the amount of attenuation of near visible radiation due to carbon dioxide (Hanel, 1961).

Kreiss (1968) assumed that the sea surface acts as a smooth, flat surface -- even under raining clouds. Rain falling on the sea surface creates bubbles and foam. This would tend to raise the radiance of the cloud at microwave frequencies.

CHAPTER VII

MICROWAVE RADIOMETRY

General

The historical development of microwave radiometry from radio astronomy to a discipline of terrestrial remote sensing was given in Chapter I. The three basic components of a microwave radiometer are its antenna system, its receiver, and its output recorder.

The antenna system intercepts a portion of the total electromagnetic radiation incident upon it and transfers this power to the input terminals of the receiver along connecting transmission lines or wave guides. Antennas used in microwave radiometry are highly directive, that is, they receive energy mostly from a certain set of directions relative to the axis of the antenna.

The power supplied to the input terminals of the receiver is greatly amplified and filtered so that only power having frequencies from $\nu - \Delta\nu/2$ to $\nu + \Delta\nu/2$ is passed to its output terminals. $\Delta\nu$ is the band pass of the radiometer, and ν is the central frequency of the radiometer.

The output from the amplifier is converted to direct current and may be recorded on a strip chart or on magnetic tape.

Since microwave radiation is weak, the contribution of thermal emission in the antenna, transmission lines, and first

stages of amplification may be comparable to the radiational power intercepted by the antenna.

The purpose of this chapter is to present certain concepts necessary to allow one to relate the field of polarized brightness temperatures present at some location in space to measurements made by typical microwave radiometers. The concepts presented in the next sections are discussed in great detail by Bracewell (1962) in his paper on techniques of radio astronomy.

Microwave Receivers

The functions of the receiver portion of a microwave radiometer are to amplify the power supplied to its input terminals by the antenna system, to convert this power to more suitable frequencies, and to tune the output to a certain band of frequencies. It is important to remember that the radiometer is not monochromatic. A typical bandwidth of microwave radiometers used today is 0.1 GHz.

A block diagram of a typical microwave receiver of a Dicke radiometer is shown in Figure 16.

The antenna system supplies a small amount of power to the input terminals of the microwave receiver. This power is typically 10^{-20} watts per Hertz and is carried by a wide range of frequencies. The antenna system displays some degree of selectivity and does not deliver all of the power incident upon its physical area to the input terminals. This tuning effect is small, however,

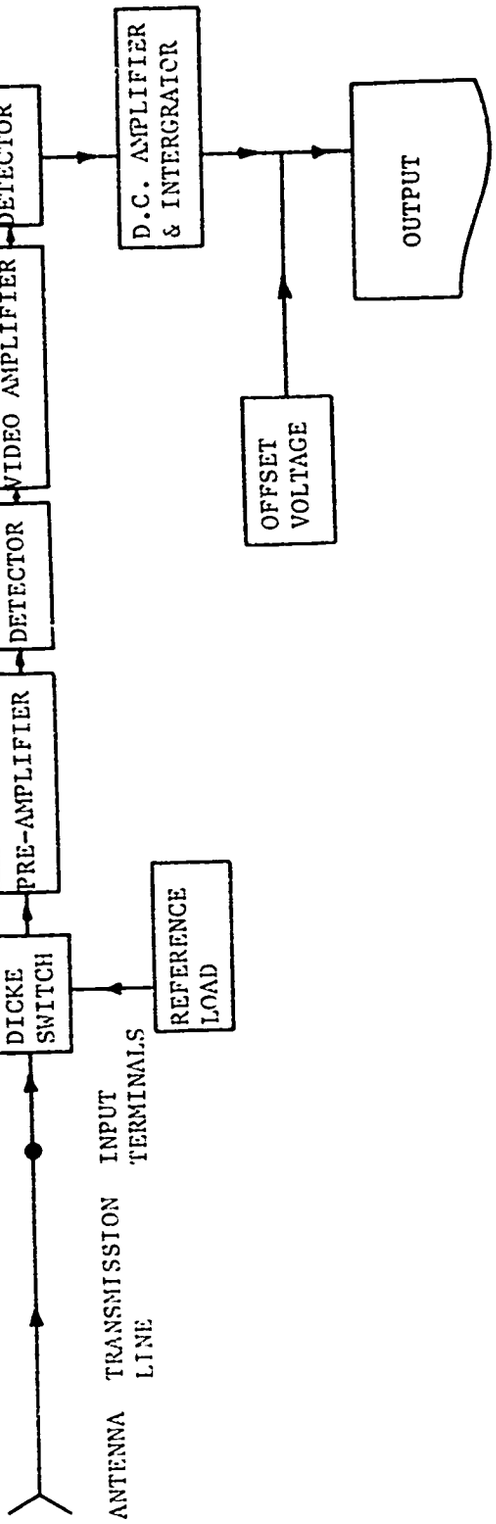

Figure 16. Block diagram of a typical microwave radiometer.

compared to tuning that occurs in the detectors of the microwave receiver. The antenna system does exhibit one important aspect of selectivity, viz., it chooses a certain polarization. If the input power is essentially constant with frequency, one defines the bandwidth ($\Delta\nu$, Hertz) as "the difference between the frequencies at which the output voltage (or other output indication) falls to the value corresponding to a halved power input at the mid-frequency, ν" (Bracewell, 1962). The shape of the band pass is usually assumed to be Gaussian.

Let P_i be the power supplied by the antenna system to the input terminals and carried by frequencies from $\nu - \Delta\nu/2$ to $\nu + \Delta\nu/2$. Formally, one may say that the actual power passed by the reciver is P_i times a constant factor since power is passed outside $\Delta\nu$ and since not all the power existing in $\Delta\nu$ is passed. On the other hand, calibrations of the radiometer consist of comparing this power to the power produced by a matched resistor or produced when the antenna is surrounded by a blackbody. One would expect the same biasing effect on the calibration power as on the power supplied by the antenna system. It is further assumed that P_i is constant over $\Delta\nu$.

Microwave frequencies are much too high to be handled by ordinary components of radio amplifiers. If ν is less than 10 GHz, however, P_i may be amplified before the signal is converted to lower frequencies by mixing the original signal with a lower

frequency signal.

The video amplifier then boosts the power to a level that is recordable. The signal is rectified, integrated, and fed to the output recorder.

The most serious limitation placed on early microwave receivers was drift in amplification. Dicke (1946) proposed a method whereby the effect of relatively slow fluctuations in amplification could be lessened. The power from a fixed, known, internal source is fed into a switch which alternately passes power from the antenna and the internal source at a rapid pace. Any drift in amplification affects the amplification of the antenna power and the internal power in the same amount; therefore, the difference between these signals should not be affected by amplification fluctuations. The signal from the reference generator which drives the Dicke switch also is supplied to the final detector stage. The antenna power is then recovered.

Since a continuous spectrum of frequencies is passed by the microwave receiver, modulations are evident on the wave form of the amplified signal. Bracewell (1962) shows that the root-mean-square deviation in the output voltage is proportional to the mean value of the output voltage divided by the square root of the integration time multiplied by the bandwidth.

The power (P_j, watts) produced by a matched resistor at temperature, T (°K), over the frequency range from $\nu - \Delta\nu/2$ to

$\nu + \Delta\nu/2$ is called Johnson noise and is given by Bracewell (1962) as:

$$P_J = kT\,\Delta\nu \qquad (°K), \qquad (162)$$

where k is Boltzmann's constant.

Using (162) it is possible to express P_i in terms of the temperature of a matched resistor (T_i, °K) which produces a power P_i. Thus,

$$T_i = P_i / k\Delta\nu \qquad (°K). \qquad (163)$$

T_i is called the apparent input temperature.

The value of T_i is determined by the total amount of power received by the antenna system of the radiometer and supplied to the input terminals. A significant portion of P_i may originate in the antenna system and connecting transmission lines since these devices also emit Johnson noise.

The output of the radiometer may be expressed in terms of apparent input temperature. From the preceeding discussion of voltage accuracies, one may say that the root-mean-square deviation of the measured apparent input temperature $\overline{\Delta T_i}$ is given by:

$$\overline{\Delta T_i} = (T_N + T_i)/(t_i\,\Delta\nu)^{1/2} \qquad (°K), \qquad (164)$$

where T_N is the contribution to the overall signal due to noise emission in the radiometric components (°K), and t_i is the

integration time (seconds).

T_N is called the apparent temperature of the receiver noise and may be found in the literature in terms of the noise figure (NF) where:

$$T_N = (NF - 1)290 \quad (°K). \qquad (165)$$

Currently used microwave receivers have noise figures close to unity.

Typical values of $\overline{\Delta T}_i$ are 5° K in airborne microwave radiometers. The next generation of airborne microwave radiometers should have values of $\overline{\Delta T}_i$ near 0.5° K. Some radio telescopes have values of $\overline{\Delta T}_i$ near 0.01° K.

Now it is necessary to relate T_i to the field of brightness temperature and certain antenna parameters.

Antenna Effects

It is convenient to define a new set of direction angles relative to the axis of a high gain antenna. Let (θ,ϕ) be this set as shown in Figure 17. The angle, θ, lies in the vertical plane of polarization, and ϕ lies in the horizontal plane of polarization. The axis of the antenna may be inclined to the vertical by an angle ψ which is called the angle of incidence or angle of viewing. If ψ is zero, the vertical and horizontal planes lose their significance. In this case the 'vertical plane' is defined as the vertical plane that contains the path of the

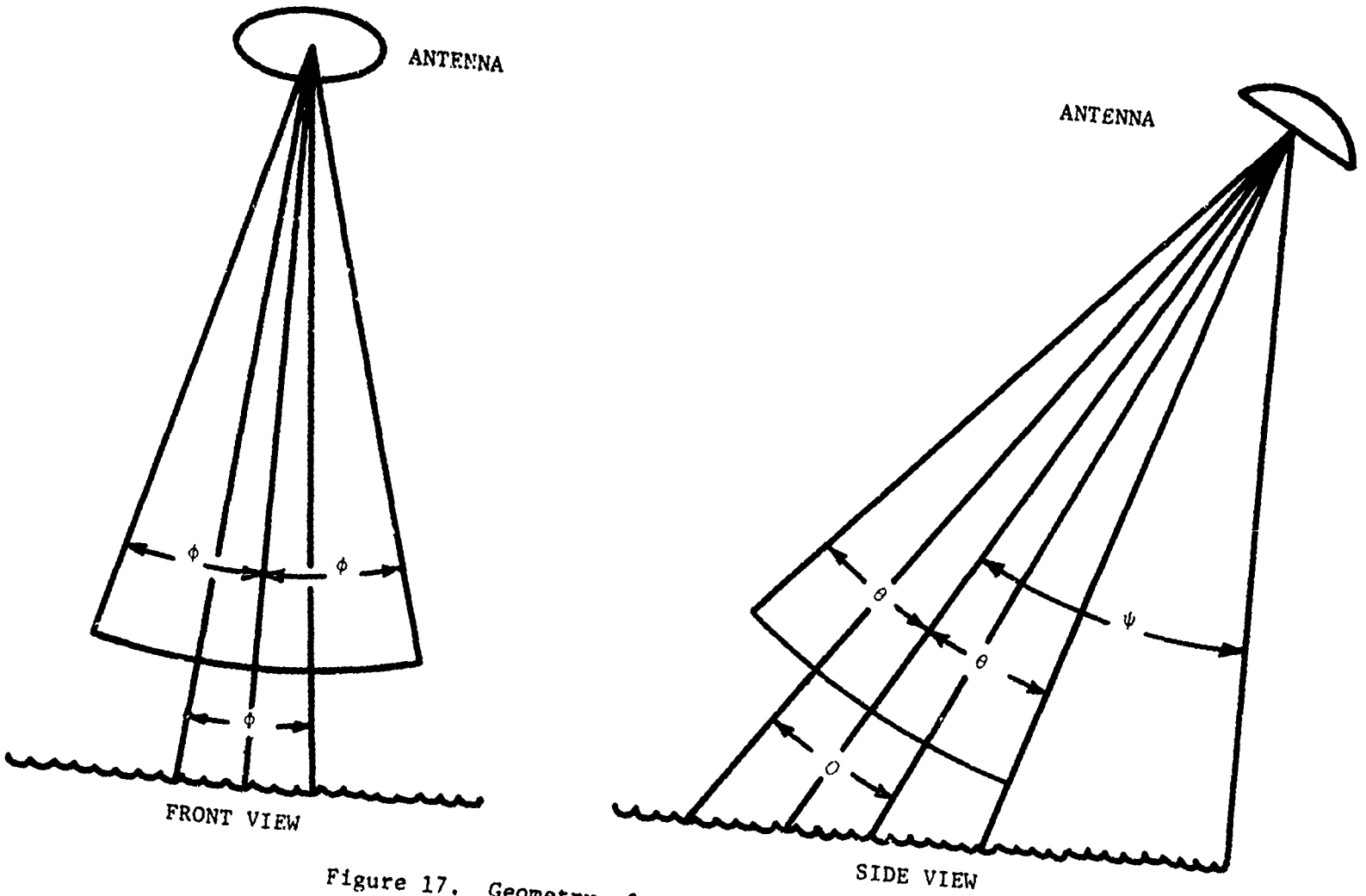

Figure 17. Geometry of antenna parameters.

platform carrying the microwave radiometer. In most cases, the field of intensity is symmetrical to the normal.

The characteristic of an antenna system are described in terms of its radiating properties. Let P_t be the total power radiated by an antenna. It follows, then, that the average power ($\bar{P}$, watts/steradian) radiated per unit solid angle is $P_t/4\pi$. Antennas are usually highly directive, that is, they radiate unevenly with (θ,ϕ). Let $P(\theta,\phi)$ describe the distribution of the radiated power where:

$$P_t = \int_{4\pi} P(\theta,\phi)\, d\Omega \qquad \text{(watts)}. \qquad (166)$$

If P_i is the power supplied to the antenna terminals, then one defines an antenna efficiency factor, η_a, such that:

$$\eta_a = P_t \,/\, P_i \qquad \text{(dimensionless)}. \qquad (167)$$

Let

$$D(\theta,\phi) \equiv P(\theta,\phi) \,/\, \bar{P} \qquad \text{(dimensionless)}, \qquad (168)$$

and

$$G(\theta,\phi) \equiv P(\theta,\phi)\, 4\pi \,/\, P_i \qquad \text{(dimensionless)}. \qquad (169)$$

$D(\theta,\phi)$ is called the directive gain pattern of the antenna, and $G(\theta,\phi)$ is called the gain pattern of the antenna.

From (167), (168), and (169) it follows that:

$$G(\theta,\phi) = \eta_a \; D(\theta,\phi) \qquad \text{(dimensionless)}. \qquad (170)$$

Let $I_p\ (\theta,\phi)$ be the distribution of the polarized intensity of the upwelling radiation with respect to the antenna axis. The total amount of power (P_a, watts) in polarization p intercepted by the antenna is given from (39) by:

$$P_a = \int_{4\pi} \int_{\Delta\nu} \int_{\text{area}} I_p\ (\theta,\phi)\ \cos\theta'\ dA\ d\nu\ d\Omega \qquad \text{(watts)}. \quad (171)$$

It is assumed tha $I_p\ (\theta,\phi)$ is constant over the area of the antenna and over the bandwidth. The angle θ' is the angle between the axis of the antenna and the direction, (θ,ϕ). The effective area of the antenna, (A_e, square meters) is introduced in (171) and represents the efficiency of the antenna in gathering electromagnetic energy as well as the lessening of the physical area of the antenna due to the factor, $\cos\theta'$. Thus, (171) becomes:

$$P_a = \int_{4\pi} I_p\ (\theta,\phi)\ A_e(\theta,\phi)\ \Delta\nu\ d\Omega \qquad \text{(watts)}. \quad (172)$$

According to Jordon (1950),

$$A_e\ (\theta,\phi) = (c^2/4\pi\nu^2)\ G\ (\theta,\phi) \qquad (m^2), \qquad (173)$$

where c is the speed of light in a vacuum.

Using (54) to express $I_p\ (\theta,\phi)$ in terms of $T_p\ (\theta,\phi)$ and using (173), one obtains the following expression for P_a:

$$P_a = (k\Delta\nu/4\pi) \int_{4\pi} T_p\ (\theta,\phi)\ G\ (\theta,\phi)\ d\Omega \qquad \text{(watts)}. \quad (174)$$

Using (162), one may express P_a in terms of the temperature of a matched resistor, (T_a, °K) or simply antenna temperature where:

$$P_a = k\Delta\nu T_a \quad \text{(watts)}. \tag{175}$$

Thus, (174) becomes:

$$T_a = (1/4\pi) \int_{4\pi} T_p(\theta,\phi)\, G(\theta,\phi)\, d\Omega \quad (°K). \tag{176}$$

When a radome is used to protect the antenna, one must consider the effects of absorption and emission of energy by the radome. If L_R is the transmissivity of the radome, then:

$$T_i = (L_R/4\pi) \int_{4\pi} T_p(\theta,\phi)\, G(\theta,\phi)\, d\Omega + T_R(1 - L_R) \quad (°K), \tag{177}$$

where T_R is the effective thermometric temperature of the radome and T_i is the apparent input temperature as measured by the radiometer. In practice, L_R and T_R have been difficult to determine.

The shape of $G(\theta,\phi)$ is usually assumed to be Gaussian for (θ,ϕ) near $(0,0)$. In this case, one may describe $G(\theta,\phi)$ by giving $G(0,0)$, and the beamwidths, Θ and Φ. The beamwidths are the angles between values of θ and ϕ where the gain is equal to half of the gain along the axis. In most cases, the gain is given in terms of decibel reduction relative to $G(0,0)$. Thus, the gain is 3 decibels below $G(0,0)$ when $\theta = \pm\Theta$ or $\phi = \pm\Phi$

In some cases the angular widths, Θ_M and Φ_M, of the solid angle containing the main lobe of the gain pattern are given.

The power delivered to the input terminals of the receiver by the antenna comes from all portions of the 4π steradians surrounding a location is space. Thus, one cannot assume, summarily, that the radiometer is 'seeing' one particular area under view. This is especially important when T_p varies strongly with θ and ϕ. Over the ocean, however, it has been shown in past chapters that T_p varies slowly with ψ especially for ψ near zero degrees.

Consider the case of an antenna placed in a constant temperature enclosure. In this case:

$$T_a = (T_p/4\pi) \int_{4\pi} G(\theta,\phi)\, d\Omega = T_p \qquad (^\circ K), \qquad (178)$$

since

$$\int_{4\pi} G(\theta,\phi)\, d\Omega = 4\pi. \qquad (179)$$

In a similar fashion, one may break the integral in (176) into parts and say that:

$$\begin{aligned} T_a = {} & (T_p(0,0)/4\pi) \int_{\substack{\text{main}\\ \text{lobe}}} G(\theta,\phi)\, d\Omega \\ & + \left\{ T_p^{\overline{\text{side}}}/4\pi \right\} \int_{\substack{\text{side}\\ \text{lobes}}} G(\theta,\phi)\, d\Omega \\ & + \left\{ T_p^{\overline{\text{back}}}/4\pi \right\} \int_{\substack{\text{back}\\ \text{lobes}}} G(\theta,\phi)\, d\Omega \qquad (^\circ K). \end{aligned} \qquad (180)$$

In each term of (180), the integrals have the dimensions of

solid angle and may be referred to as the equivalent solid angle of the main lobe (Ω_M), the side lobes (Ω_S), and the back lobes (Ω_B), respectively.

In most cases, $\Omega_M / 4\pi$ is 0.7 to 0.9. It will be assumed that the antenna temperature is equal to the brightness temperature along the antenna axis as a first approximation. The mean brightness temperature for side lobes ($\overline{T}_p^{side}$, °K) is usually as high or higher than T_p for ψ near zero degrees, and the mean brightness temperature for back lobes ($\overline{T}_p^{back}$, °K) is much lower than T_p (0,0).

An excellent discussion of these antenna parameters is given by Ko (1964) for several specific cases.

In summary, one should note that T_i is measured by the radiometer. If one knows L_g and $G(\theta,\phi)$, it is still impossible to obtain $T_p(\theta,\phi)$ without making certain simplifying assumptions. In the case of measurements over the ocean, it is assumed that T_i does relate only to the value of T_p at (θ,ϕ) equal to zero, i.e.,

$$T_p(\psi) = [T_i - T_R(1 - L_R)] / L_R \quad (°K), \qquad (182)$$

where T_i is the calibrated reading of the radiometer.

If no radome is used, it is assumed that:

$$T_p(\psi) \simeq T_a(\psi) \quad (°K). \qquad (183)$$

In any event, one would be able to measure relative changes in apparent antenna temperature that occur along a flight line

and assume that the corresponding change in relative polarized brightness temperature would be comparable.

CHAPTER VIII

RESULTS OF MICROWAVE MEASUREMENTS

General

Few measurements have been made of microwave radiance over sea water under conditions in which the distributions of essential atmospheric and hydrospheric parameters were known adequately. Indeed, it may be impossible to determine the distribution of liquid water in a cloud field by in situ measurements. Atmospheric temperature and humidity soundings often are not available over the ocean. Surveys of the ocean's surface by research vessels do not result in truly synoptic measurements. The nature of the small-scale roughness of the sea surface is difficult to deduce from standard wave instruments.

The National Aeronautics and Space Administration (NASA) has been actively sponsoring research and development in applied remote sensing. Under NASA's Earth Resources Survey Program, many airborne tests have been made of a set of remote sensors that will probably be placed in a spacecraft in the 1970's. Applications are being developed under this program for all of the earth sciences. At the present time, the Goddard Space Flight Center and the Environmental Sciences and Service Administration are actively sponsoring research in remote sensing for meteorology. It is really impossible to separate meteorology from the other earth sciences since one must always look through the

atmosphere when one is trying to study some aspect of the land or the ocean from space. Over the ocean, one must always be aware of the mutual influences between the atmosphere and hydrosphere.

The Spacecraft Oceanography Project has been sponsoring studies at Texas A&M University of possible applications of remote sensing over the Mississippi Delta as a part of NASA's Earth Resources Survey Program. One of the objectives of this study is to determine whether or not remote sensors can be used from aircraft and spacecraft to study the distribution of the outflow of the Mississippi River into the Gulf of Mexico. The chief indicators of outflow distribution are the temperature and salinity fields. Sharp boundaries exist between masses of river, coastal, and ocean water in the mixing area. Microwave radiometers have been flown over this area during various seasons of the year at altitudes of 458 meters and 3048 meters. These radiometers operate at the central frequencies of 9.2, 15.8, 22.235, and 34.0 GHz. Calibrated apparent input temperatures have been supplied to the author by the Jet Propulsion Laboratories and the Manned Spacecraft Center from aircraft missions flown in February 1967 and February 1968.

The Goddard Space Flight Center conducted tests of several remote sensors over portions of the Gulf of Mexico in June 1967 using a Convair 990. Included among these remote sensors was a microwave radiometer which scans, electronically, up to 50°

to either side of the flight track and which operates at a central frequency of 19.35 GHz. Dr. William Nordberg and Dr. Jack Conaway of the Goddard Space Flight Center have courteously supplied the author with calibrated temperatures obtained by this radiometer along with certain supporting photographs and infrared data.

It has been possible to obtain some surface measurements made during these aircraft flights. The purpose of this chapter is to describe the microwave radiometers flown on the Convair 240A and Convair 990, to present their measurements in a concise form, and to discuss their scientific value for oceanography and meteorology.

Microwave Radiometers in the NASA 926

System description

Blinn (1967a) has written a fairly complete description of the microwave radiometers installed in a Convair 240A which has been designated as the NASA 926. There are two separate microwave radiometers in this system -- the MR-62 and the MR-64. The MR-62 is practically identical to the microwave radiometers flown on the Mariner II spacecraft near Venus in 1962. It operates at 15.8 GHz and 22.235 GHz and uses a common antenna. The MR-64 operates at 9.2 GHz and 34 GHz and uses another antenna. The antennas of these systems are shown in Figure 18. The parabolic reflector of the MR-62 is shown on the left side of

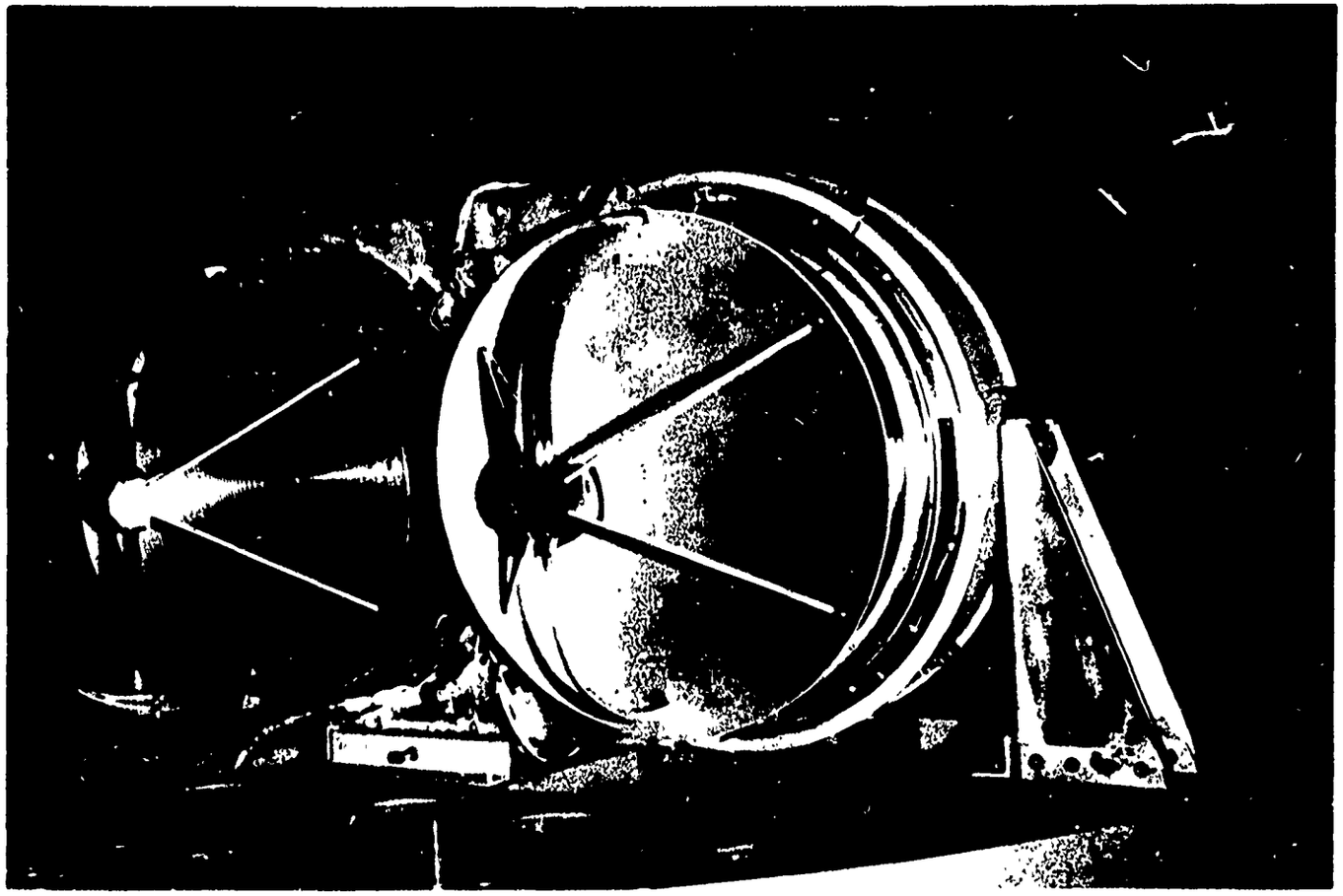

Figure 18. Antennas of the MR-62 and MR-64 microwave radiometers.

Figure 18, and one can easily see the series of concentric, flat reflectors which reflect visible light back to space and which concentrate microwave radiation into the horn in front of the reflectors. One should notice the size and orientation of the waveguides which transfer the microwave signal from the horn to internal parts of the radiometers. The MR-62 is cross polarized and the MR-64 is polarized in the same plane for both channels. Both of these antennas may be rotated through 90° to change the polarization planes. These antennas are mounted in the nose of the NASA 926 (see Figure 18 and 19) and may be tilted to zenith angles between 0° and 45°.

A radome, consisting of eleven layers of several dielectric materials, protects the antennas from the airstream. The transmissivities (L_R) of this radome are given in Table XXVIII along with some other parameters of the radiometers.

Table XXVIII. Significant parameters of the MR-62 and MR-64 microwave radiometers on board the NASA 926 (after Blinn, 1967a).

Frequency (ν, GHz)	9.2		15.8		22.235		34.0	
Polarization (p)	h	v	h	v	h	v	h	v
Transmissivity (L_R)	1.0	1.0	0.91	0.891	0.912	0.901	0.751	0.705
Beamwidth	3.4°	3.8°	3°	3°	2.2°	1.8°	1.25°	1.15°
Integration time	1.0		1.2		1.3		1.1	
Sensitivity (ΔT)	1.84		0.31		0.70		0.71	

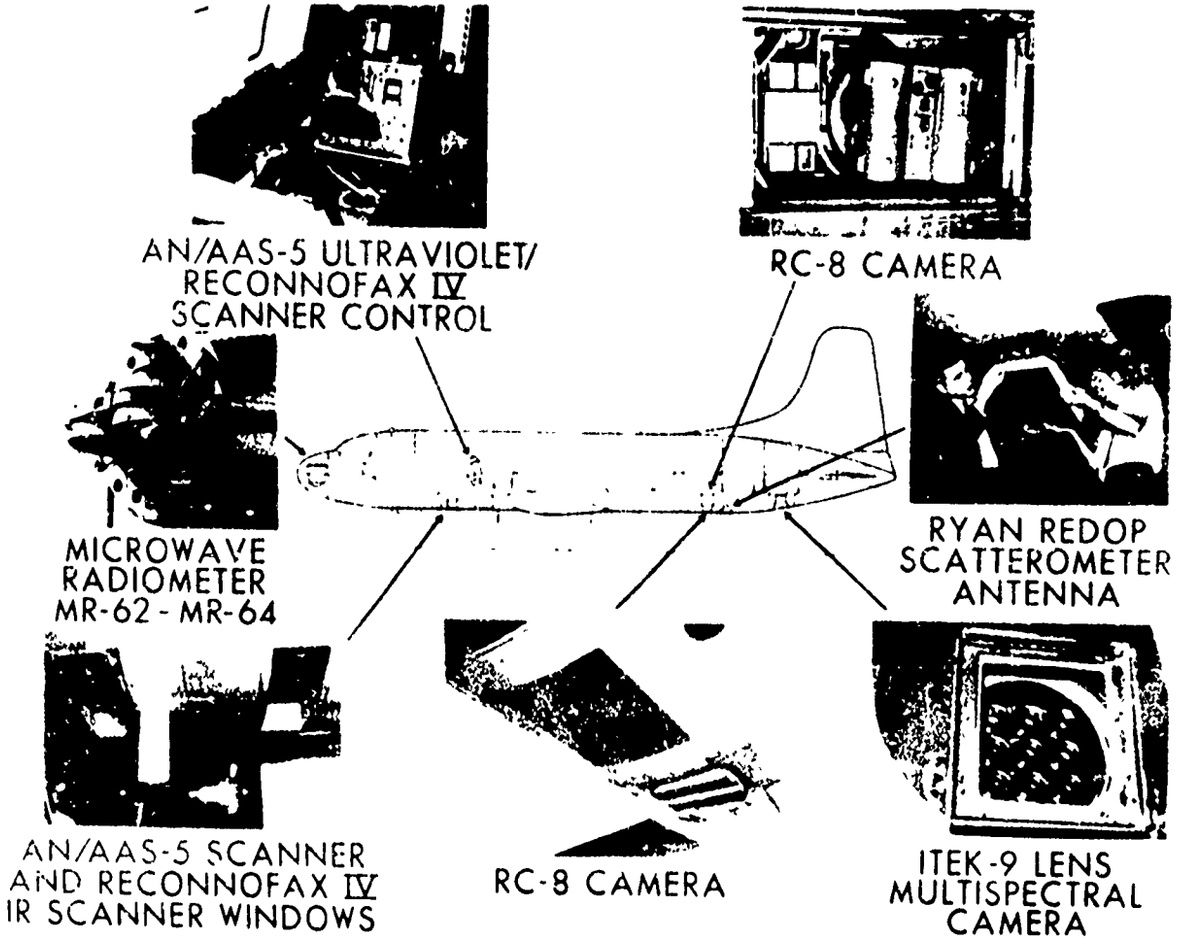

Figure 19. Location of remote sensors in the NASA 926.

During a flight, the temperature of the radome is recorded by using two thermistors embedded in the radome. It was not possible, however, to calibrate these thermistors. Blinn (1967a) suggests that one should assume that the radome temperature is equal to the temperature of the air recorded by standard aircraft instruments.

Pre-flight and post-flight calibrations of both radiometers are performed on the ground by filling the horns of the antenna with highly absorptive material. Readings are made of the antenna temperature of this material which is assumed to act as a blackbody. This method of calibration is liable to produce inaccurate calibration points. The 'accuracy' of these measurements is suspect; however, the relative values can be used with confidence.

The output of the radiometers are recorded on magnetic tape by modulating the frequency of a 54 KHz carrier frequency. Known increments of internal noise occasionally are added to the power received by the antenna system to provide scale calibration.

These microwave radiometers have been used to make measurements of the flux of upwelling microwave radiation over an area south of the main mouths of the Mississippi River along certain radial flight lines emanating from South Pass. Three extensive aircraft missions have been conducted over this area in the past two years with these radiometers. Figure 20 shows the basic flight lines flown on these missions. Data taken along Lines 1, 4, and 3 will be discussed in this chapter.

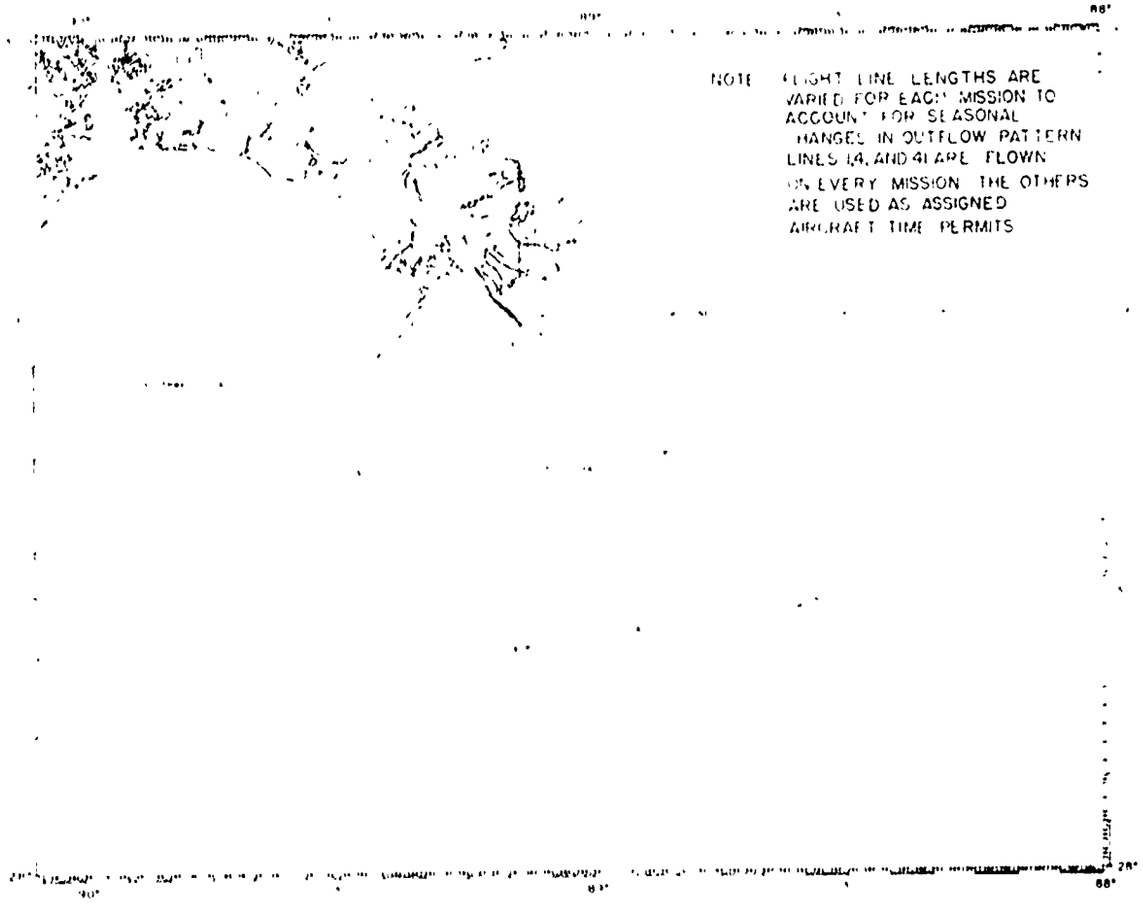

Figure 20. Basic flight lines flown over Mississippi Delta over past two years.

Mission 41

Mission 41 was flown on February 24, 1967, at an altitude of 458 meters. Table XXIX summarizes the significant flight parameters and radiometric parameters for this mission.

The sky was clear during this mission. A strong cold front had swept over the area in the last 24 hours before the mission was flown. The wind was about 7 meters per second from the north at flight level. No surface measurements were available. The rate of river outflow was above normal.

The measurements obtained by the microwave radiometers during Mission 41 were calibrated and converted to digital form by Blinn (1967b). These data show that the microwave radiance was fairly constant over the entire area when polarization and zenith angles were held constant. Occasionally, the data would indicate large increases or decreases on all four channels. These changes took place over a period of three to five seconds. Further investigations revealed that these changes were approximately equal to the noise levels occasionally introduced into the radiometric system to allow one to calibrate the scale of the output. Thus, it appears that these excursions in the data were due to improper calibration procedures. Ignoring these excursions, one may use the calibrated data to obtain some information about the marine environment on this particular day. It will be shown in the analysis of data taken on Mission 66 that the temperature and salinity

Table XXIX. Flight parameters and radiometric parameters for Mission 41.

Flight Number	Line Number	True Heading (degrees)	Ground Speed (knots)	Start Time of Line (GMT)	Stop Time of Line (GMT)	Angle	Polarization 9.2, 15.8, 34 GHz	Polarization 22.235 GHz
2	4	132	163	19:00:25	19:16:05	10°	v	h
2	1	012	145	19:32:00	19:46:50	10°	v	h
2	3	286	145	21:37:30	21:41:50	45°	h	v
3	1	352	150	01:51:05	02:02:00	45°	v	h

of the water had virtually no effect on the microwave radiance of the sea for these frequencies.

The values of apparent input temperatures furnished to the author by Blinn (1967a) are averages over one-second. From these data, ten-second averages were calculated for certain times along the flight track.

An examination of these values showed that no steady trends in antenna temperature were evident as one moved from river water to sea water. Average values of apparent input temperature were selected for each of the flight lines, and these values were corrected for radome effects by using values of L_R given in Table XXIX in (182). The temperature of the radome was assumed to be 279° K which was the reported temperature of the air outside the aircraft during the flights. The resulting values of estimated brightness temperatures are shown in Table XXX.

The slight disagreement between values of estimated brightness temperature over lines 4 and 1 underscores the lack of absolute accuracy of these measurements. It is apparent from the detailed computations involved in arriving at values of T_b given in Table XXX that the emissive temperature of the radome is quite appreciable. The air temperature at flight level was reported to be 279° K throughout the daytime and nighttime flights.

The main difference between Flights 2 and 3 on Line 1 is the change in incidence angle from 10° to 45°. Marandino (1967)

Table XXX. Mean values of brightness temperatures for Mission 41.

Flight Number	Line Number	Polarization (p)	Incidence Angle, ψ	Frequency ν (GHz)	Estimated Brightness Temp. T_b (°K)
2	4	v	10°	9.2	148
		v	10°	15.8	131
		h	10°	22.2	156
		v	10°	34.0	167
2	1	v	10°	9.2	149
		v	10°	15.8	134
		h	10°	22.2	155
		v	10°	34.0	170
2	3	h	45°	9.2	132
		h	45°	15.8	114
		v	45°	22.2	172
		h	45°	34.0	154
3	1	v	45°	9.2	188
		v	45°	15.8	133
		h	45°	22.2	133
		v	45°	34.0	174

has calculated the distribution of T_b with incidence angle for a flat sea surface using Fresnel's Law of Reflection. His calculations show an increase of 34° K, 37° K, and 36° K in vertically polarized brightness temperature when ψ changes from 10° to 45° for frequencies of 9.2, 15.8, 22.234, and 34 GHz, respectively. The observed values of these increases given in Table XXX are 40° K, 2° K, 19° K, and 7° K, respectively. The discrepancies in the latter three values are probably due to sea roughness and foam since some white caps were visible in the photographs taken on this mission. Mandino's calculations for horizontal

polarization show a decrease in the brightness temperature of 27° K, 28° K, 17° K, and 24° K, respectively, for these same frequencies. The observed values of these decreases given in Table XXX are approximatley 16° K, 17° K, 1° K, and 13° K if one assumed that T_h equals T_v at ψ equal to 10°. Again. it appears that roughness causes the horizontally polarized brightness temperature to be higher for a rough surface than for a smooth surface for ψ near 45°. Using the apparent wind speed at flight level, one would estimate the surface wind to be about 7 meters per second. Stogryn (1967) predicted that the difference between T_h (10°) and T_h (45°) for a frequency of 35 GHz and for average conditions is 14° K. This value is remarkably close to the 13° K difference observed. Due to the extremely short fetch in this case, one must conclude that the local wind is the controlling factor in determining the effect of roughness on microwave radiation for these high frequencies.

The only other information that might be inferred from the data in Table XXX is about the humidity of the atmosphere. The curves in Figure 12 are valid if one is viewing the atmosphere from an altitude greater than 20 kilometers. Values of T_b for a frequency of 22.234 GHz were computed for an altitude of 458 meters for various values of precipitable water (W, cm) using Kreiss' values of sky temperature and values of absorption coefficients for molecular oxygen and water vapor listed in Table X. From

these values and the value of T_p in Table XXX, it appears that W was approximately 2 centimeters. This value appears to be higher than one would expect on a cold winter day. The increase in apparent brightness may be due to a small amount of breaking waves on the surface.

Mission 50

Mission 50 was flown on June 12, 1967 at 458 meters above sea level. The measurements made by the microwave radiometers during this mission have neither been calibrated nor reduced to digital form. The flight lines flown on this mission are shown in Figure 21 as solid lines. The dashed lines in this figure are the approximate flight lines flown by the Convair 990 on June 6, 1967, sponsored by the Goddard Space Flight Center. The data obtained by this flight (Flight 13) will be discussed later in this study.

Mission 66

Mission 66 was flown on February 5 and 10, 1968 at an altitude of 3048 meters and 458 meters, respectively. The raw output from the MR-62 and MR-64 microwave radiometers was calibrated and converted to digital form by the Manned Spacecraft Center (1968). There were no irregularities in these data as there were in the reduced data for Mission 41. The 9.2 GHz channel, however, did

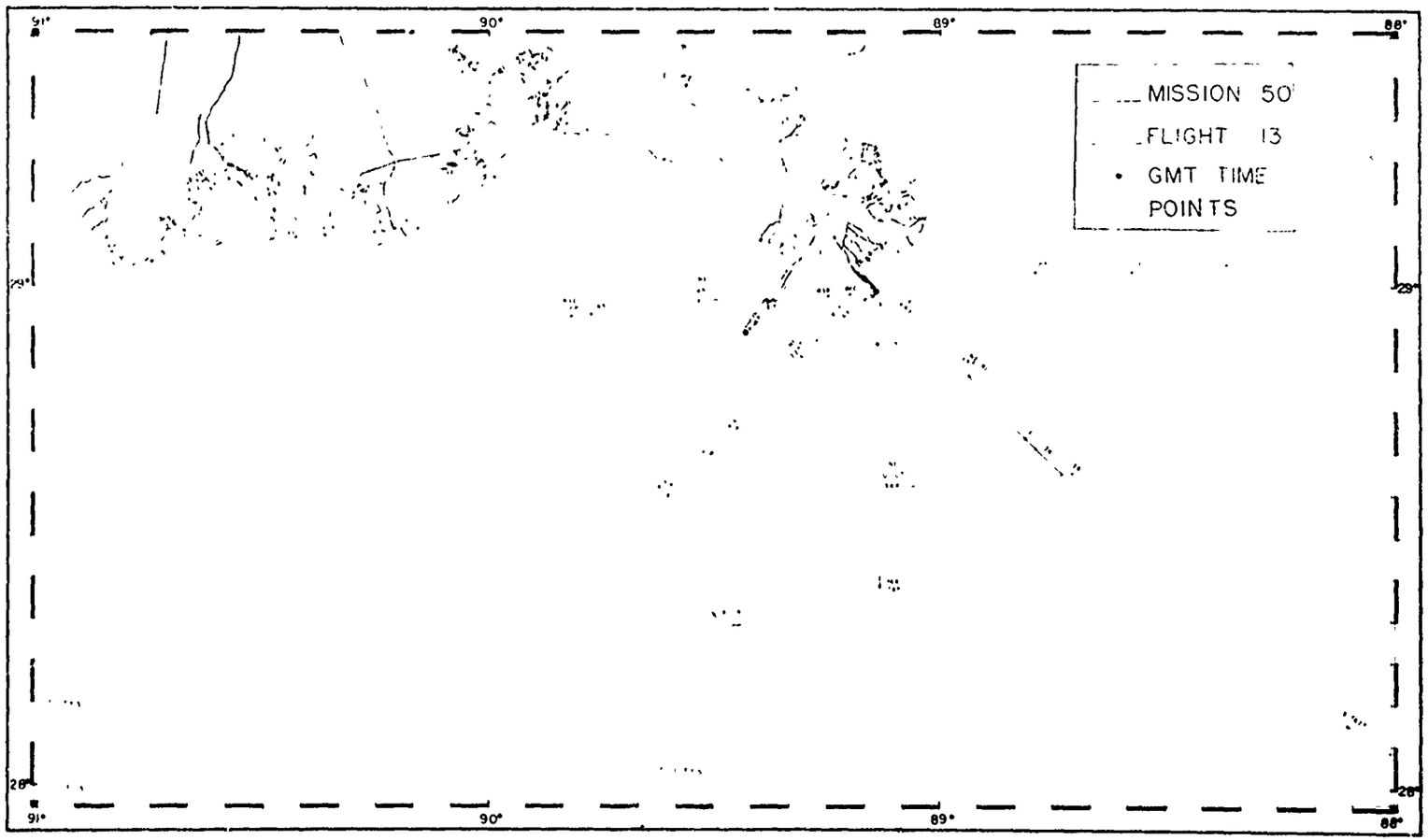

Figure 21. Flight lines flown over Mississippi Delta during Mission 50 and during Flight 13.

not function properly except for one brief segment.

Flight 1 of Mission 66 was flown on February 5, 1968 from 19:23:30 Z[8] to 19:29:00 Z at an altitude of 3048 meters over Line 1 only. Turbulence and fuel problems forced a cancellation of the rest of this flight. The air temperature at flight level was 274° K.

Flight 11 of Mission 66 was flown on February 10, 1968, from 16:08:55 Z to 16:50:52 Z at an altitude of 458 meters and covered Lines 1, 41, and 4. The air temperature was 283° K at flight level during Lines 1 and 41, and it was 284° K during Line 4.

An extensive survey of the test site was conducted by R/V ALAMINOS, the departmental research vessel of Texas A&M University, from February 9 to February 13, 1968, during cruise 68-A-1. The track chart for this cruise is shown in Figure 22. Figures 23 and 24 show the distributions of surface temperature and surface salinities based on the data obtained during cruise 68-A-1.

The temperature and salinity of the surface layer are plotted versus the distance from South Pass (d, miles) along Flight Line 1 in Figure 25.

The actual measurements made by the microwave radiometers were furnished to the author as one-second averages of apparent input temperature versus the time (z). Ten-second averages were computed for every 20 seconds to smooth the data. The apparent

[8] Z refers to Greenwich Meridian Time.

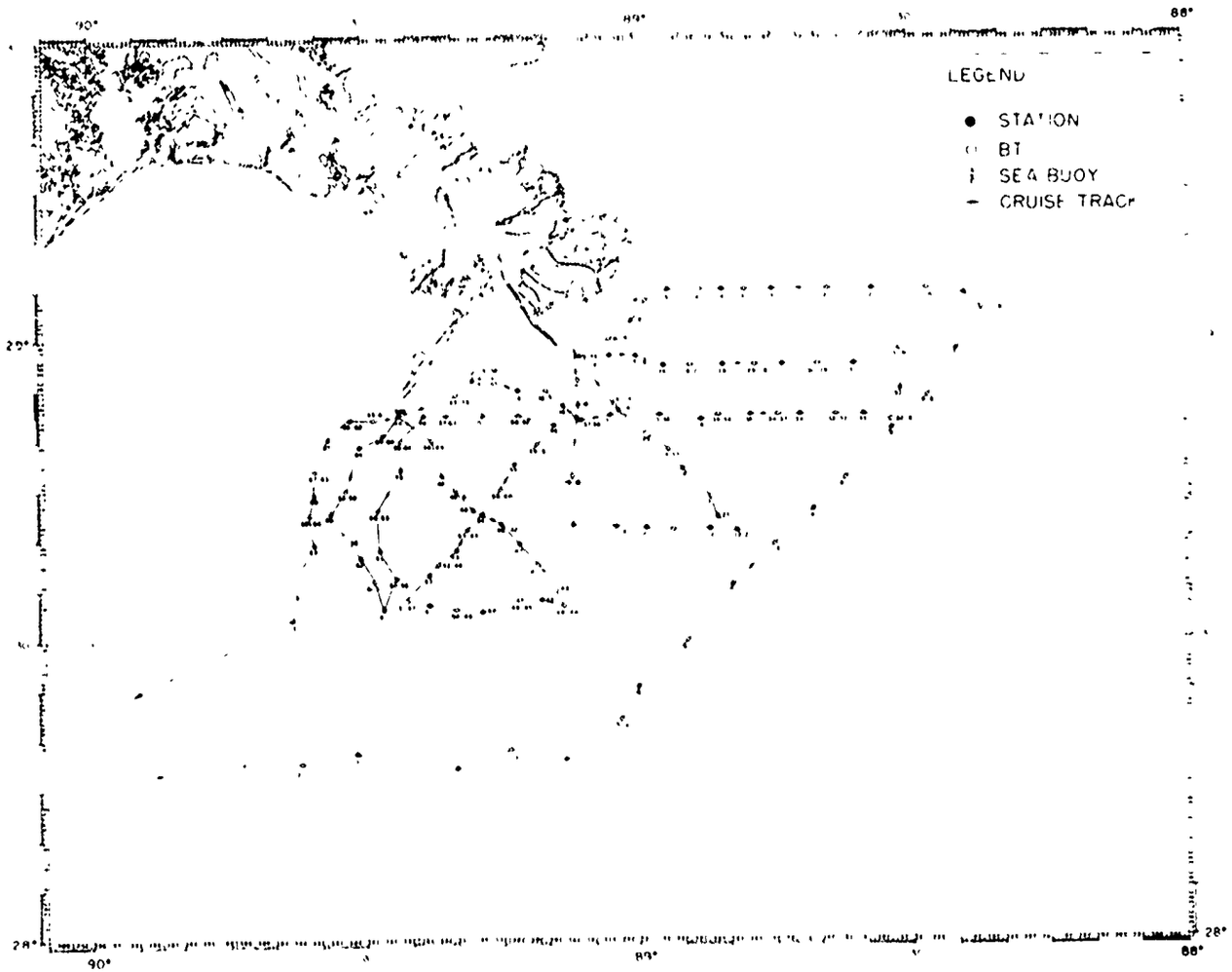

Figure 22. Cruise track of R/V ALAMINOS during Cruise 68-A-1.

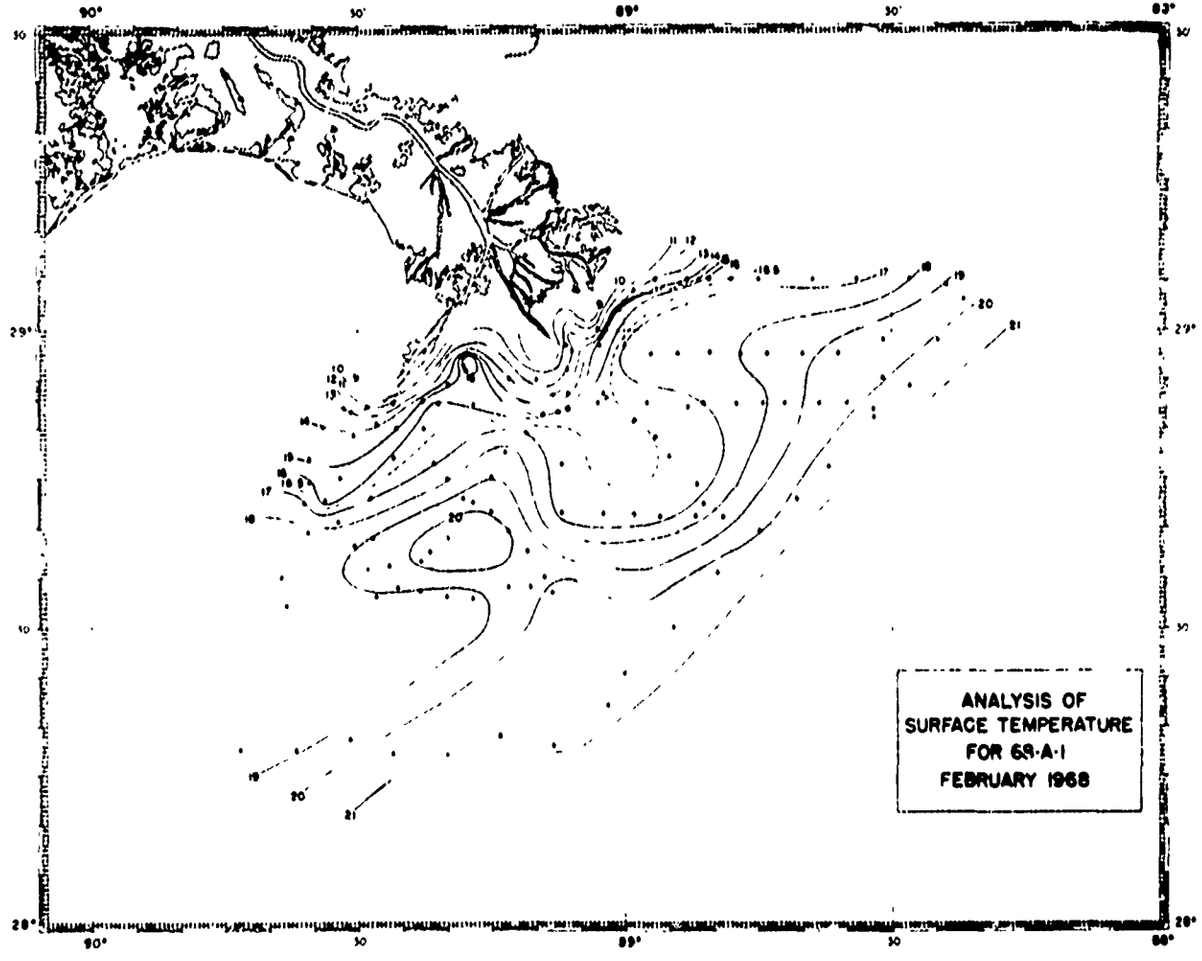

Figure 23. Analysis of surface temperature for 68-A-1, February 1968.

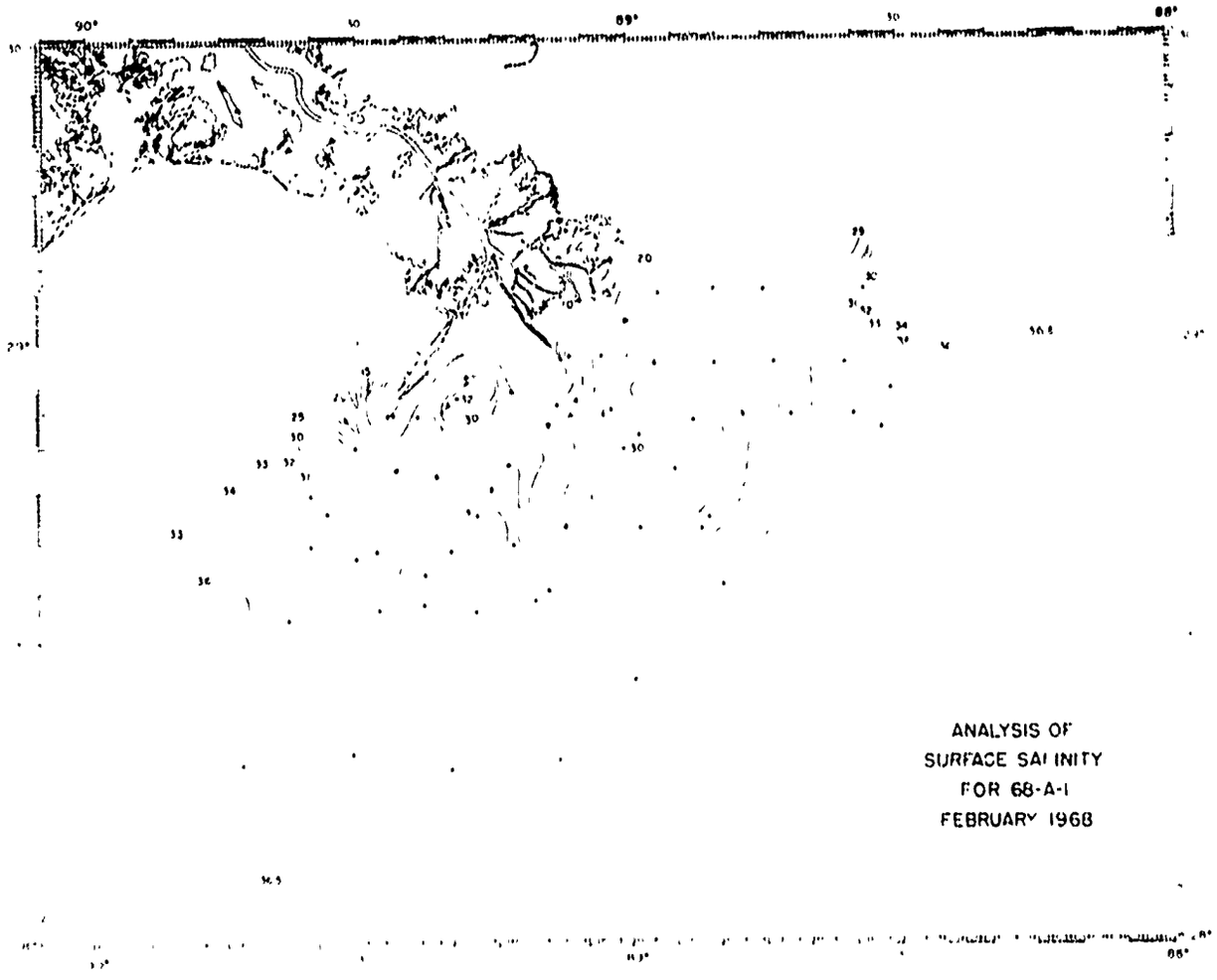

Figure 24. Analysis of surface salinity for 68-A-1, February 1968.

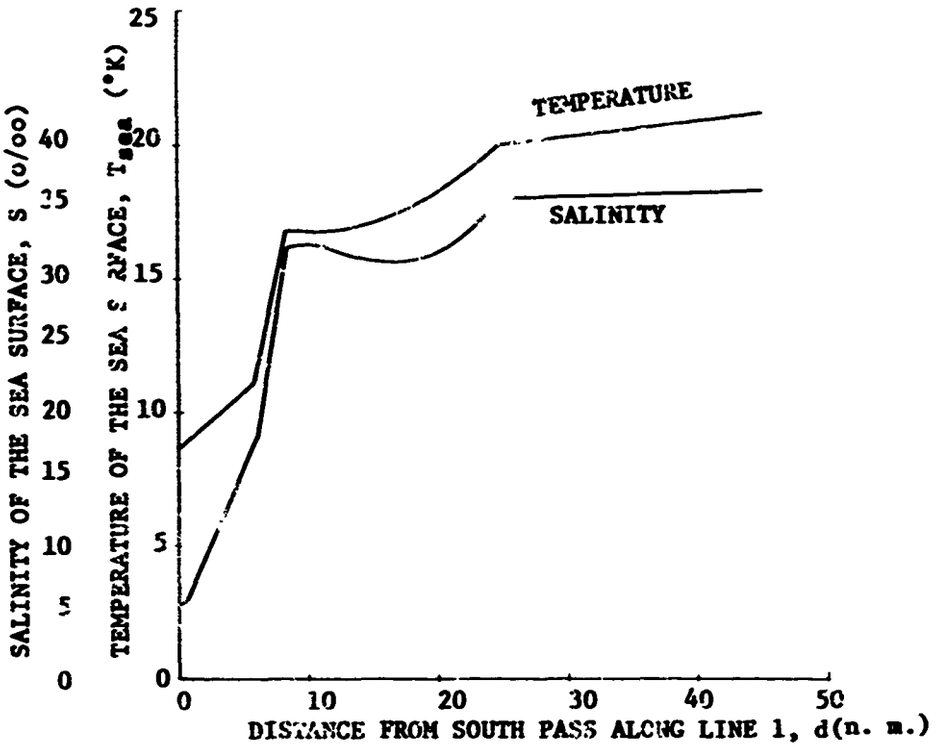

Figure 25. The distribution of temperature and salinity along Line 1 from analyses in Figures 23 and 24.

input temperatures were corrected for radome effects as before. The resulting estimated brightness temperatures are plotted versus d in Figures 26 and 27 along with the theoretical values based on the distributions of temperature and salinity given in Figure 25. The measured values are shown as circles, triangles, or squares on the following figures. The theoretical values are plotted as solid lines, these lines are adjusted in absolute value to allow one to compare the relative changes that occurred as the flight line was flown.

The measured values of brightness temperature at a frequency of 9.2 GHz show that this channel was not operating properly. The shape of the theoretical curve for 15.8 GHz fits the general shape of the measured profile. There appears to be a regular fluctuation in the signal measured at 458 meters at the frequencies of 15.8, 22.234, and 34 GHz. On the other hand, an overall drift is apparent in the readings at 3048 meters.

In all cases, there appears to be no information in these measurements about the distribution of temperature or salinity. The fact that the readings of the 34 GHz channel are much higher for low levels than for middle levels gives one reason to suspect the readings from the MR-64 on both of these flights.

The mean value of the readings of the 22.235 GHz channel indicate that the precipitable water was approximately 2.5 cm.

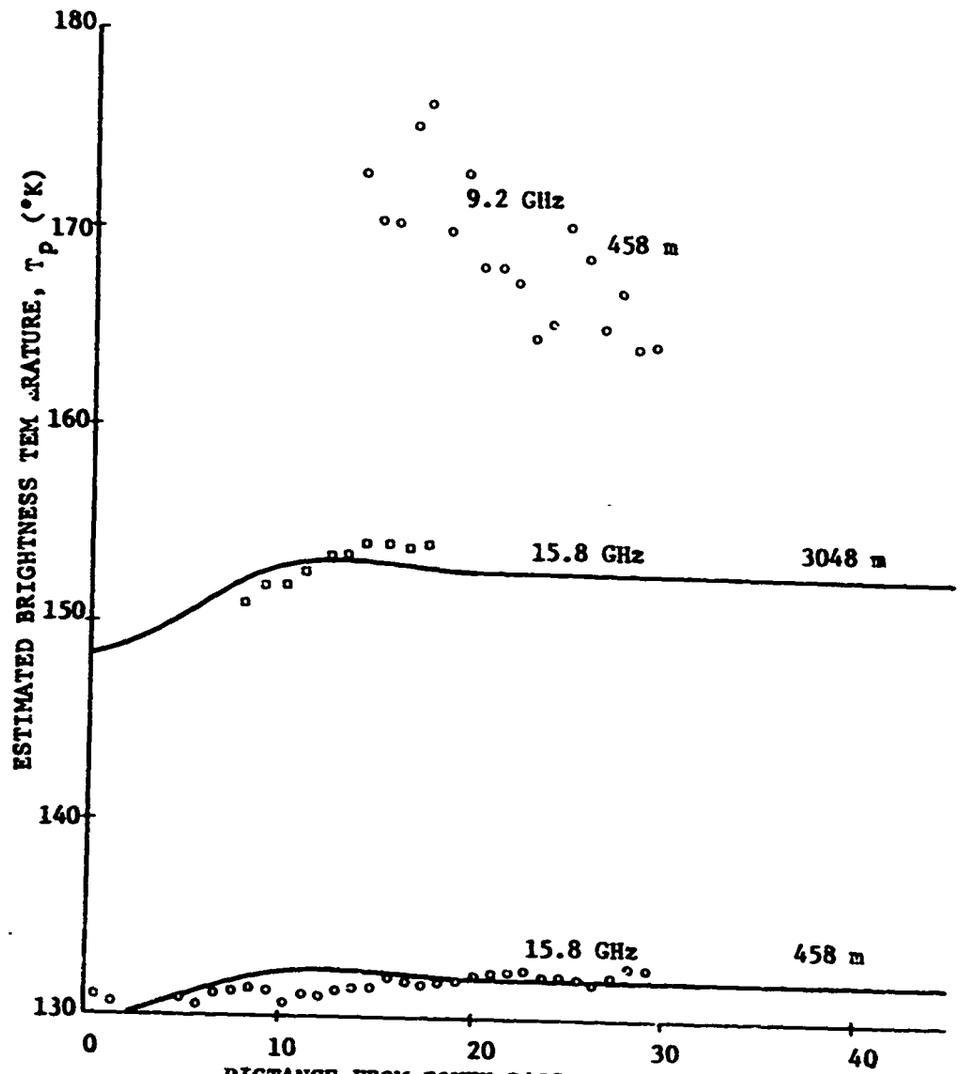

Figure 26. Estimated brightness temperatures measured over Line 1 of Mission 66 at altitudes of 3048 meters (squares) and 458 meters (circles) and corresponding theoretical values of brightness temperatures (solid lines) versus distance from South Pass for frequencies of 9.2 GHz and 15.8 GHz.

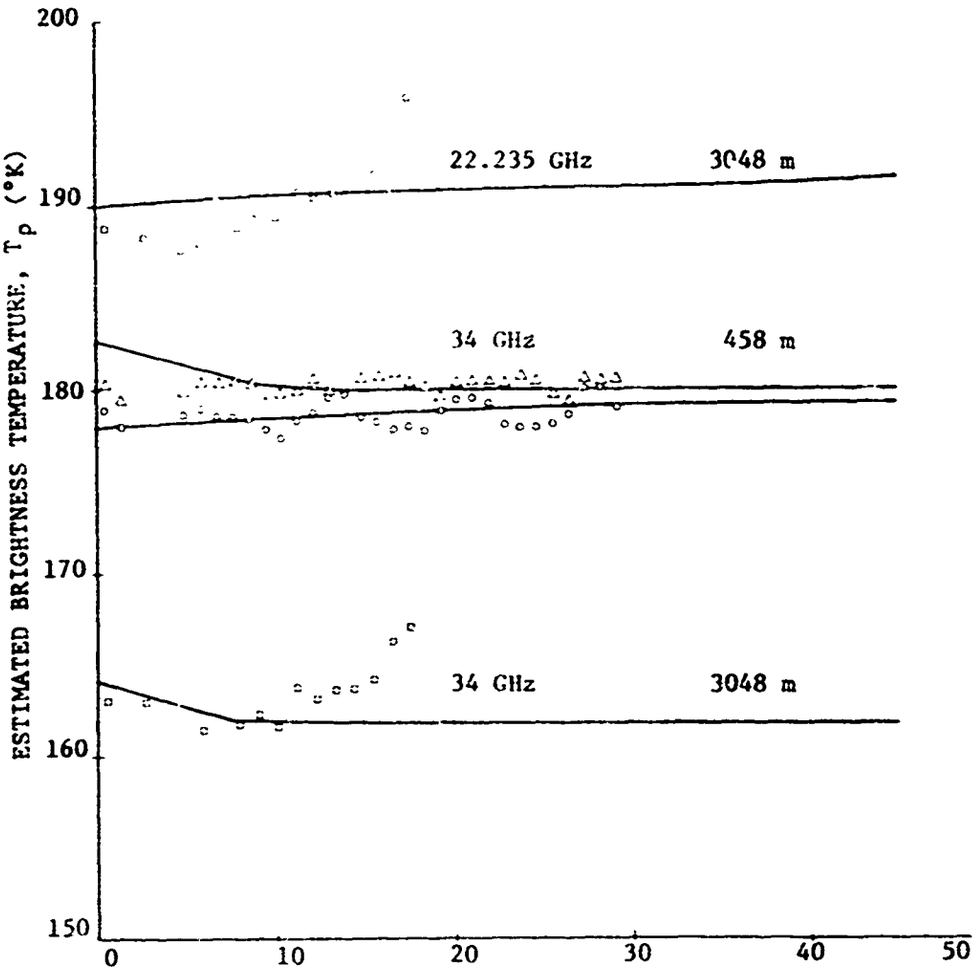

Figure 27. Estimated brightness temperatures measured over Line 1 of Mission 66 at altitudes of 3048 meters (squares) and 458 meters (circles & triangles) and corresponding theoretical values of brightness temperatures (solid lines) versus distance from South Pass for frequencies of 22.235 GHz and 34 GHz.

Implications for future missions

Using the distribution of temperature and salinity shown in Figure 25, the author computed theoretical values of polarized brightness temperature for each nautical mile along Line 1 for an incidence angle of 0° and for the frequencies of 5.4 GHz and 1.0 GHz. The effects of the intervening atmosphere between the observer and the sea surface were neglected in these calculations. The zenith sky temperatures were assumed to be 10° K at 1.0 GHz and 5° K at 5.4 GHz. The results of these calculations are shown in Figure 28. It has been shown in Chapters V and VI that the polarized brightness temperature of the sea is a function of sea temperature only at 5.4 GHz. The polarized brightness temperature radiation at a frequency of 1.0 GHz is strongly dependent on salinity and slightly dependent on sea temperature. Therefore, it appears that one should be able to survey the distribution of temperature and salinity along coastal areas using a dual-frequency radiometer which operated at 5.4 GHz and 1.0 GHz.

In the summer, the discribution of temperature along coastal regions is often inconclusive; however, the salinity distribution does act as an indicator of coastal mixing and other coastal processes. A survey was made of the area south of the Mississippi Delta by the R/V ALAMINOS in late August 1967. Figures 29 and 30 show the distributions of surface temperature and surface salinity, respectively, derived from the data obcained during this cruise

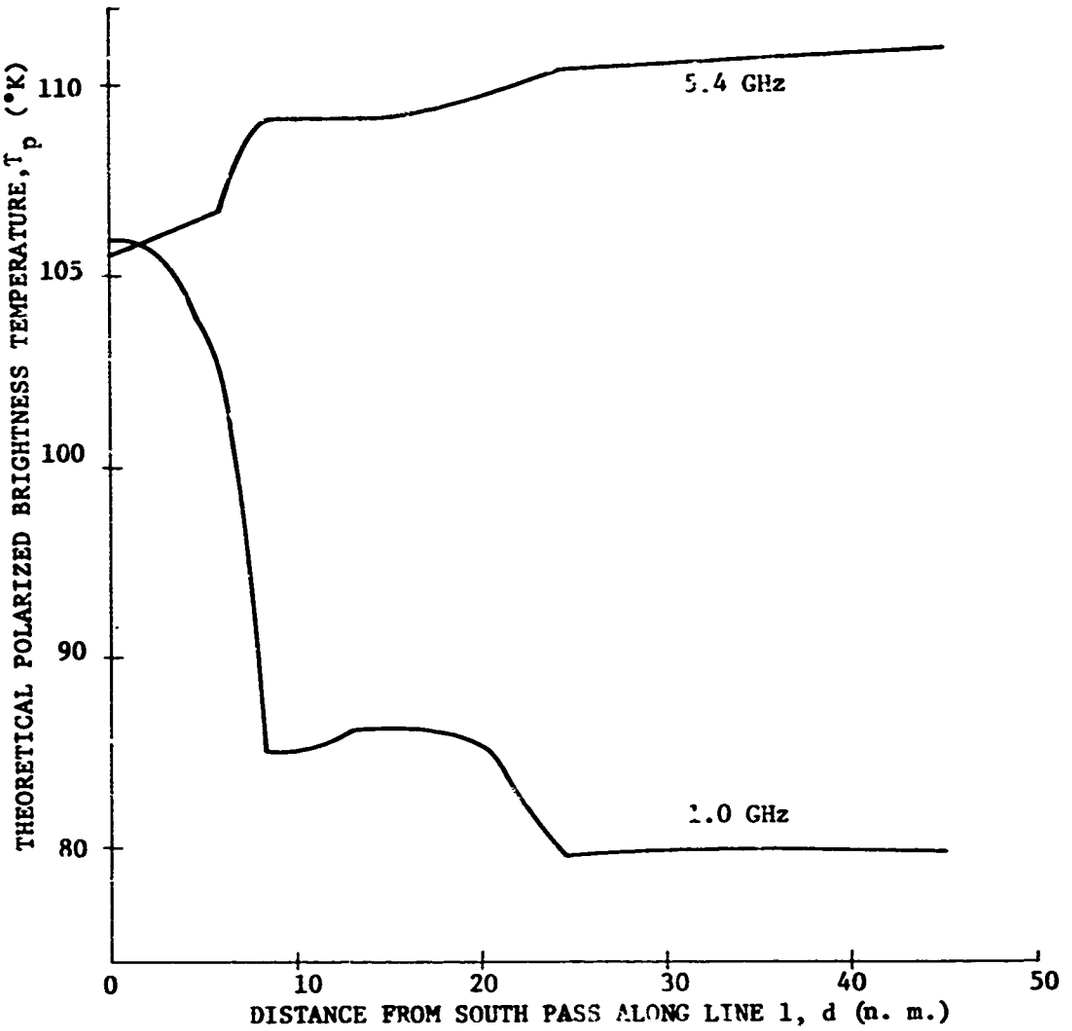

Figure 28. Theoretical polarized brightness temperatures versus distance from South Pass for the distribution of temperature and salinity given in Figure 24, for frequencies of 5.4 GHz and 1.0 GHz, and for an incidence angle of 0°.

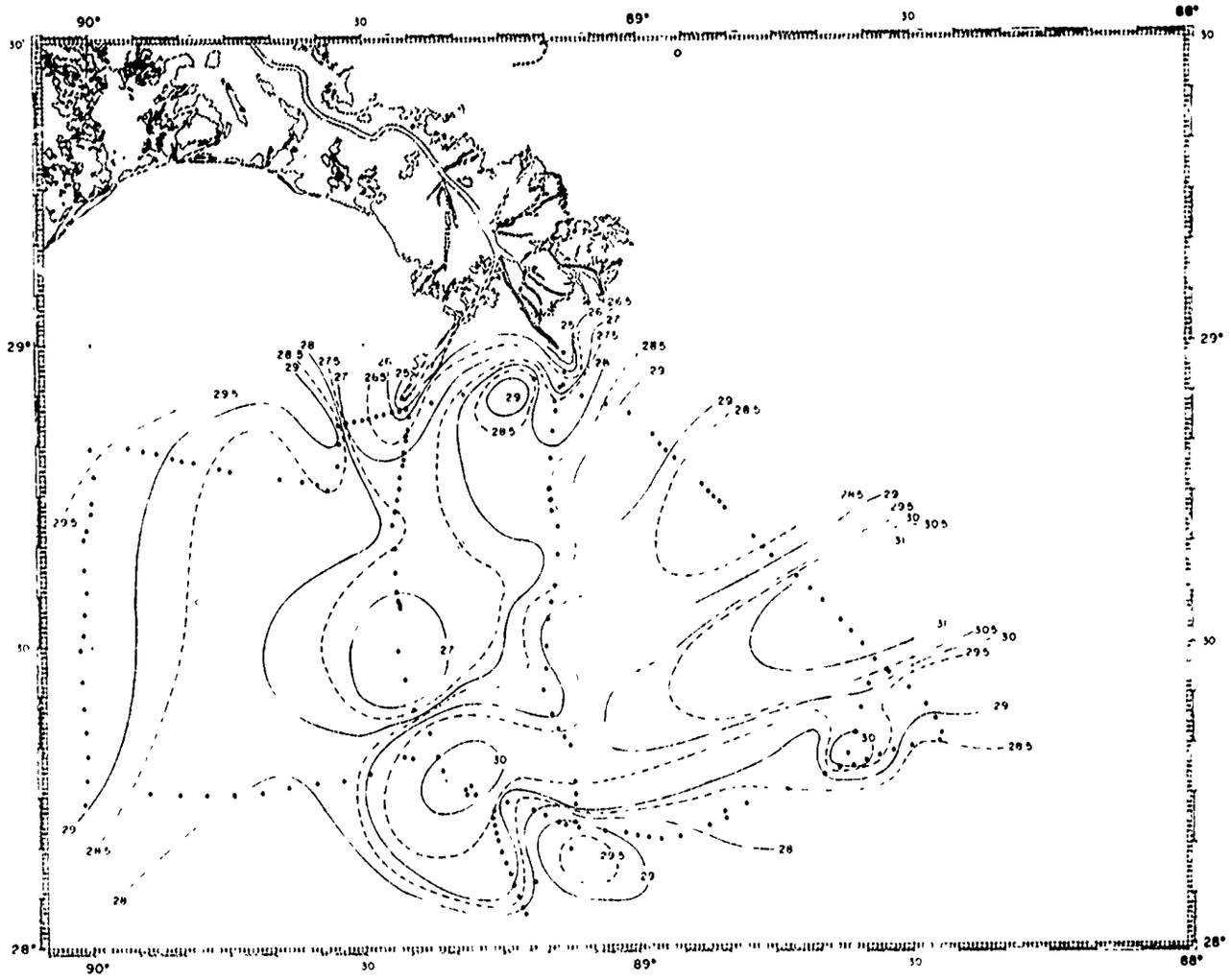

Figure 29. Analysis of surface temperature for 67-A-7 based on readings of the infrared radiometer on the R/V ALAMINOS.

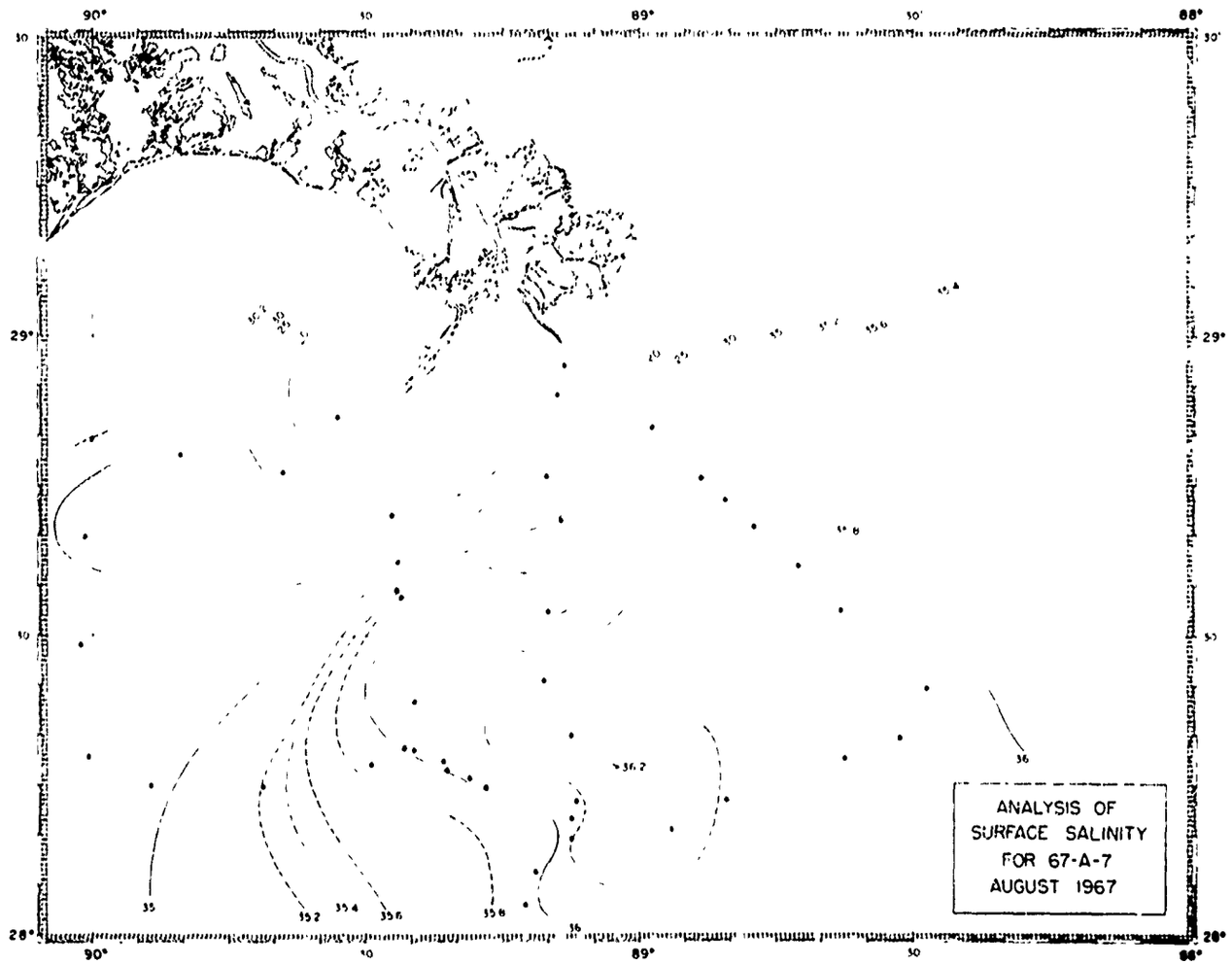

Figure 30. Analysis of surface salinity for 67-A-7, August 1967.

(67-A-7). These figures show the consistency of salinity as an indicator of coastal and river phenomena.

A new set of microwave radiometers is scheduled to be installed in the P3A aircraft sponsored by NASA as a part of the Earth Resources Survey Program. One channel of these radiometers operates at a frequency of 1.4 GHz. It is hoped that these radiometers can be used in April 1969 to test the hypothesis presented in this report.

Microwave Radiometers in the Convair 990

Systems description

Under the sponsorship of the Goddard Space Flight Center, an electronically scanned radiometer operating at a frequency of 19.35 GHz with a bandwidth of 400 MHz has been flown over parts of the Gulf of Mexico during June 1967 (Catoe, et al., 1967). This radiometer uses an 18 inch by 18 inch array of dipoles as an antenna. The phase relationships between respective dipoles are controlled in such a manner as to form a highly directive gain pattern that can be step scanned sideways up to ±50° from the nadir. The ratio of the effective solid angle of the main lobe of this gain pattern to 4π steradians is about 0.9 or higher depending on the looking angle. This indicates that the phased dipole antenna is quite directive and surpresses sidelobes efficiently. The sensitivity of the measured antenna temperatures

is claimed to be about 2° K (Catoe, et al., 1967). The polarization is horizontal. The Goddard Space Flight Center has calibrated and digitized the readings of this radiometer. The output is displayed as apparent antenna temperature versus incidence angle and time. The entire angular span of 100° is broken into 39 separate angles, and the readings are presented for each of the scan lines which are approximately 2 sec apart in time.

It has been mentioned in Chapter VI that there appear to be three applications for this instrument. First, one may be able to determine the roughness of the sea surface by comparing the measured values of horizontally polarized radiation for ψ near zero degrees to those at ψ near 50°. Secondly, the amount of precipitable water in the atmosphere may be inferred from the absolute value of horizontally polarized radiation for ψ near zero degreees under conditions of clear sky. Thirdly, it may be possible to determine the concentration of liquid water in undercast clouds. These three applications will be treated briefly in the next sections.

Roughness

This microwave radiometer was flown over the central western Gulf of Mexico on June 5, 1967, at an altitude of about 10,000 meters. Reports from surface ships indicated that the sea temperature was approximately 18.0° C over the area and that the salinity

was approximately 36.5 o/oo (Arnold, personal communication, 1968). Photographs taken from the Convair 990 during this flight (Flight 12) indicated that the sky was practically clear and that the surface was practically smooth and flat for the portion of this flight from 18:13:00 Z to 18:13:30 Z. The readings of the radiometer were averaged over this period for each angular position. These averages are plotted in Figure 31 versus scan angle (ψ) and are connected by a dashed line. The theoretical distribution of horizontally polarized brightness temperature with incidence angle given by Stogryn (1967) for a flat sea surface is shown in Figure 31 as a solid line. The measured antenna temperatures and the theoretical brightness temperatures agree for ψ near 0° and for ψ near ±50°. The disagreement between these values for ψ near ±20° is probably due to antenna effects. During the time near 18:04 Z the sea surface was reported by the pilot to be a rough sea surface, no white caps---sea rough enough for Doppler to operate (Tobin, 1967). During this period of time, the horizontally polarized brightness temperature at ±50° was about 4° K lower than that at 0°. From Table XXVIII, it appears that this decrease would be caused by a surface wind of about 10 meters per second. This value exceeds the critical wind speed at which waves would begin to break on the surface. Considering the accuracy of these measurements and effects of the antenna, one should be satisfied that the emissivity of the water

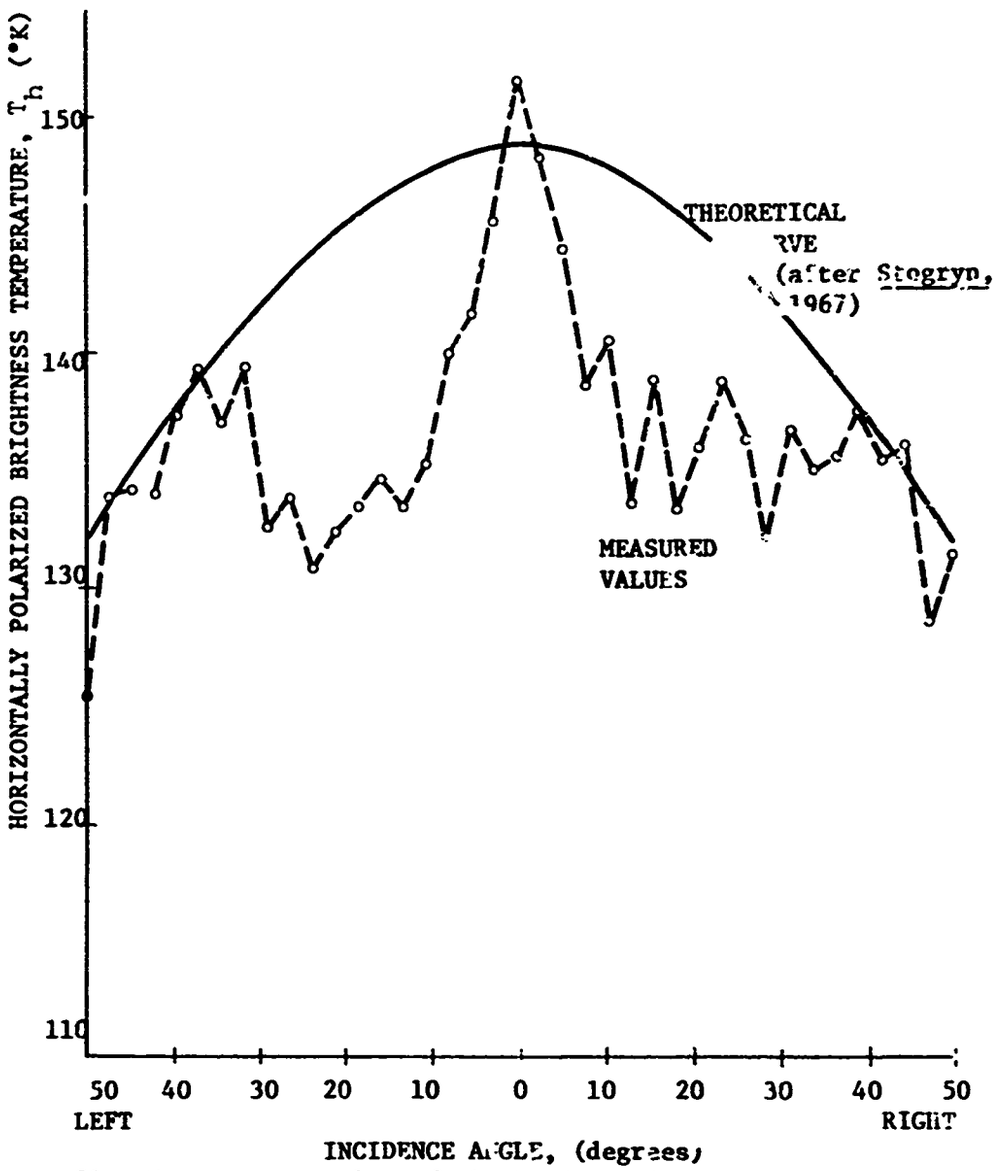

Figure 31. The average value of the horizontally polarized brightness temperature (circles and dashed line) measured during Flight 12 from 18:13:00Z to 18:13:30Z versus incidence angle and corresponding theoretical values (solid line) from Stogryn (1967) for a frequency of 19.35 GHz.

had apparently risen for ψ near 50° due to the increase in surface roughness.

Precipitable water

The highest altitude flown by the Convair 990 was about 11,000 meters above the sea surface. Figure 32 shows the distribution of the estimated brightness temperature for an incidence angle of 0° versus time for a portion of Flight 12. The coast of Texas near Houston, Texas, was crossed during this time. One should note, incidentally, the large decrease that occurs in the estimated brightness temperature when one goes from land to water. One may even distinguish between the Intercoastal Canal and the narrow strip of land that separates it and the Gulf of Mexico. It appears that the average value of the brightness temperature observed over the land was about 148° K. The curves in Figure 12 may be used to estimate the amount of precipitable water in the atmosphere for this June day as being about 1.9 centimeters. This value appears to be reasonable for the season and the observed clear sky.

Liquid water

On June 6, 1967, the Convair 990 was able to fly over various types of clouds in the Gulf of Mexico. One portion of this flight (Flight 13) passed directly over a small group of cumulus clouds. The calibrated values of brightness temperature from the 19.35 GHz

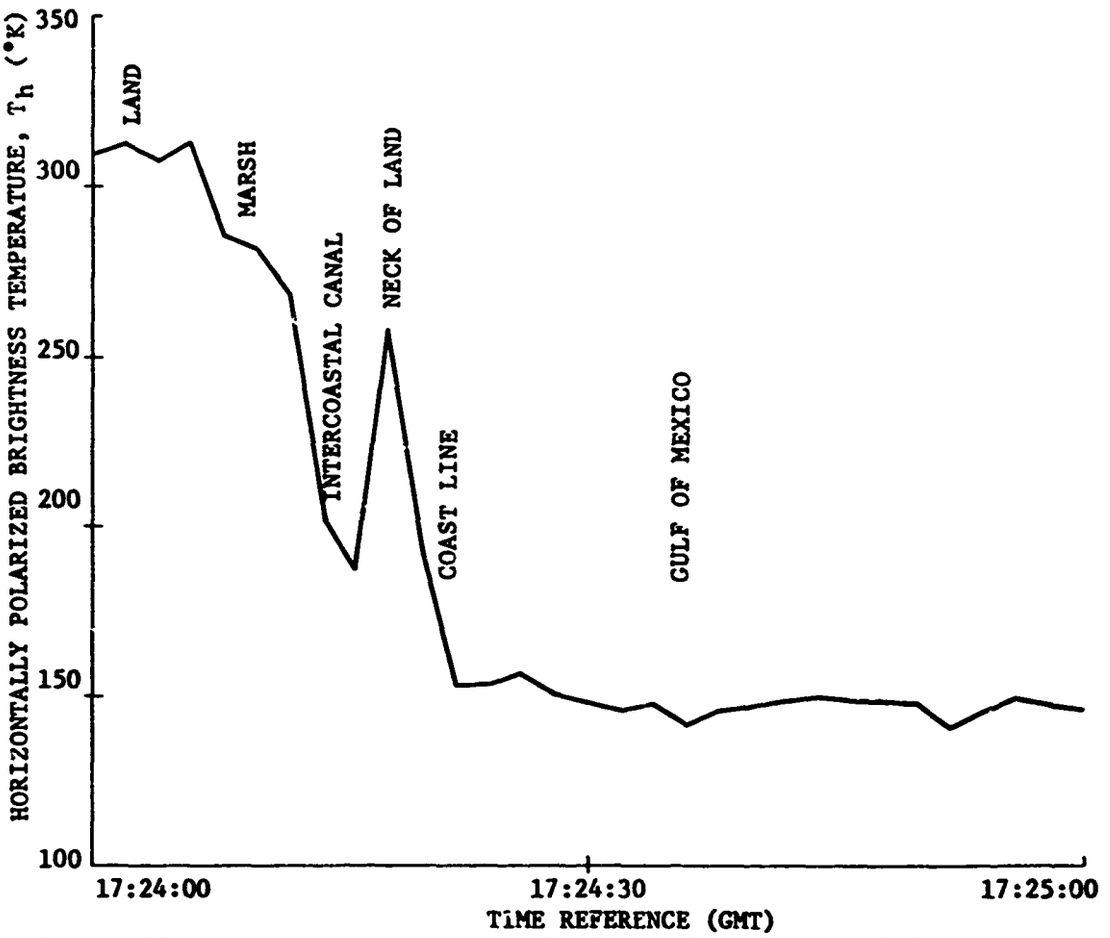

Figure 32. Measured values of the horizontally polarized brightness temperature from 17:24 Z to 17:25 Z during Flight 12 versus time for an incidence angle of 0° and for a frequency of 19.35 GHz as the aircraft flew from land to water.

radiometer are plotted in Figure 33 versus time for an incidence angle of 0°. The actual values are shown as circles in this figure and the smoothed analysis of these data is indicated by the solid line. One should note that a slight increase occurred in the readings when the visible edge of the cloud was passed. When the aircraft was over the core of the cloud, an enormous increase was noted in the brightness temperature. It is probable that this increase occurs over portions of the cloud which contain water droplets large enough and dense enough to fall as rain. The top of the cloud was estimated to be at an altitude of 4600 meters. The cloud bases were estimated to be about 600 meters above the sea surface. The thickness of this cloud seems to correspond most closely to the case of a 'thick stratus' cloud considered before in Chapter VI. If one assumed that the curve for thick stratus in Figure 14 is valid for the cloud overflown in Figure 32, one may compute a horizontal profile of the mean concentration of liquid water in this cloud. The computed values for the curve in Figure 15 were reduced by a factor of 0.6 to allow for the difference in cloud thickness. The resulting distribution of the mean concentration of liquid water (M, g/m^3) is plotted versus time (Z) in Figure 34. The increase in brightness temperature over the brightness temperature observed over the clear ocean was used in the computations. The actual distribution of liquid water in this particular cloud was unknown. The raindrops probably

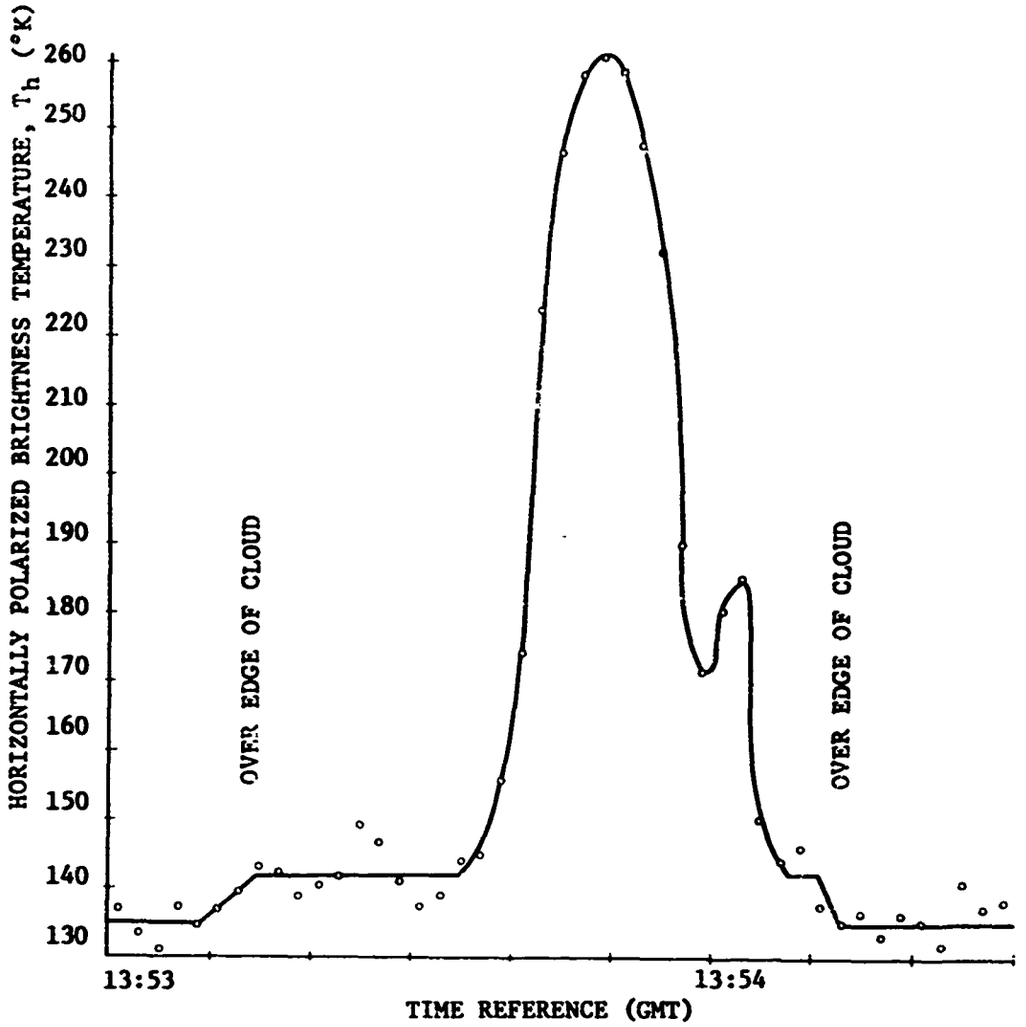

Figure 33. The estimated horizontally polarized brightness temperature from 13:53:00 Z to 13:54:30 Z during Flight 13 versus time for an incidence angle of 0° and for a frequency of 19.35 GHz as the aircraft flew over raining clouds at sea.

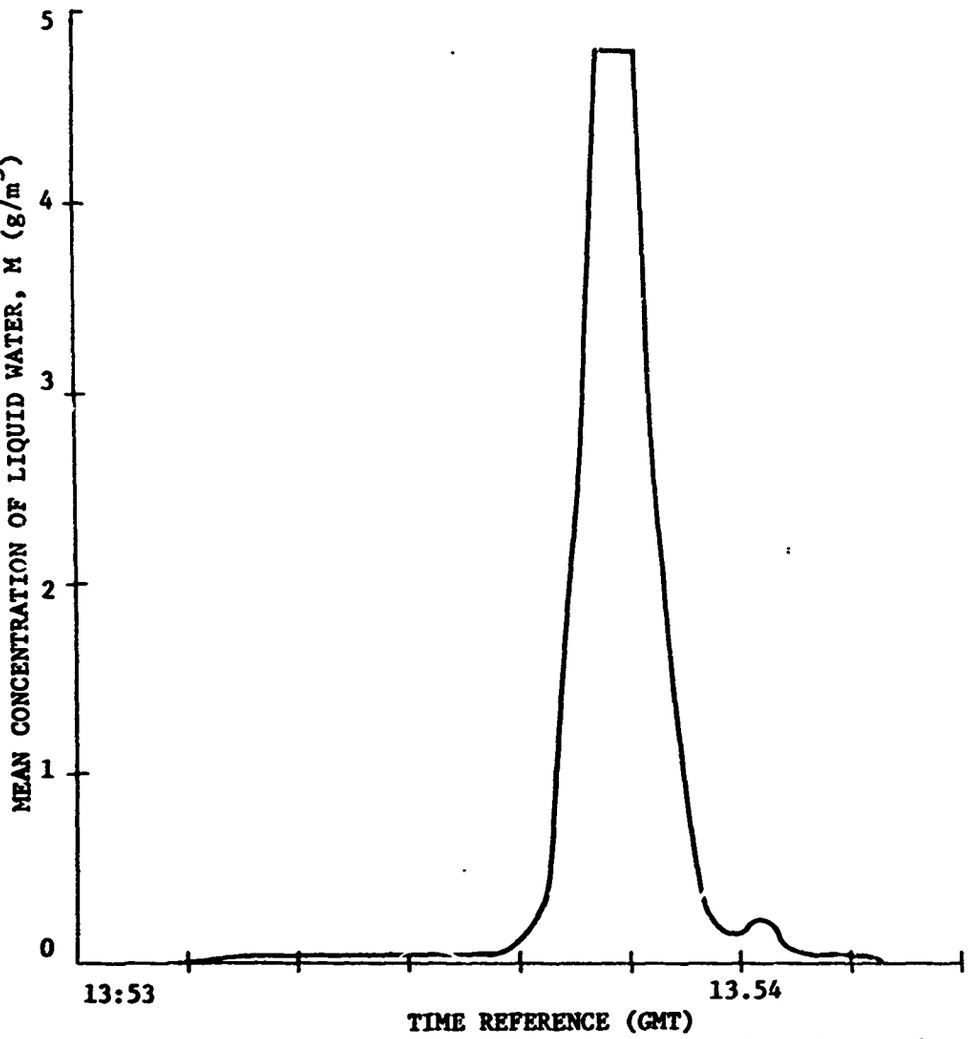

Figure 34. The distribution of the concentration of liquid water in the clouds under the aircraft as derived from the measurements given in Figure 33.

produced bubbles on the sea surface. In this case, it is inadvisable to use Kreiss' curves for obtaining M.

The microwave radiometer on board the Convair 990 scans sideways to the path of the aircraft, and it is possible to obtain an image or map radiometric values along a strip. It is hoped that this radiometer could be flown on one of the Nimbus spacecraft. Using this one radiometer alone, it should be possible to survey rainbands at sea, determine the moisture content of the atmosphere over the oceans and possibly determine the roughness of the sea surface. Land-water boundaries and water-ice boundaries could be surveyed in remote areas of the world.

CHAPTER IX

CONCLUSIONS AND RECOMMENDATIONS

Conclusions

Microwave radiometry has a great potential as an observational tool in meteorology and oceanography. The greatest disadvantage is that there are the large number of variables that significantly affect the intensity field of microwave radiation at some location above the surface of the sea. Nevertheless, further research in microwave radiometry is fully justified.

There appear to be no serious gaps in the state of knowledge concerning the various aspects of microwave radiometry; however, all aspects must be investigated more fully to enable one to use this tool with confidence. There is a lack of accurate measurements of microwave radiance over the sea under conditions in which appropriate environmental support measurements are available. Most of the theoretical predictions that have been made of microwave radiance have yet to be confirmed by actual measurements over the ocean.

Dielectric properties of water

The ability to predict the emission and extinction of sea water is dependent upon one's knowledge of its complex dielectric constant as a function of salinity, temperature, and frequency

of observation. The fundamental basis of these investigations, at the present time, are the observations by Lane and Saxton of the electric behavior of an aqueous solution of sodium chloride made in the 1940's. Although there is no reason to expect that the electric properties of such a solution and that of actual sea water differ significantly, it is desirable to determine as accurately as possible the electric properties of sea water under various conditions of salinity and temperature throughout the microwave region of the electromagnetic spectrum.

Radiative transfer

It is possible to specify the intensity of microwave radiation in a horizontally homogenous, non-scattering atmosphere overlying a homogenous water surface by solution of the equation of radiative transfer if one can specify the distributions of temperature and absorption coefficient with height and depth. This approximation to the real atmosphere and hydrosphere is valid as long as there are no clouds of large water droplets in the atmosphere and as long as the sea surface is relatively undisturbed. Otherwise, scattering cannot be neglected. If one is to consider scattering, the problem of solving the equation of radiative transfer becomes enormously complicated since the entire field of intensity must be specified at each point in the atmosphere. In many cases, the real atmosphere is not horizontally uniform, for example, in the vicinity of thunderstorms and fronts. These situations, too,

must be considered in the future.

Thermodynamic equilibrium

The source function for thermal emission by atmospheric and hydrospheric constituents is assumed to be Planckian for all cases considered. This form is valid only if a condition of thermodynamic equilibrium exists throughout the entire environment. It has been noted that the amount of thermal energy transferred as microwave radiation is much smaller than that transferred as infrared radiation. Suppose that a radiational imbalance existed in some location in the atmosphere as far as a particular band of microwave frequencies is concerned. One would expect the resultant rate of heating or cooling to be insignificantly small. Thus, the idea that this imbalance would be lessened greatly through changes in internal energy appears to be invalid in this case. A final proof for any theory, of course, lies in its ability to predict results that agree with measurements under controlled conditions or well-known conditions in the environment.

Water vapor and molecular oxygen

The theory of absorption and emission by water vapor and molecular oxygen in the atmosphere was formulated by Van Vleck in the 1940's. The distributions of these atmospheric constituents are easily specified in the case of oxygen, but the distribution of water vapor is usually unknown. It appears that the

natural variability of water vapor in the atmosphere has little effect on the amount of microwave energy absorbed or emitted by the atmosphere when the frequency is less than 8 GHz. Most studies of the microwave emission of water vapor are made by assuming a simple exponential decay of its density with height. Real distributions should be considered to determine fully if this variable can be surveyed remotely through measurements of appropriate microwave radiances.

It appears that the several engineering approaches to the problem of emission of water vapor in the atmosphere yield only approximations. If one is able to use relative measurements of microwave radiance as opposed to absolute measurements, it is not necessary to be able to predict accurately the contribution of the overall radiation that comes from the atmosphere.

Hydrometers

The effect of extinction or emission by ice crystals in the atmosphere can be neglected in most cases. The extinction of liquid water is linearly proportional to the concentration of liquid water in a cloud of water droplets if the maximum size of the droplets is small, for example, as in the case of droplets in fog and non-raining clouds. Extinction in raining clouds becomes more complicated and scattering must be considered. Since scattering and absorption of clouds of large droplets must be

treated by the precise theory developed by Mie, the distribution of drop sizes in the cloud becomes a factor. The investigations in this area are elementary at present and much work is needed. One needs to ascertain the effect of bubbles and foam that are formed on the sea surface where rains fall into the sea.

Air-sea interface

Since the ocean returns approximately two-thirds of the microwave radiation incident upon its surface to the atmosphere as scattered or reflected radiation, it is necessary to determine the effect of various configurations of sea surfaces. Emipirical methods must be used to specify the scattering of the rough sea as a function of incidence angle, polarization, sea temperature, sea salinity, electromagnetic frequency, and roughness. Based on meager evidence to date, it appears that the sea surface behaves as a specular reflector for viewing angles near normal incidence (Stogryn, 1967). If foam exists on the sea surface as a result of large surface shearing stresses, one must expect roughness to be a factor at all angles.

Sea temperature

Due to the relaxation of water molecules, the emissivity of sea water decreases with increasing temperature for frequencies above about 8 GHz. Current microwave measurements lie in this range of frequencies, therefore, it is not possible to determine

the temperature of the sea surface by available radiometers. It appears that the emissivity of sea water remains fairly constant or increases slightly with temperature for frequencies near 5.4 GHz.

Salinity

The effect of changes in the salinity of sea water on the brightness temperature of sea water is negligible for frequencies above 4 GHz. Investigations of this effect for frequencies above 1 GHz revealed that the effect of salinity is dominant for frequencies between 1 GHz and 3 GHz and that the effect of salinity is largest at 1.0 GHz and for viewing angles near normal incidence. It appears that microwave radiometers operating at 1.0 GHz and 5.4 GHz could be used to survey remotely temperature and salinity along coastal and river regions of the world. Imaging radiometers operating at these frequencies might be able to map the location of major water mass boundaries.

Foam, bubbles, ice, and land

Microwave measurements and theory indicate that one should be able to determine the amount of foam or ice covering the ocean surface at some location and to survey land-sea and ice-sea boundaries remotely by using scanning microwave radiometers. Accurate measurements are needed to determine the effect of foam under various environmental conditions.

Microwave radiometry

The current generation of microwave radiometers should be accurate enough to allow scientists to make microwave measurements that can be used, practically, for a large number of applications. Sensitivities of 0.5° K are needed in most applications to oceanography. Presently available microwave radiometers are sufficiently accurate for meteorological applications.

Applications

In summary, the following oceanographic measurements appear feasible from airborne or spaceborne microwave radiometers: (1) determination of surface roughness, (2) determination of surface temperature, (3) determination of surface salinity, (4) detection of icebergs, (5) survey of ice fields, (6) determination of foam cover, and (7) survey of precipitation.

The following meteorological measurements seem feasible: (1) measurement of moisture content of atmosphere from spacecraft, (2) survey of rainbands, (3) determination of concentration of liquid water in non-raining clouds, and (4) sounding of temperature (not covered in detail in this study).

Recommendations

The following suggestions are offered for future research and action:

1. Numerous measurements of the microwave radiance over the ocean are needed under known environmental conditions so that existing microwave theory may be tested throughly and so that certain empirical determinations can be made, for example, the nature of the bistatic scattering cross-section for a real ocean surface. Atmospheric soundings of temperature, humidity, and pressure are needed to support any measurement program for meteorological applications. An appropriate set of microwave radiometers should be mounted on a research vessel so that accurate surface measurements can be made of the brightness temperature of the sky and the sea. To avoid the effects of being in the near field, one would mount antennas on a high platform.

2. Flights should be made of the microwave radiometers scheduled to be placed on the P3A aircraft sponsored by NASA over the outflow region of the Mississippi Delta to test the feasibility of measuring salinity with the 1.4 GHz channel.

3. Extensive studies of the electric properties of sea water as a function of its temperature, its salinity, and its dissolved gases should be made for frequencies throughout the microwave regions. Controlled studies of the emission of sea foam and bubbles should be included in this study.

4. The effects of liquid water in the atmosphere should be studied rigorously using the Mie equations to specify scattering and using realistic models of atmospheric clouds. This study

would constitute a major study into practically all area of concern to microwave physics. Computer programs would have to be developed. Simultaneous surveys of the atmosphere by radiometer, radar, and in situ instruments would need to be made under various meteorological conditions.

BIBLIOGRAPHY

Abbott, R.L., Width of the microwave lines of oxygen and their relationship to the thermal noise emission spectrum of the atmosphere, Proc. 3rd Symp. Remote Sensing of Environ., Ann Arbor, Michigan, 257-269, November, 1965.

Aden, A.L., Back-scattering of Electromagnetic Waves from Spheres and Spherical Shells, Air Force Cambridge Research Center Geophys. Res. Papers No. 15, 42 pp., 1952.

Aden, A.L., and M. Kerker, Scattering of electromagnetic waves by two concentric spheres, J. Appl. Phys., 22, p. 1242, 1951.

Anderson, L.J., J.P. Day, C.H. Freres, and A. Stokes, Attenuation of 1.25 cm radiation through rain, Proc. I.R.E. 35, p. 351, 1947.

Barath, F.T., Microwave radiometry and application to oceanography, Oceanography from Space, Woods Hole, Massachusetts, 235-239, 1965.

Barath, F.T., Radiometric calibration, a lecture at the Passive Microwave Team Workshop, Univ. of Nevada, Reno, Nevada, August 15-16, 1967.

Barath, F.T., A.H. Barrett, J. Copeland, D.E. Jones, and A.E. Lilley, Mariner 2 microwave radiometer experiment and results, Astronomical J., 69 (1), 49-58, February, 1964.

Barrett, A.H., and V.K. Chung, A method for the determination of high-altitude water-vapor abundance from ground-based microwave observations, J. Geophys. Res., 67 (11), 4259-4266, October, 1962.

Basharinov, A.E., A.B. Gorelik, V.V. Kalashnikov, and B.G. Kutuza, The determination of cloud and rain characteristics by means of simultaneous microwave radiometric and radar measurements, Proc. 13th Radar Met. Conf., McGill Univ., Montreal, 536-539, August, 1968.

Battan, L.J., Radar Meteorology, University of Chicago Press, Chicago, 161 pp., 1959.

Becker, G.E., and S.H. Autler, Water vapor absorption of electromagnetic radiation in the centimeter wavelength range, Phys. Rev., 70 (5 & 6), 300-307, September, 1946.

Beckmann, P., and A. Spizzichino, The Scattering of Electromagnetic Waves from Rough Surfaces, 503 pp., Pergamon Press, Oxford, 1963.

Blanchard, D.C., Electrification of the atmosphere by particles from bubbles in the sea, Progress in Oceanography, 1, 71-202, 1963.

Blinn, J.C., Microwave Radiometer Data, Antenna Temperatures from Mississippi Delta Test Site, Mission 41, February 24, 1967, 218 pp., Jet Propulsion Laboratories, Pasadena, California, November 30, 1967a.

Blinn, J.C., System description: Aircraft Microwave Radiometers Model MR-62 and MR-64, 37 pp., Jet Propulsion Laboratories, Pasadena, California, July 1, 1967b.

Bracewell, R.N., Radio astronomy techniques, Handbuch der Physik, 54, 42-129, 1962.

Buettner, K.J.K., Microwave emission of raining clouds, Oceanography from Space, Woods Hole, Massachusetts, 287, 1965.

Buettner, K.J.K., On the Uses of Intermediate Infrared and Microwave Infrared in Meteorological Satellites, Semi-Annual Report, Contract NASA NsG-632, 25 pp., Univ. of Washington, Seattle, Washington, June, 1968.

Buettner, K.J.K., Regenortung vom Wettersatelliten mit Hilfe von Zentimeterwellen (Location of rain from weather satellites using centimeter-wavelength radiation), die Naturwissenshaften, 50, 591-592, 1963.

Catoe, C., W. Nordberg, P. Thaddeus, and G. Ling, Preliminary Results from Aircraft Flight Tests of an Electrically Scanning Microwave Radiometer, Report No. X-622-67-352, 35 pp., Goddard Space Flight Center, Greenbelt, Maryland, August, 1967.

Chandrasekhar, S., Radiative Transfer, 393 pp., Clarendon Press, Oxford, 1950.

Chemical Rubber Company, Handbook of Chemistry and Physics, 40th Edition, 3456 pp., Chemical Rubber Publishing Company, Cleveland, Ohio, 1959.

Chen, S.N.C., and W.H. Peake, Apparent temperatures of smooth and rough terrain, I.R.E. Trans. Ant. Prop., AP-9, 567-572, November, 1961.

Cole, R.H., Theories of dielectric polarization and relaxation, Progress in Dielectrics, 3, 47-67, John Wiley and Sons, Inc., New York, 1961.

Collie, C.H., J.B. Hasted, and D.M. Ritson, The dielectric properties of water and heavy water, Proc. Phys. Soc. London, 60, 145-160, 1948.

Conway, W.H., and R.T. Sakamoto, Microwave radiometer measurements program, Proc. 3rd Symp. Remote Sens. of Environ. Ann Arbor, Michigan, 339-356, November, 1965.

Cox, C.S., and W.H. Munk, Measurements of the roughness of the sea surface from photographs of the Sun's glitter, J. Opt. Soc. Am., 44, 838-850, November, 1954a.

Cox, C., and W. Munk, Statistics of the sea surface derived from sun glitter, J. Marine Res., 13, 198-227, February, 1954b.

Croom, D.L., Stratospheric thermal emission and absorption near the 22.235 Gc/s (1.35 cm) rotational line of water-vapor, J. Atmos. Terr. Phys., 27, 217-233, 1965.

Cummings, C.A., and J.W. Hull, Microwave radiometric meteorological observations, Proc. 4th Symp. on Remote Sensing of Environ., Ann Arbor, Michigan, 263-271, April, 1966.

Debye, P., Polar Molecules, 289 pp., The Chemical Catalogue, New York, 1929.

Decker, M.T., and E.J. Dutton, Radiometric observations of thunderstorm cells, Proc. 5th Symp. Remote Sensing of Environ., Ann Arbor, Michigan, 617-629, April, 1968.

Deirmendjian, D., Scattering and Polarization Properties of Polydispersed Suspensions with Partial Absorption, RM-3228-PR, July, 1962.

Deirmendjian, D., Complete microwave scattering and extinction properties of polydispersed cloud and r in elements, R-422-PR, The Rand Corporation, 1963.

Dicke, R.H., The measurement of thermal radiation at microwave frequencies, Rev. Sci. Instr., 17 (7), 268-275, July, 1946.

Dicke, R.H., R. Beringer, R.L. Kyhl, and A.B. Vane, Atmospheric absorption measurements with a microwave radiometer, Phys. Rev., 70 (5 & 6), 340-348, September, 1946.

Dunsmuir, R., and J. Lamb, The Dielectric Properties of Ice at Wavelengths of 3 and 9 cm., Manchester Univ. Rept. No. 61, 1945.

Edison, A.R., Calculated Cloud Contributions to Sky Temperature at Millimeter-wave Frequencies, NBS Report 9138, 29 pp., U.S. Department of Commerce, National Bureau of Standards, February, 1966.

Ewen, H.I., F. Haneman, R.M. Kalafus, M.E. Louapre, R. Maillous, and D.G. Steinbrecher, Microwave radiometric capabilities and techniques, 5th Symp. Remote Sensing of Environ., Ann Arbor, Michigan, 9-58, April, 1968.

Ewing, G.C. (ed), Proc. Conf. Feasibility of Conducting Oceanographic Explorations from Aircraft, Manned Orbital and Lunar Laboratories (Short Title: Oceanography from Space), Ref. No. 65-10, Woods Hole, Massachusetts, 469 pp., April, 1965.

Falcone, V.J., Jr., Calculations of apparent sky temperature at millimeter wavelengths, Radio Science, 1 (10), 1205-1290, October, 1966.

Flugge, S., (ed.), Handbuch der Physik, 16, 753 pp., Springer-Verlag, Berlin, 1956.

Flugge, S. (ed.), Handbuch der Physik, 17, 406 pp., Springer-Verlag, Berlin, 1958.

Flugge, S. (ed.), Handbuch der Physik, 54, 308 pp., 1962.

Franz, K., (Title unknown), Hochfrequenztechnik und Electroakustik, 55, 141, 1940.

Gille, J.C., (ed.), Proc. 3rd Interdisciplinary Workshop on Inversion of Radiometric Measurements, T.R. 68-2, Department of Meterology, Florida State University, Tallahassee, Florida, 40 pp., May, 1968.

Giorgi, G., (Title unknown), Assoc. Elettrot, Italiana, Atti, 5, 402, 1901.

Glasstone, S., Sourcebook on the Space Sciences, 937 pp, D. Van Nostrand Co., Inc., Princeton, New Jersey, 1965.

Goldstein, H., Attenuation by condensed water, Propagation of Short Radio Waves, 671-692, McGraw-Hill Book Co., New York, 1951.

Goody, R.M., Atmospheric Radiation, 436 pp., Clarendon Press, Oxford, 1964.

Greene, D.R., An Investigation of Precipitation Attenuation and Its Application in a Dual-Frequency Radar Morphology of Subtropical Precipitation, M.S. Thesis, 108 pp., Department of Meteorology, Texas A&M University, College Station, Texas, January, 1964.

Gunn, K.L.S., and T.W.R. East, The microwave properties of precipitation particles, Quart. J. Met. Soc., 80, 522-545, 1954.

Hanel, R.A., Determination of cloud altitude from a satellite, J. Geophys. Res., 66 (4), 1300, April, 1961.

Hasted, J.B., The dielectric properties of water, Progress in Dielectrics, 3, 102, John Wiley and Sons, Inc., New York, 1961.

Hogg, D.C., Effective antenna temperature due to oxygen and water vapor in the atmosphere, J. Appl. Phys., 30 (9), 1417-1419, September, 1959.

Hogg, D.C., and R.A. Semplak, Estimated sky temperatures due to rain for the microwave band, Proc. I.E.E.E., 51, 499-500, March, 1963a.

Hogg, D.C., and R.A. Semplak, Measurement of microwave interference at 4 Gc due to scatter by rain, Proc. I.E.E.E., 51, p. 500, March, 1963b.

Holter, M.R., and R.R. Legault, The motivation for multispectral sensing, Proc. 3rd Symp. Remote Sensing Environment, Ann Arbor, Michigan, 71-78, November, 1965.

Hyatt, H.A., Analysis of Measurements of Microwave Emission from the Earth's Surface and Atmosphere, Report No. DAC-60693, 50 pp., Douglas Missile & Space Systems Division, Douglas Aircraft Company, California, June, 1967.

Imai, I., Attenuation of microwaves through rain for various drop-size distributions, 75th Anniversary Volume of J. Met. Soc. Japan, 65-71, 1957.

Janza, F.J., A Comparison of the Microwave Scatterometer and Radiometer for Sea-State Measurements, Ryan Electronics and Space Systems, San Diego California, 1968.

Joos, G., Theoretical Physics, translated from original German by I.M. Freeman, 885 pp., Hofner Publishing Co., New York, 1950.

Jordan, E.C., Electromagnetic Waves and Radiating Systems, 710 pp., Prentice-Hall, Inc., New York, 1950.

Kaplan, L.D., Inference of atmospheric structure from remote radiation measurements, J. Opt. Soc. Am., 49 (10), 1004-1007, October, 1959.

Keigler, J.E., and L. Krawitz, Weather radar observations from Earth satellite, J. Geophys. Res., 65 (9), 2793-2808, September, 1960.

Kerr, D.E., (ed.), Propagation of Short Radio Waves, 728 pp., McGraw-Hill Book Co., New York, 1951.

Ko, H.C., Radio-telescope antenna parameters, I.E.E.E. Trans. Mil. Electronics, MIL-8 (3 & 4), 225-232, 1964.

Kraus, J.D., Radio and radar astronomy and the exploration of the universe, I.E.E.E. Trans. Mil. Electronics, MIL-8 (3 & 4), 232-235, 1964.

Kraus, J.D., Radio Astronomy, 481 pp., McGraw-Hill Book Co., New York, 1966.

Kreiss, W.T., Meteorological Observations with Passive Microwave Systems, 198 pp., Boeing Scientific Research Laboratories Document D1-82-0692, Boeing Aircraft Company, Seattle, Washington, February, 1968.

Kutuza, B.G., Investigation of radiowave attenuation and radiation of rain in the microwave range, Proc. 13th Radar Met. Conf., McGill Univ., Montreal, 540-542, August, 1968.

Lane, J.A., and J.A. Saxton, Dielectric dispersion in pure polar liquids at very high radio-frequencies. I. Measurements on water, methyl and ethyl alcohols, Proc. Roy. Soc. London, 213, 400-408, 1951.

Lane, J.A., and J.A. Saxton, Dielectric dispersion in pure polar liquids at very high radio-frequencies. III. The effect of electrolytes in solution, Proc. Roy. Soc. London, 214, 531-545, 1952.

Laws, J.O., and D.A. Parsons, The relation of raindrop size to intensity, Trans. Am. Geophys. Union, 24, p. 452, 1943.

Lowan, A., (ed.), Tables of Scattering Functions for Spherical Particles, National Bureau of Standards, Washington, D.C., 1949.

Manned Spacecraft Center, Mission 66, Flight 1, Test Site 128, Passive Microwave Data Antenna Temperatures, 24 pp., Houston, Texas, 1968.

Manned Spacecraft Center, Mission 66, Flight 11, Test Site 128, Passive Microwave Data Antenna Temperatures, 190 pp., Houston, Texas, 1968.

Marandino, G.E., Microwave Signatures from Various Terrain, B.S. Thesis, 59 pp., Department of Physics, M.I.T., Cambridge, Massachusetts, May 19, 1967.

Mardon, A., Part II: Application of microwave radiometers to oceanography, Oceanography from Space, Woods Hole, Massachusetts, 254-271, 1965.

Marshall, J.S., and W. McK. Palmer, The distribution of raindrops, with size, J. Meteorology, 5 (4), 165-166, August, 1948.

Maxwell, J.C., A Treatise on Electricity and Magnetism, Vol. II., Clarendon Press, Oxford, 1892.

McAlister, E.D., and W.L. McLeish, 1. Oceanographic measurements with airborne infrared equipment and their limitations (and) 2. A two-wavelength microwave radiometer for temperature and heat exchange measurements at the sea surface of possible use in manned satellites, Oceanography from Space, Woods Hole, Massachusetts, 189-214, 1965.

McLellan, H.J., Elements of Physical Oceanography, 150 pp., Pergamon Press, New York, 1965.

Meeks, M.L., and A.E. Lilley, The microwave spectrum of oxygen in the Earth's atmosphere, J. Geophys. Res., 68 (6), 1683-1703, March, 1963.

Mie, G., Beitrage zur Optik truber Medien, speziell kolloidaler Metallosungen, Ann. Phys., 25, 377-445, 1908.

Munk, W.H., A critical wind speed for air-sea boundary processes, J. Marine Res., 6, (3), p. 203, 1947.

Paris, J.F., Investigations into the applications of passive microwave radiometry to oceanographic and meteorological problems, Tech. Papers, 9th Ad Hoc Spacecraft Oceanography Advisory Group, Spacecraft Oceanography Project, U.S. Naval Oceanographic Office, Washington, D.C., January 23-25, 1968a.

Paris, J.F., Preliminary Results from Convair 240A Mission 50, 12 June 1967, Over Mississippi Delta Area, Ref. No. 68-6T, 33 pp., Department of Oceanography, Texas A&M University, College Station, Texas, May 3, 1968b.

Pascalar, H.G., and R.T. Sakamoto, Microwave radiometric measurements of ice and water, Proc. 3rd Symp. Remote Sensing of Environ., Ann Arbor, Michigan, 803-812, November, 1965.

Peake, W.H., Interaction of electromagnetic waves with some natural surfaces, I.R.E. Trans. Ant. Prop., AP-7, S324-S329, December, 1959.

Peake, W.H., The microwave radiometer as a remote sensing instrument with applications to geology, notes prepared for a short course on geological remote sensing, 34 pp., Stanford U., December, 4-8, 1967.

Peake, W.H., R.L. Riegler, and C.H. Schultz, The mutual interpretation of active and passive microwave sensor outputs, Proc. 4th Symp. Remote Sensing of Environ., Ann Arbor, Michigan, 771-777, April, 1966.

Planck, M., Theorie der Warmestrahlung, Barth, Leipzig, 1906.

Porter, Ronald A., Microwave Radiometric Measurements of Sea Water, Concrete, and Asphalt, Raytheon Co., Space and Information Systems Division, Sudbury, Massachusetts, June 20, 1966.

Ramo, S., J.R. Whinnery, and T. van Duzer, Fields and Waves in Communication Electronics, 754 pp., John Wiley & Sons, Inc., New York, 1965.

Rice, S., Reflection of electromagnetic waves from slightly rough surfaces, Comm. Pure and Appl. Math, 4, 351-378, 1951.

Roeder, R.S., Airborne Measurements with the AN/AAR-33 Radiometric Search Set, 6 pp., Sperry Microwave Electronics Company, a division of Sperry Rand Corp., January 10, 1967.

Roll, H.U., Physics of the Marine Atmosphere, 426 pp., Academic Press, New York, 1965.

Ryde, J.W., The attenuation and radar echoes produced at centimeter wavelengths by various meteorological phenomena, Meteorological Factors in Radio-Wave Propagation, 169-189, 1946.

Ryde, J.W., and D. Ryde, Attenuation of Centimeter and Millimeter Waves by Rain, Hail, Fogs and Clouds, G.E.C. Res. Lab., London, Report Number 8670, 1945.

Saunders, P.M., and C.H. Wilkens, Precise airborne radiation thermometry, 4th Symp. Remote Sensing of Environ., Ann Arbor, Michigan, 815-826, June, 1966.

Saxton, J.A., The anomalous dispersion of water at very high radio frequencies. Part II. Relation of experimental observations to theory., Meteorological Factors in Radio-wave Propagation, 292-306, 1946a.

Saxton, J.A., The anomalous dispersion of water at very high radio frequencies. Part III. The dipole relaxation time and its relation to the viscosity, Meteorological Factors Radio-Wave Propagation, 306-316, 1946b.

Saxton, J.A., The anomalous dispersion of water at very high radio frequencies. Part IV. A note on the effect of salt in solution., Meteorological Factors in Radio-Wave Propagation, 316-325, 1946c.

Saxton, J.A., Dielectric dispersion in pure polar liquids at very high radio-frequencies. II. Relation of experimental results to theory, Proc. Roy. Soc. London, 213, 473-492, 1951.

Saxton, J.A., and J.A. Lane, Electrical properties of sea water, Wireless Engineer, 269-275, October, 1952.

Saxton, J.A., and J.A. Lane, The anomalous dispersion of water at very high radio-frequencies. Part I. Experimental determination of the dielectric properties of water in the temperature range 0° C. to 40° C. for wavelengths of 1.24 cm. and 1.58 cm., Meteorological Factors in Radio-Wave Propagation, 278-292, 1946.

Servey, T.E., Digital Computer Program for Calculations of Apparent Sky Temperature and Atmospheric Transmission Factor, 37 pp., Raytheon Co., Bedford, Massachusetts, September 9, 1964.

Silver, S., Antenna theory and design, MIT Radiation, 582 pp., Laboratory Series, 12, McGraw-Hill, New York, 1949.

Singer, S.F., and G.F. Williams, Jr., Microwave Detection of Precipitation Over the Surface of the Ocean, University of Miami, Coral Gables, Florida, 1968.

Sirounian, V., The effect of temperature, angle of observation, salinity, and thin ice on the microwave emission of water, J. Geophys. Res., 73 (14), 4481-4486, July 15, 1968.

Smith-Rose, R.L., Allocation of frequencies for radio astronomy and space science, Nature, 203 (4940), 7-11, July, 1964.

Staelin, D.H., Measurements and interpretation of the microwave spectrum of the terrestrial atmosphere near 1-centimeter wavelength, J. Geophys. Res., 71 (12), 2875-2881, June, 1966.

Stephens, J.J., Radar cross-sections for water and ice spheres, J. Meteorology, 18, 348-359, June, 1961.

Stogryn, A., The apparent temperature of the sea at microwave frequencies, I.E.E.E. Trans. Ant. Prop., AP-15(2), 278-286, March, 1967.

Stratton, J., (Title unknown), Proc. I.R.E., 18, p.1064, 1930.

Stratton, J., Electromagnetic theory, 615 pp., McGraw Hill Book Co., New York, 1941.

Sucher, M., and J. Fox, Handbook of Microwave Measurements, Vols. I, II, and III, Interscience Publishers, John Wiley & Sons, Inc., New York, 1963.

Taylor, H.P., and J.A. Campbell, Technique of observing the 5-mm self-emission from the oxygen of the Earth's atmosphere to obtain a vertical sense, Radio Science, 1 (10), 1209-1213, October, 1966.

Tobin, M.S., Support Data for Convair 990 Meteorological Flight II, Goddard Space Flight Center, Greenbelt, Maryland, July, 1967.

Townes, C.H., and A.L. Schawlow, Microwave Spectroscopy, McGraw-Hill Book Co., New York, 698 pp., 1955.

Valley, S.L., Handbook of Geophysics and Space Environments, McGraw-Hill Book Co., New York, 1965.

Van de Hulst, H.C., Light Scattering by Small Particles, John Wiley and Sons, Inc., New York, 470 pp., 1957.

Van Vleck, J.H., The absorption of microwaves by oxygen, Phys. Rev., 71 (7), 413-424, April, 1947a.

Van Vleck, J.H., The absorption of microwaves by uncondensed water vapor, Phys. Rev., 71 (7), 425-433, April, 1947b.

Van Vleck, J.H., Theory of absorption by uncondensed gases, Propagation of Short Radio Waves, McGraw-Hill Book Co., New York, 646-664, 1951a.

Van Vleck, J.H., The relation between absorption and dispersion, Propagation of Short Radio Waves, McGraw-Hill Book Co., New York, 641-646, 1951b.

Van Vleck, J.H., and V.F. Weisskopf, On the shape of collision broadened lines, Rev. Mod. Phys., 17, 227-236, 1945.

Von Hippel, A.R., Dielectrics and Waves, 284 pp., The M.I.T. Press, Cambridge, Massachusetts, 1954.

Walsh, Don, The Mississippi River Outflow, Its Seasonal Variations and Its Surface Characteristics, Ph.D. Dissertation, 220 pp., Department of Oceanography, Texas A&M University, College Station, Texas, August, 1968.

Weger, E., Apparent sky temperature in the microwave region, J. Meteorology, 17, 159-165, April, 1960.

Wells, D.R., The Apparent Temperature of the Ocean Surface at Microwave Frequencies, 7 pp., Space-General Corp., El Monte, California, January 17, 1967.

Westwater, E.R., A method for determination of the tropospheric temperature structure from ground-based measurement of oxygen emission, Proc. 3rd Symp. Remote Sensing of Environ., Ann Arbor, Michigan, 245-256, November, 1965.

Williams, G.F., Microwave radiometry of the ocean, Tech. Report, 9th Ad Hoc Spacecraft Oceanography Advisory Group, Spacecraft Oceanography Project, U.S. Naval Oceanographic Office, Washington, D.C., January 23-25, 1968.

Wulfsberg, K.N., Apparent Sky Temperatures at Millimeter Wave Frequencies, 29 pp., Physical Sciences Research Papers, No. 38, Air Force Cambridge Research Laboratories, USAF, Hanscom Field, Massachusetts, July, 1964.

Wulfsberg, K.N., Atmospheric attenuation at millimeter wavelengths, Radio Science, 2 (3), 319-324, March, 1967.

Yamamoto, G., and D.Q. Wark, Discussion of the letter by R.A. Hanel, 'Determination of cloud altitude from a satellite', J. Geophys. Res., 66 (10), p. 2596, October, 1961.

Zimmerer, R.W. and M. Mizushima, Precise measurement of the microwave absorption frequencies of the oxygen moleucle and the velocity of light, Phys. Rev., 121(1), 152-160, 1961.

UNCLASSIFIED

Security Classification

DOCUMENT CONTROL DATA - R & D

(Security classification of title, body of abstract and indexing annotation must be entered when the overall report is classified)

1. ORIGINATING ACTIVITY (Corporate author) Department of Oceanography, Texas A&M University, College Station, Texas through the Texas A&M Research Foundation.	2a. REPORT SECURITY CLASSIFICATION Unclassified 2b. GROUP Unclassified

3. REPORT TITLE
Microwave Radiometry and Its Applications to Marine Meteorology and Oceanography

4. DESCRIPTIVE NOTES (Type of report and inclusive dates)
Technical Report

5. AUTHOR(S) (First name, middle initial, last name)
Jack F. Paris

6. REPORT DATE January, 1969	7a. TOTAL NO. OF PAGES 212	7b. NO. OF REFS 138
8a. CONTRACT OR GRANT NO Nonr 2119(04) b. PROJECT NO. Texas A&M Project 286-13 c. d.	9a. ORIGINATOR'S REPORT NUMBER(S) Ref. No. 69-1T 9b. OTHER REPORT NO(S) (Any other numbers that may be assigned this report)	

10. DISTRIBUTION STATEMENT
No limitation; Price: Cost of reproduction

11. SUPPLEMENTARY NOTES	12. SPONSORING MILITARY ACTIVITY Funding by National Aeronautics and Space Administration through the Office of Naval Research

13. ABSTRACT

Past developments in microwave radiometry are reviewed to establish a continuity between microwave physics, engineering, and applications to marine meteorology and oceanography. Molecular oxygen, water vapor, and liquid water absorb, emit, and scatter microwave radiation. The ocean reflects or scatters a majority of the microwave radiation incident upon its surface and emits microwave energy. The functional relationship between these interactions and the physical state of the atmosphere and hydrosphere are described in detail. The emission of sea water is almost constant with temperature and salinity for frequencies of 8 GHz to 30 GHz, is linearly proportional to temperature for frequencies near 5.4 GHz, and is strongly dependent upon salinity for frequencies near 1 GHz. Sea foam causes the microwave emission of the sea to increase greatly for all microwave frequencies and angles of viewing. The natural variability of water vapor in the atmosphere affects the absolute value of upwelling microwave radiation greatly for frequencies near 22.235 GHz. The attenuation and emission of the atmosphere are predictable for frequencies less than 8 GHz. Microwave measurements near 5.4 GHz and 1 GHz may be used to survey, remotely, the temperature and salinity of coastal water. Microwave measurements near 22.235 GHz may be used to measure the precipitable water in the atmosphere. It is recommended that (1) electric properties of sea water be measured precisely, (2) controlled environmental tests of current microwave theory be conducted, (3) the problem of the microwave emission and extinction of raining clouds over water be studied in great detail using realistic models and the Mie theory, and (4) the emissive properties of sea foam, bubbles, and rough sea surfaces be determined through empiricism.

DD FORM 1 NOV 65 1473 (PAGE 1)

S/N 0101-807-6801

UNCLASSIFIED

Security Classification